ON THE CONCEPT OF THE RECONFIGURABLE MULTI-SOURCE INVERTER FOR ELECTRIFIED VEHICLE POWERTRAINS

ON THE CONCEPT OF THE RECONFIGURABLE MULTI-SOURCE INVERTER FOR ELECTRIFIED VEHICLE POWERTRAINS WITH A HYBRID ENERGY STORAGE SYSTEM

BY

MEGAN SPENCER WOOD, B.Eng.

A THESIS

SUBMITTED TO THE DEPARTMENT OF ELECTRICAL & COMPUTER ENGINEERING

AND THE SCHOOL OF GRADUATE STUDIES

OF MCMASTER UNIVERSITY

IN PARTIAL FULFILMENT OF THE REQUIREMENTS

FOR THE DEGREE OF

MASTER OF APPLIED SCIENCE

Master of Applied Science (2020) McMaster University

(Electrical & Computer Engineering) Hamilton, Ontario, Canada

TITLE:	On the Concept of the Reconfigurable Multi-Source Inverter for Electrified Vehicle Powertrains with a Hybrid Energy Storage System
AUTHOR:	Megan Spencer Wood B.Eng. (Electrical Engineering), McMaster University, Hamilton, Canada
SUPERVISOR:	Dr. Ali Emadi
NUMBER OF PAGES:	xv, 91

Lay Abstract

One of the main factors affecting the cost of electrified vehicle is the expense of building a high voltage battery pack. Motor's used in electric vehicle applications typically operate at higher voltages and therefore require large battery pack or costly power electronics to step the voltage of the pack up to a suitable operating level. A Reconfigurable Multi-Source Inverter uses a combination of two sources to create different voltage levels. This novel inverter can be used to maximize the voltage of smaller packs to help reduce the overall cost of vehicle electrification.

Abstract

This thesis focuses on the concept, design, and simulation of the Reconfigurable Multi-Source Inverter for EV applications and its effectiveness when combined with a HESS.

The current trends in the automotive market, including different vehicle types, and the adoption of electrified vehicles by the public are discussed. The benefits and logistics of different vehicle architectures are analyzed and compared. Hybrid vehicles will be essential in helping transition society from conventional internal combustion engine vehicles to purely electric vehicles. The individual components of these electrified vehicles are reviewed, and common topologies are discussed with the benefits of each system compared.

The batteries required for these electric vehicles are costly and require many individual cells in order to operate efficiently. Many hybrids vehicles make use of expensive power electronics, such as DC/DC converters to help boost the operating voltage of the battery pack without adding additional cells. A Reconfigurable Multi-Source Inverter in introduced and its switching structure is explained in depth. Its' ability to make use of multiple DC sources to create four different voltage levels is outlined and possible modulation techniques are presented. This thesis aims introduce a novel Reconfigurable Multi-Source Inverter using a Space Vector Pulse Width Modulation

(SVPWM) scheme and is further investigated through simulations and with plans for experimental validation on an R-L load.

To my parents, Susan and Dave

Thank You

Acknowledgements

This research was undertaken, in part, thanks to funding from the Canada Excellence Research Chair (CERC) Program, McMaster and Institute for Automotive Research and Technology (MacAUTO). I would like to thank my supervisor, Dr. Ali Emadi, for always believing in me, and pushing me to challenge myself both personally and professionally.

I would like to also thank the many members of the McMaster Formula Hybrid and McMaster Engineering EcoCAR Teams, without which my time at McMaster would have been very different. Each of these teams became a family to me, and I will cherish my memories with both teams fondly.

I would like to thanks all of my friends and colleagues who supported me throughout the many ups and downs of university life. Most importantly I would like to thank my family, without your support I know I could not have made it this far. To my mom, Susan, and my dad, Dave, I couldn't have asked for a better support system both growing up and throughout my university career. To my brother Connor, thanks for always sticking by my side.

Finally, I would like to thank all of the different professors, administrators and staff who have helped me through my many years at McMaster.

Contents

Lay Abstract **iii**

Abstract **iv**

Acknowledgements **vii**

Notation **xiii**

1 Introduction **1**

1.1 Automotive Electrification 1

1.2 Contributions 6

1.3 Thesis Outline 8

2 Electrified Powertrains **10**

2.1 Electric Motors 11

2.2 DC/DC Converters 12

2.3 Inverters 13

2.4 Hybrid Vehicle Architectures 17

3 Energy Storage Systems **21**

3.1 Exotic Energy Storage Systems 23
3.2 Hybrid Energy Storage Sytems 24
3.3 Battery Modelling 26

4 Reconfigurable Multi-Source Inverter 29
4.1 Operating Voltages 31
4.2 Inverter Control 33

5 Modelling & Simulation of an ReMSI in an Electrified Vehicle 40
5.1 Inverter Modelling and Control 41
5.2 Inverter Modelling with a HESS 45
5.3 Vehicle Modelling 46
5.4 ReMSI in an Electrified Powertrain 48

6 Power Circuitry and Plans for Experimentation of the ReMSI 50
6.1 Existing Experimental Setup 50
6.2 IGBT Setup 52
6.3 Challenges 54

7 Conclusion 55
7.1 Future Work 57

A Commutation Paths 59

B Printed Circuit Board Schematics 64

List of Figures

1.1 Example Conventional ICE Vehicle Architecture 3

1.2 Example Electric Vehicle Architecture 4

1.3 Example Hybrid Vehicle Architecture 5

2.1 Motor Positioning Nomenclature 11

2.2 A Hybrid Vehicle Architecture with a DC/DC Converter 13

2.3 Voltage Source Inverter Topology 15

2.4 Multi Source Inverter Topology 16

2.5 Multi-Source Inverter in a Hybrid Vehicle 16

2.6 Example Series Hybrid Architecture 18

2.7 Example Parallel Hybrid Architecture 19

2.8 Example Power-Split Hybrid Architecture 20

3.1 Battery Cell Configurations 22

3.2 5S3P Battery Pack 22

3.3 Parallel Passive HESS 25

3.4 Parallel Active HESS 26

3.5 n-order R-RC-RC Equivalent Circuit Model 27

4.1 Reconfigurable Multi-Source Inverter in a Power-Split Hybrid Vehicle 30

4.2 Ideal Switch Topology for an ReMSI 31

4.3 ReMSI Operating Modes Switching Paths 32
4.4 Sinusoidal Pulse Width Modulation Scheme 35
4.5 Alpha-Beta Reference Plane 39
5.1 Block Diagram of SVPWM Control Strategy for the ReMSI 41
5.2 Gating Signals for each Phase Output 42
5.3 Line-to-Line Voltage and Output Phase Current 43
5.4 Output Phase Current 43
5.5 Output Voltages 44
5.6 SOC of V_{DC2} Throughout the Different Operating Modes 48
6.1 Experimental Test Setup 51
6.2 NPC vs. TNPC IGBT Setup 52
6.3 TNPC Switch Topology for an ReMSI 53
A.1 Original TNPC ReMSI Circuit 59
A.2 Commutation Paths in Operating Mode 1 60
A.3 Commutation Paths in Operating Mode 2 61
A.4 Commutation Paths in Operating Mode 3 62
A.5 Commutation Paths in Operating Mode 4 63

List of Tables

4.1 Switching States of the ReMSI with Ideal Switches 34

Notation

Abbreviations

AC	Alternating Current
Ah	Amp-hours
APM	Auxiliary Power Module
AVTC	Advanced Vehicle Technology Competition
BEV	Battery Electric Vehicle
BSG	Belted Starter Generator
CO_2	Carbon Dioxide
DC	Direct Current
EM	Electric Motor
ESS	Energy Storage System
EV	Electrified Vehicle

GHG	Green House Gas
HESS	Hybrid Energy Storage System
HEV	Hybrid Electric Vehicle
HV	High Voltage
ICE	Internal Combustion Engine
IGBT	Insulated Gate Bipolar Transistors
KVL	Kirchhoff's Voltage Law
kW	Kilowatts
kWh	Kilowatt Hours
Li-Ion	Lithium-Ion
LV	Low Voltage
MAAS	Mobility as a Service
MSI	Multi-Source Inverter
MTDM	machine-tool-die-and-mould
NPC	Neutral Point Clamped
OEM	Original Equipment Manufacturers
PCB	Printed Circuit Board
PHEV	Plug-In Hybrid Electric Vehicle

PWM	Pulse Width Modulation
ReMSI	Reconfigurable Multi-Source Inverter
SPWM	Sinusoidal Pulse Width Modulation
SVPWM	Space Vector Pulse Width Modulation
TNPC	T-Type Neutral Point Clamped
UC	Ultracapacitor
VSI	Voltage Source Inverter

Chapter 1

Introduction

1.1 Automotive Electrification

The Canadian automotive market has been growing for many years, expanding from 1.43 vehicles per household in 2000 to 1.47 in 2009 [1]. As of 2019, Canada was ranked as one of the world's top 10 producers for commercial automobiles, making it one of our countries largest manufacturing sectors [2]. There are five global Original Equipment Manufacturers (OEM's) who assemble, on average more than 2 million vehicles at their Canadian plants per year. These plants are supplied by almost 700 automotive parts suppliers, including Tier 1 companies such as Magna, and Linamar. Additionally, Canada is home to one of only five machine-tool-die-and-mould (MTDM) making clusters in the world. Canadians have been building vehicles for over a century, and this industry directly employs more than 125,000 Canadians, with an additional 400,000 people in aftermarket services, maintenance, and dealerships [2].

For the average consumer, vehicles can be divided into two major fuel types: fossil

fuels or electric potential energy, while there are other options such as fuel cells, or hydrogen, they are significantly less common. Taking the chemical energy of the fossil fuel, an Internal Combustion Engine (ICE) converts it to rotational mechanical energy to produce power for the wheels. Through the use of a transmission gear set, the vehicle can operate at a variety of speeds and torques to best suit the driver's needs. While fossil fuels are very energy-dense chemically, most of that potential energy is lost through the combustion process in the ICE; conventional fossil-fueled vehicles have an efficiency ranging from 12-30% [3]. This is the most popular type of vehicle on the road today, an example of this architecture can be seen below in Figure 1.1.

The infrastructure that is globally in place makes owning and operating an ICE vehicle very convenient with gas stations in every major city and located along highways, and side roads, meaning the average driver will rarely need to worry about running of fuel. As an ICE vehicle burns fossil fuels, various Green House Gases (GHG) are produced, the majority of which is Carbon Dioxide (CO_2). These harmful gasses are a significant contributor to climate change. On average, for every litre of gasoline burned by passenger vehicles, approximately 2.3 kg of CO_2 is generated [4]; in 2014, road vehicles accounted for almost 50% of the world's oil usage [5]. Governments across the globe are increasing fuel economy and emissions standards, causing the automotive industry to become more electrified in order to combat climate change. In 2011, the Obama administration implemented improved fuel efficiency standards for light-duty passenger vehicles for the first time since 1990 [6]. Vehicle electrification will be crucial in achieving these improved fuel consumption values.

Vehicles using purely electric potential energy are called Battery Electric Vehicles

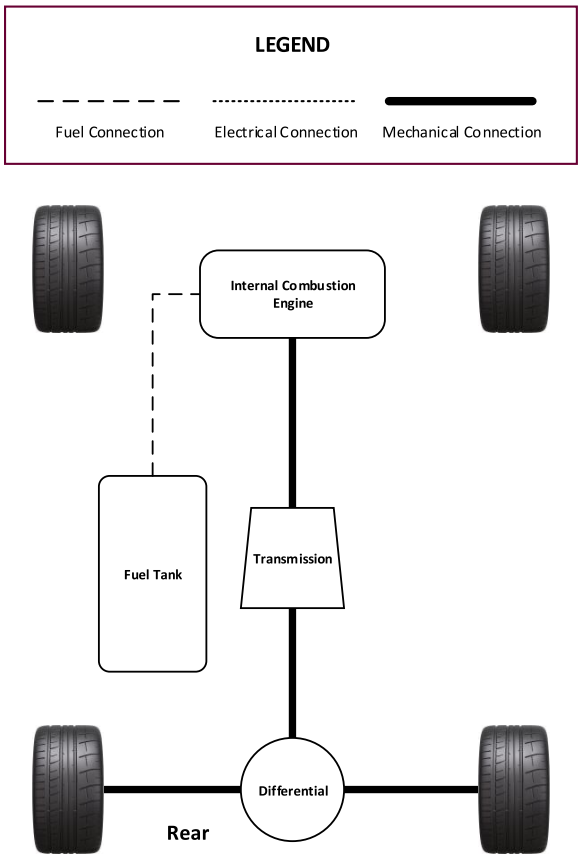

Figure 1.1: Example Conventional ICE Vehicle Architecture

(BEV). The BEV system is simpler to design and model then the ICE option due to having significantly fewer moving components. The powertrain for a BEV, shown in Figure 1.2, consists of a battery pack, or Energy Storage System (ESS), a tractive Electric Motor (EM), and power electronics. While batteries generally contain less energy potential than fossil fuels, the power electronics and components of a BEV system have a much higher operating efficiencies. Through the use of regenerative braking, a BEV, on average, has an overall system efficiency of around 77% [3]. Electric vehicle charging stations are less common than gas stations; the infrastructure is being put in place, with governments offering incentives for consumers to opt for

Electrified Vehicles (EVs) over there conventional counterparts. Electric vehicles are expected to grow from 2% of the world's total passenger vehicles in 2016 to 22% by 2030 [4].

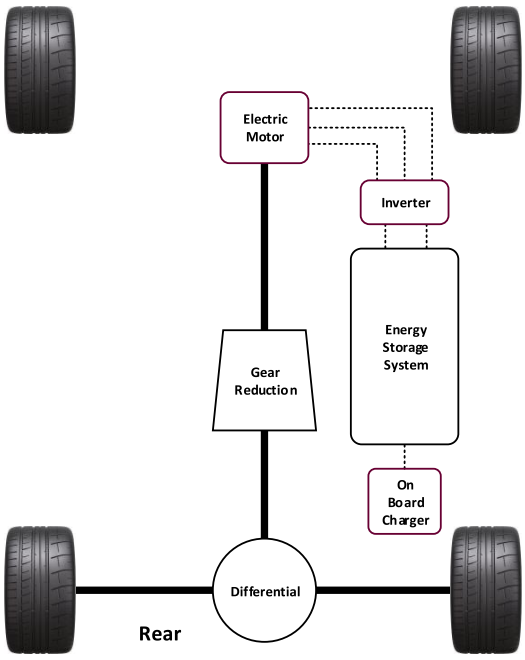

Figure 1.2: Example Electric Vehicle Architecture

Hybrid Electric Vehicles (HEV) use a combination of both fossil fuels and electrical energy. An HEV vehicle powertrain is similar to an ICE vehicle but has the addition of a second alternative powertrain as well. These systems can be bulky and expensive as they require twice the number of components and design work compared to their ICE or BEV counterparts. HEVs can be split into many different categories depending on their level of electrification. The lowest level of electrification is considered a micro HEV, which utilizes engine start/stop functionality with a small EM to reduce emissions while idling, which sees an improvement of about 5-10% efficiency over a conventional vehicle [3]. The next level is a mild HEV, which can begin to contain

High Voltage (HV) systems to improve efficiency up to 20% above a purely ICE vehicle [3].

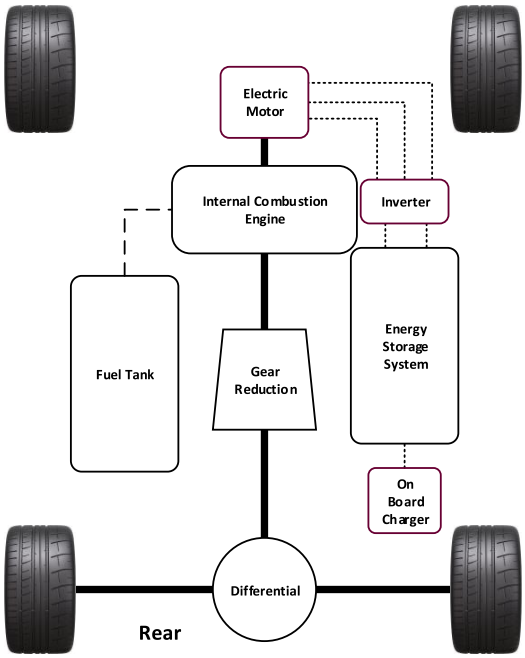

Figure 1.3: Example Hybrid Vehicle Architecture

Further electrification would be considered a full HEV, which would make use of a tractive EM to apply power to the wheels and recharge the system by making use of regenerative braking. The powertrain of a full HEV can have an efficiency of up to 50% [3]; a typical example of a full hybrid would be the first generation Toyota Prius. Finally, there is a Plug-In Hybrid (PHEV), Figure 1.3, which allows the HV battery to be recharged through the use of a wall plug and an external charging cable, as seen with the Chevrolet Volt. PHEV's can be up to 70% more efficient than purely fossil fuel vehicles [3], which makes them a popular choice, having the flexibility and option to refuel at either a gas station or charging station.

1.2 Contributions

The author, during her time at McMaster, has contributed to several different areas including but not limited to the following.

- Was the electrical team lead of the EcoCAR 3 team
- Played a crucial role in the design, build, and integration of the Hybrid Energy Storage System (HESS) used by the MAC team throughout the EcoCAR 3 competition.
- Was the Engineering Manager of the EcoCAR Mobility Challenge team for two years throughout her master's degree.
- Was a co-author on two papers outlining the significance of the HESS and its uses in EV applications.

1.2.1 Advanced Vehicle Technology Competitions

The Advanced Vehicle Technology Competition (AVTC) series is a decades-long unique collaboration of government, industry, and academic partners who combine resources to explore sustainable transportation solutions. Sponsored by the United States Department of Energy, and managed by Argonne National Laboratory, it is North America's premier collegiate-level automotive engineering competition. Students work in interdisciplinary teams to solve real-world problems and help meet future automotive market needs.

McMaster has been participating in AVTC's since 2014, starting with the EcoCAR 3 challenge, a four-year-long competition sponsored by General Motors. The

competition consisted of 16 North American universities, who were tasked with the goal of re-engineering and electrifying a 2016 Chevrolet Camaro. The overarching goal was to maintain the performance expected from the Camaro while minimizing its environmental impact through the implementation of high-performance hybrid technologies. With that goal in mind, the team set their sights on the Chevrolet Z/28 Camaro, a track performance vehicle, as the car to beat. Thus the E/28 Camaro was born, a hybrid vehicle boasting 600 HP and 750 ft-lbs of torque while increasing the vehicle's fuel economy to 42 miles per gallon (5.6 L/100km). The team hoped to break the stereotype of hybrid vehicles being low range, low performance, and prove that electrified powertrains can be track-ready, sports cars while still being environmentally conscious and consumer-friendly.

The E/28 was more than just a student project car; it also featured an advanced driver assistance system and the level of safety expected from a production vehicle. Together the MAC team designed a PHEV with a 2.0L LTG engine, an 8-speed automatic transmission, and two electric motors. The innovation opportunities were endless with such a unique project, and the team continually chose to push the boundaries even further by incorporating a HESS (HESS). A HESS is a combination of both batteries and ultracapacitors; the system capitalizes on the power density of ultracapacitors of the charge-sustaining characteristics of a conventional battery pack. The Mac team has used these competitions as a stage for combining cutting edge research with industry design requirements. By continually pushing the envelope of hybrid architectures, the team was able to showcase the viability of a HESS successfully.

In 2018 McMaster began participating in the newest AVTC, the EcoCAR Mobility Challenge. Another four yearlong engineering design competition, this time sponsored

by General Motors and Mathworks, 12 teams were tasked with re-engineering, electrifying, and adding autonomous features to a 2019 Chevrolet Blazer for the Mobility as a Service (MAAS) market. Therefore, the proposed architectures are designed for ride-sharing and should be efficient as an everyday versatile commuter vehicle. The McMaster team is currently comprised of approximately 150 engineering students from a range of engineering disciplines, including mechanical, electrical, software, mechatronics, automotive, and others. The students on the team range in level from first-year students new to automotive design to masters-level students who have experience working in the automotive industry. Together they have designed and built a parallel through the road mild-hybrid powertrain.

1.3 Thesis Outline

This thesis is organized into seven chapters. It focuses on the concept, design, and simulation of the Reconfigurable Multi-Source Inverter for EV applications and its effectiveness when combined with a HESS.

Chapter 1 covers trends in the automotive market, different vehicle types, and the adoption of electrified vehicles by the public. Additionally, the authors' thesis contributions are discussed with emphasis on her work with the McMaster EcoCAR team.

Chapter 2 presents the fundamentals of the power electronics found within an electrified powertrain. EM's, traction inverters, and power converters are discussed along with their design characteristics and various applications. The primary hybrid powertrain architectures are introduced, and their power flow requirements are detailed.

Chapter 3 discusses energy storage systems found in hybrid vehicle systems and discusses the benefits and costs associated with different storage methods. Battery cell modelling and simulation strategies are also discussed in this chapter as battery cells are unequivocally the most common form of an energy storage system, apart from fossil fuels.

Chapter 4 introduces the concept of the Reconfigurable Multi-Source Inverter (ReMSI). The converter topology is initially introduced using ideal switches, which are later replaced with power semiconductors. The theoretical behaviour of the ReMSI is discussed in its' four unique operating modes. Pulse Width Modulation (PWM) techniques are presented and compared to each other and their applications in the novel inverters.

Chapter 5 consists of the modelling and simulation of the ReMSI using Simulink to prove operation using Insulated Gate Bipolar Transistors (IGBTs) in place of ideal switches. The inverter is first modelled individually, and the results of the different operating voltages and currents are shown. The model is added to a larger vehicle model to highlight the mode switching within the inverter, and its potential use cases.

In Chapter 6, a prototype bench has been built to create an experimental setup using an induction motor and a load. Closed-loop control experiments with speed and torque references are planned to validate the concept of the proposed topology.

Chapter 7 is dedicated to conclusions and future work.

Chapter 2

Electrified Powertrains

Depending on the level of electrification and the powertrain configuration, power electronics are used to control the Electric Motors (EMs) and the supplemental powertrain. The EMs can be used as a motor or generator to either apply force to the powertrain or help recuperate powertrain losses and can be used in both the tractive torque producing powertrain and as supplementary systems. Power electronics can be used to convert Direct Current (DC) into Alternating Current (AC) or be used to step to a different operating DC voltage. The onboard inverters can also operate as rectifiers and make use of an integrated motor controller is used to control EM. DC-DC boost converters are used as an option to help step voltage levels up or down as needed between the ESS and the EM to reduce ESS size. Other power converters can be integrated into the supplemental powertrain to ensure the proper operation of the vehicle. Such as a DC-DC buck converter or Auxiliary Power Module (APM), which is connected between the HV and Low Voltage (LV) batteries to run the accessory loads or an onboard charger to allow the battery to charge with the grid. These additional electronics add cost and complexity to the overall design of the vehicle.

2.1 Electric Motors

An electric machine is a general term used for machines that make use of electromagnetic forces, such as motors and generators. While EM's found in EV applications can act as both motors and generators, they are primarily used for torque production and are therefore often referred to as electric motors rather than machines. EM's can be used to help improve the overall efficiency of the powertrain in several different ways. Depending on the purpose and location of the motor in the powertrain, the nomenclature changes. The Figure 2.1 outlines the various motor positions in an electrified drivetrain.

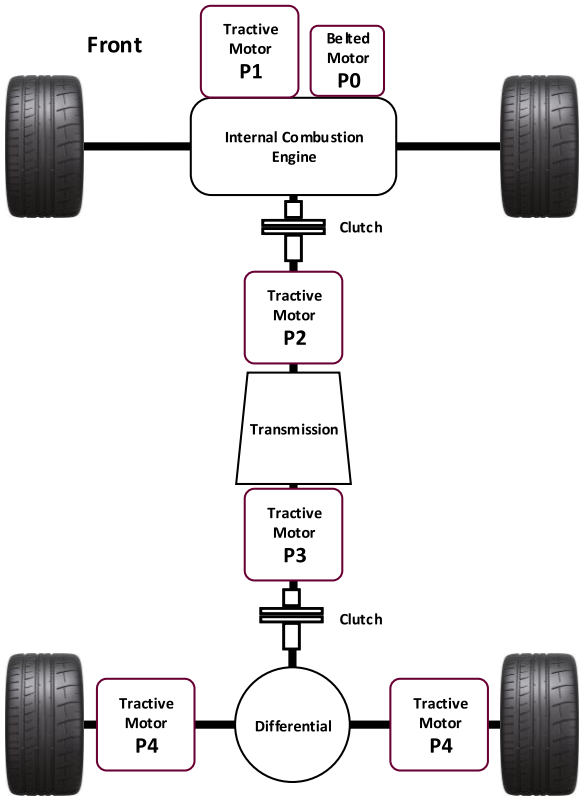

Figure 2.1: Motor Positioning Nomenclature

In mild hybrid systems, they are often used to help reducing engine idling during

frequent stopping; this is referred to as a start-stop system. This motor placement is sometimes referred to as a P0 placement motor, or a Belted Starter Generator (BSG). For tractive applications, most production powertrains make use of a three-phase AC EM. These motors usually have an operating voltage of 300V+ and can produce anywhere between 80kW and 120kW of power [4], therefore requiring a sizable onboard Energy Storage System (ESS). Depending on the placement of the tractive motor, it may be referred to as P1 through P4, respectively, as shown in the Figure 2.1 above. Various motor types are currently used in production vehicles such as, the induction motors used by Tesla or permanent magnet machines, which are in both the Nissan Leaf and Chevrolet Bolt.

2.2 DC/DC Converters

A DC/DC converter is a power converter that takes an input DC voltage and shifts it to another voltage level for output. In EV applications, they can be used to step voltage up or down, depending on the use case. When used to increase the input voltage, this is referred to as a boost converter and is often used to increase the output DC voltage of the vehicles ESS. These converters could allow a vehicle to have a 300V ESS but a 450V inverter to operate without increasing the size of the battery pack. These converters are often used on the output of the main DC bus of the ESS connecting to the traction inverter. This is a common design choice to help reduce the cost of the vehicle, or if the packaging is an issue.

When used to decrease the input voltage, this is called a buck converter, and are commonly used in electric vehicles as an APM in place of a conventional alternator [7]. By using a buck converter, the HV battery can be used to supply the 12V accessory

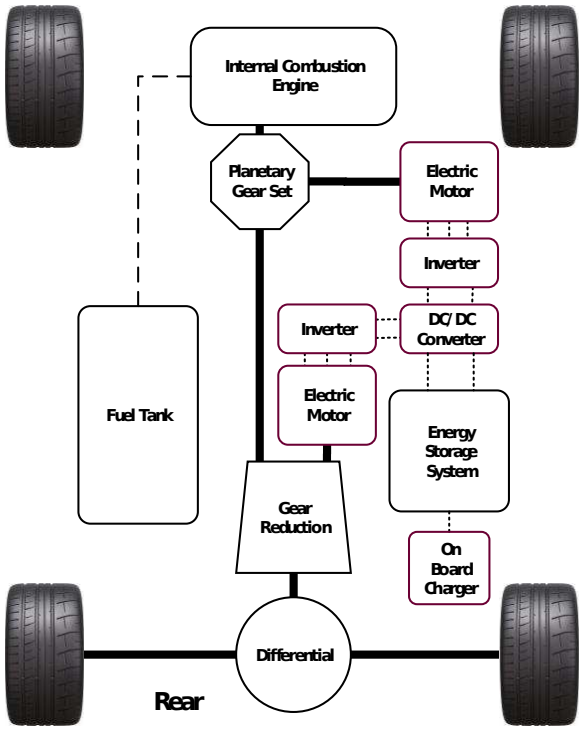

Figure 2.2: A Hybrid Vehicle Architecture with a DC/DC Converter

load bus of the vehicle.

2.3 Inverters

In most EV applications, DC electricity is fed to an onboard inverter from a DC/DC or directly from the ESS, where it is converted to AC electricity. This DC/AC power converter is referred to as an inverter and is combined and is then connected to a 3-phase AC motor. When the system is used in reverse, for regenerative braking, the converter acts as a rectifier turning AC voltage from the motor in DC voltage with is used to recharge the ESS. The inverter can change also control the speed at which the motor rotates by changing the frequency of the output current. It can also command torque from the motor by adjusting the amplitude of the signal of the output signal.

Packaging of these components has been made easier for automakers by combining power conversion and motor control into a single electric drive unit.

Inverters make use of semiconductor devices, such as Insulated Gate Bipolar Transistors (IGBT's), for the power conversion stage. These solid-state switches are controlled by small-signal circuits referred to as gate drivers. The gate driver design is of particular importance as it affects the efficiency of the IGBTs and diodes by controlling when they are in their active region. They are composed of smaller integrated circuits, such as optocouplers, to send isolated switching signals to the semiconductors. The conventional modulation techniques used by gate drivers are further discussed in Chapter Four.

2.3.1 The Voltage Source Inverter

Most electrified vehicles make use of a Voltage Source Inverter (VSI), shown in Figure 2.3, as they are relatively low cost with low switching losses and maintain their reliability [8]. Making use of IGBTs, the DC input of the inverter can be connected directly to the ESS or through a DC/DC boost converter to step up the DC voltage and supply the device with a constant DC voltage. In both setups, a sizeable DC-link capacitor can be used to smooth the current ripple and reduces the high-frequency harmonics caused by the IGBTs. This topology requires six independent switches, which are used to generate a three-phase sinusoidal AC output current to the EM. However, the VSI has the drawback of having a lower line-to-line AC output voltage than the DC input bus voltage. As a result, the torque-speed envelope of the EM is limited by the operating voltage of the ESS [8]. This would also cause the inverter and motor to have decreased efficiency at low speeds and light torque applications.

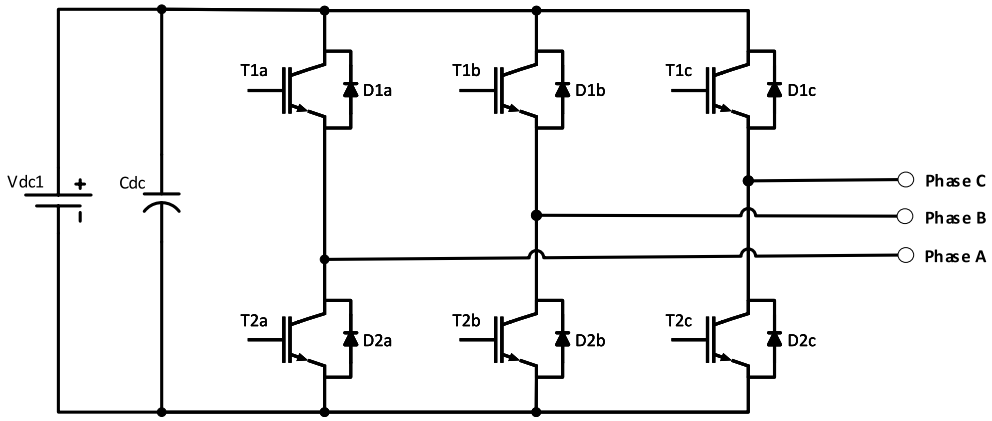

Figure 2.3: Voltage Source Inverter Topology

2.3.2 The Multi-Source Inverter

When a VSI is used to drive a three-phase traction motor, the switching losses are proportional to the DC bus voltage [9]. Therefore, the efficiency of a VSI can be increased if the DC input voltage can be variable. Multi-level inverters allow for different operating voltages on the DC input side, thus reducing the issues seen at high and low speeds with the conventional VSI. One such option is a Multi-Source Inverter (MSI), shown in Figure 2.4 below. An MSI is a multi-level inverter that aims to reduce the overall size of the ESS when used in automotive applications [9]. By implementing a buck-boost DC/DC converter in combination with the ESS to create three distinct operating voltages, V_{DC1}, V_{DC2}, and V_{DC1}-V_{DC2}. Unfortunately, the maximum achievable voltage of the system is limited to V_{DC1}, thus still requiring a large battery pack to achieve high voltages. Due to this restriction and the cost of the additional power electronics required it implement it, this inverter topology is not used in any commercially available vehicles at the moment.

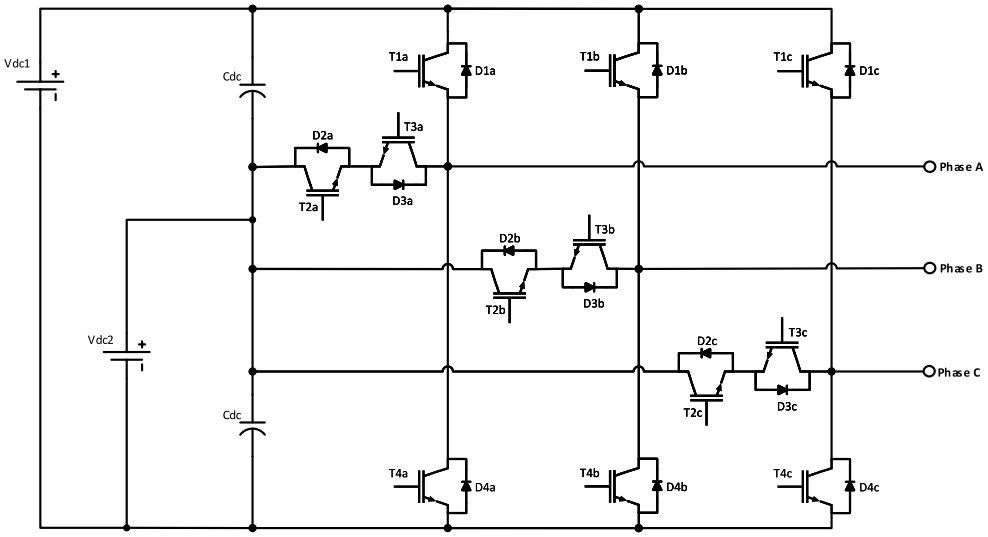

Figure 2.4: Multi Source Inverter Topology

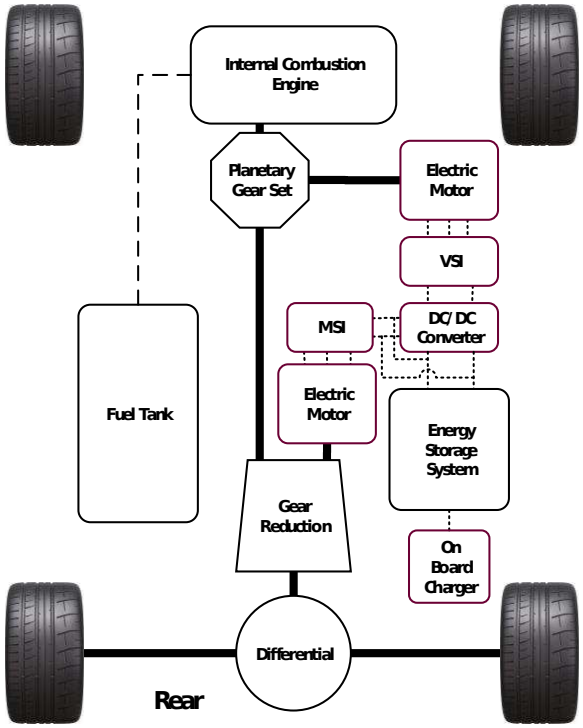

Figure 2.5: Multi-Source Inverter in a Hybrid Vehicle

2.4 Hybrid Vehicle Architectures

Vehicle electrification is a crucial step in helping reduce the world's CO_2 production, but the jump to complete vehicle electrification cannot happen overnight. Hybrid vehicles will play a critical step in moving away from fuel-burning internal combustion engines until the infrastructure for BEV vehicles is more widely implemented. HEVs make use of an internal combustion engine coupled with one or more electric motors to improve the vehicle's overall fuel consumption, efficiency. They can range in electrification from mild hybrids to PHEVs. HEV architectures can be categorized into three primary types; series, parallel, and power split configurations, based on the electrical and mechanical power flow between the propulsion components of the vehicle. Each of these respective architectures is outlined in further detail in the following sections.

2.4.1 Series Hybrid

In a series hybrid powertrain, the ICE mechanically decoupled from the wheels and provides no propulsion to the vehicle. The ICE instead acts as a generator producing mechanical energy to power the connected EM to charge the ESS. This means the speed of the ICE is independent of the vehicle speed allowing it to remain in its optimal operating range, making them ideal during stop-and-go traffic [7]. Therefore, the second EM is the only tractive component in the system, making it a mechanically simple drivetrain. However, since the ESS is being recharged through the ICE as well as regenerative braking, the efficiency of the system is limited by the efficiency of the ICE. A series hybrid configuration is shown in Figure 2.6 below—the BMW i3 an example of a production series-hybrid vehicle.

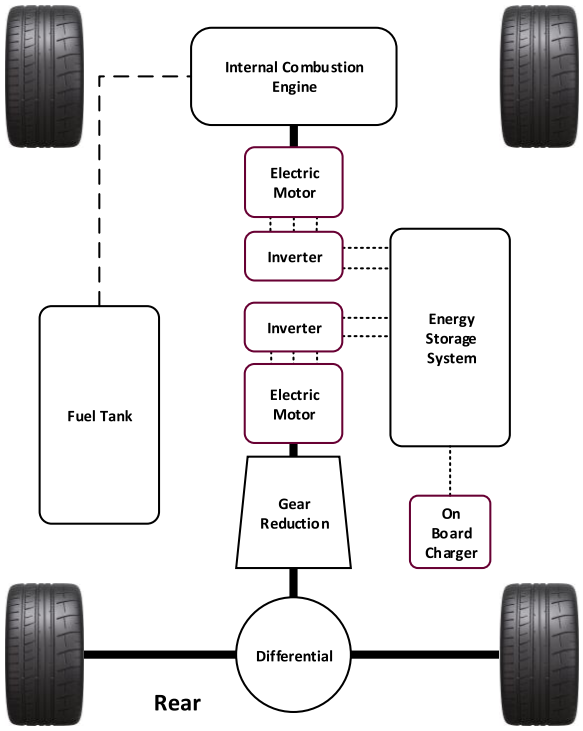

Figure 2.6: Example Series Hybrid Architecture

2.4.2 Parallel Hybrid

In a parallel powertrain configuration, the ICE is mechanically coupled to the wheels and provides a source of propulsion to the vehicle. As the chemical energy of the fuel is no longer being converted from mechanical energy into electrical potential energy at the ICE, this configuration is considered more efficient for highway driving than the series hybrid [7]. The EM helps to provide additional tractive power to the wheels and can be either directly connected to the engine or connected through a clutch to allow for electric-only drive modes. A parallel hybrid configuration is shown in Figure 2.7 below. This driveline is more complicated than the series configuration. However, it allows for multiple components to share the load at peak torque, thus allowing the ICE and the EM to be smaller than their series counterparts. Parallel systems tend

to have a smaller ESS and rely mostly on regenerative braking to keep the battery charged. These changes allow for a more power-dense driveline and a cost-effective option for manufacturers. Both the Honda Insight and the Civic hybrid are examples of production parallel hybrids.

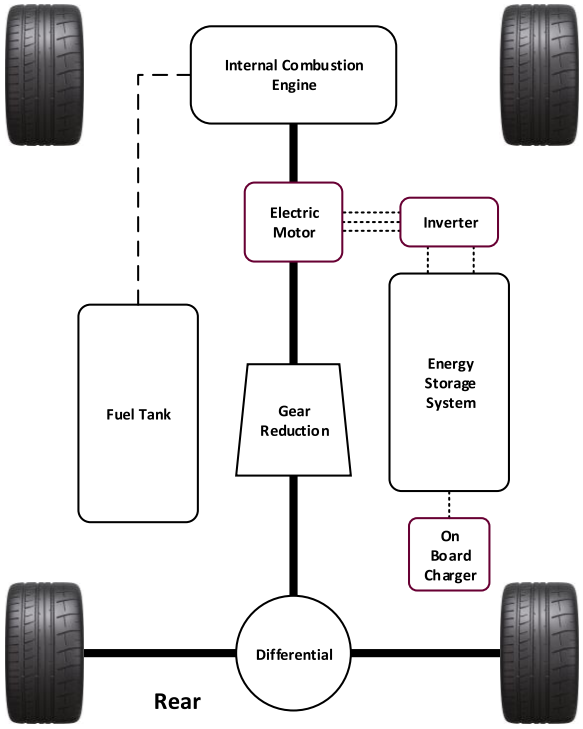

Figure 2.7: Example Parallel Hybrid Architecture

2.4.3 Power-Split Hybrid

A power-split hybrid, seen in Figure 2.8, makes use of the benefits of both a series and parallel powertrain configuration. This electrified drivetrain uses two propulsion components, a traction EM and an ICE, to power the wheels. The power from these two components is connected to a gearbox that can allow for multiple driving modes; ICE only, EV only, or any split of the two, which allows for more efficient driving [7].

Additionally, a second EM is connected to the ICE through a planetary gear set to be used as a generator to help recharge the ESS when needed. By adding additional components such as clutches or DC/DC converters expands the number of possible configurations dramatically. The increased number of components makes the control scheme more complex and increases manufacturing costs, and improved efficiency has made it the most popular choice among automakers. Both the Toyota Prius and the Chevrolet Volt make use of a power-split hybrid topology, making it the most popular commercially available architecture.

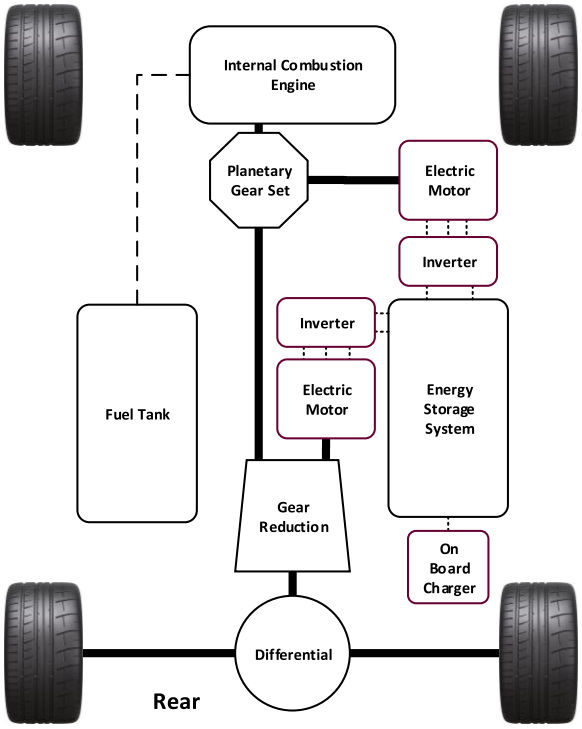

Figure 2.8: Example Power-Split Hybrid Architecture

Chapter 3

Energy Storage Systems

An Energy Storage System (ESS) is where potential energy is stored before it is turned into mechanical energy to spin the wheels of the vehicle. In a conventional vehicle, the fuel tank is considered the ESS is that it stores the chemical potential energy of the fuel before it is converted to rotational mechanical energy by the ICE. The ESS in EV applications is typically comprised of rechargeable style Lithium-Ion (Li-Ion) battery cells due to their high energy density to weight ratio [10].

Battery cells are measured using amp-hours (Ah) as a unit of electric charge. The rated output current is multiplied by time, equal to the charge transferred by a steady current of one ampere flowing for one hour. For a battery with a capacity of 10Ah, this is equivalent to a discharge current of 10A for 1 hour or 1A for 10 hours. When measuring multiple batteries connected together, the standard units include Kilowatts (kW) for power and Kilowatt-Hours (kWh) for energy. Battery cells can be connected in two ways; series, as seen in Figure 3.1a or parallel connections, as seen in Figure 3.1b to create a battery pack. Battery packs are designed to meet specific operating characteristics, such as voltage, energy, or power requirements.

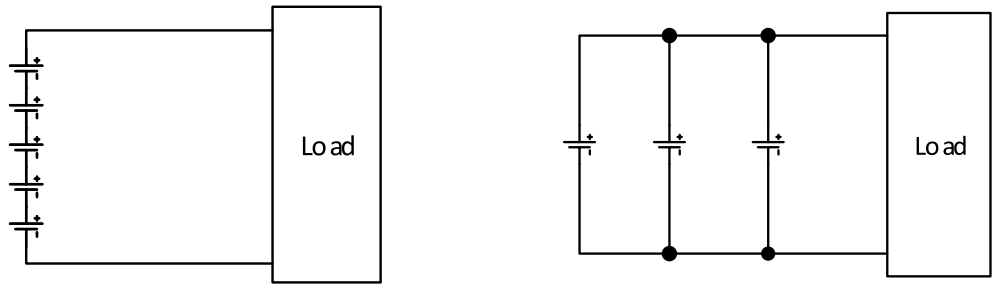

(a) Series Battery Cells (b) Parallel Battery Cells

Figure 3.1: Battery Cell Configurations

When cells are combined in series, the total voltage of the pack is the sum of all of the consecutive cell voltages, but the current remains the same as a single cell. When combined in parallel, the total current of the pack is the sum of all of the connected cell currents, but the voltage remains the same as a single cell. Therefore, battery packs need to combined cells in both series and parallel to meet their required operating characteristics. The notation used to describe the configuration of cells is S for series and P for parallel. For example, a pack consisting of 15 cells in which two strings of five are connected series and then the three strings of five are each connected in parallel would be a 5S3P configuration, shown in Figure 3.2 below.

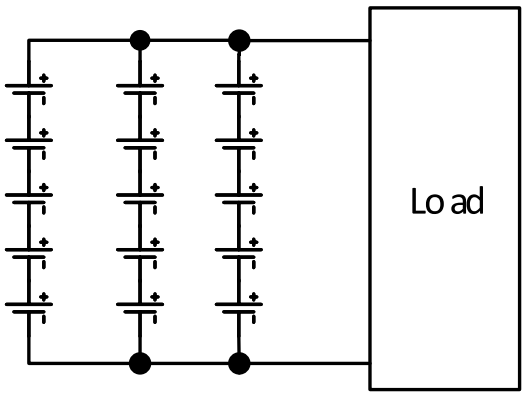

Figure 3.2: 5S3P Battery Pack

The EM's used in vehicle applications typically operate at higher voltages, thus requiring either a high voltage battery pack or costly power electronics to step the voltage of the pack up to a suitable operating level. While the cost of batteries has drastically decreased in recent years, falling 87% per kilowatt-hour since 2010, they remain the costliest component in an electrified powertrain [4].

3.1 Exotic Energy Storage Systems

3.1.1 Fuel Cell

Fuel cells generate their electrical potential energy an electrochemical reaction between hydrogen gas and oxygen, with the energy then being supplied to an onboard EM or power electronics. Therefore, instead of requiring a gas tank like ICE vehicles, a fuel cell vehicle has an onboard hydrogen tank and exhaust water since no combustion is involved. There are a few vehicle models are available in the Canadian market today which make use of a hydrogen fuel cell, namely the Hyundai NEXO, and Toyota Mirai [11]. In theory, the fuel cell technology is an excellent alternative to a battery pack as it boasts a much faster charging time, as well as a higher energy density, therefore leading to an increased range. While these vehicles have similar performance to gasoline or diesel cars, the infrastructure in Canada is not in place to make these a practical option.

3.1.2 Ultracapacitors

An ultracapacitor (UC), is a high-capacity capacitor with a capacitance value much higher than other conventional capacitors, but with lower voltage limits. Unlike other

capacitors, UCs do not use a conventional dielectric layer, but instead, make use of an electrostatic double-layer capacitance and electrochemical pseudocapacitance. The electrolyte forms an ionic conductive connection between the two electrodes, which distinguishes them from conventional electrolytic capacitors where a dielectric layer always exists. Supercapacitors are polarized by design with asymmetric electrodes, giving them an electrochemical anode (negative terminal) that is pre-doped with lithium-ions to lower the anode potential and a cathode (positive terminal) achieve a UC with a battery like characteristics [12]. UC's have help bridge the gap between electrolytic capacitors and rechargeable Li-Ion batteries while offering a higher power density, albeit at a reduced energy density.

3.2 Hybrid Energy Storage Sytems

A HESS is a combination of two or more energy storage systems working together to provide tractive energy to the wheels. In an EV to achieve higher performance, the onboard ESS needs to increase its output current, which results in a higher C-rate. A C-rate is a measure of the rate at which a battery is discharged relative to its maximum capacity. A 1C rate means that the discharge current will discharge the entire battery in 1 hour, by increasing a batteries C-rate the cell experiences plating of the solid-electrolyte interface and lowers the overall lifetime of the cell. Due to the increased power density, UCs are capable of storing and discharging current very quickly and effectively without damaging the cell, which makes them ideal for handling the peak load demands such as acceleration or braking. These events would require a primary energy source (fuel cell or battery) to be over-sized accordingly to minimize the internal resistance increase. Additionally, when connected in parallel

with each other, the UC can act as a low pass filter to the battery, thus further still increasing the battery's longevity. This thesis will focus on a UC and Li-Ion battery HESS architecture.

HESS topologies can be passively controlled systems or use an active control scheme where power converters are used to control the direction and flow of power throughout the system [13]. A passive system, shown in Figure 3.3, requires no additional power electronics to control the flow of energy, thus making it a cheaper option.

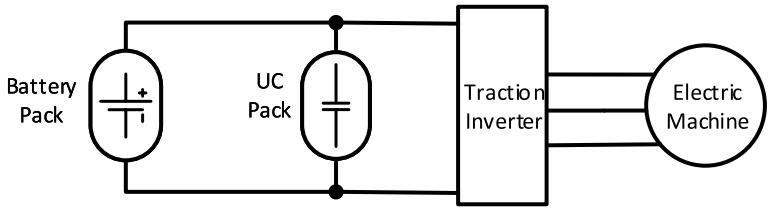

Figure 3.3: Parallel Passive HESS

As the system charges and discharges, the voltage levels of the two sources are equal due to the parallel connection, thus making accurate, effective control strategies difficult due to the variations in the internal resistance and transient response between the sources. The HESS is then directly connected to the traction inverter, and the DC output current load is the sum of the battery and the UC currents combined, making it a power-dense option. While this is advantageous for peak performance, it is not ideal for regular driving as the UC tends to discharge faster than the battery due to its lower internal resistance. In order to prevent the UC voltage from dropping below the battery voltage, the battery needs to charge the UC to keep both voltages

equal continually. As a result, more energy is required from the battery, shortening its lifetime as well as negatively affecting the overall performance of the system [14].

Active architectures allow for more control of the system but at the burden of increased electrical complexity and cost. The most straightforward active HESS topology makes use of a DC/DC converter between the battery pack and the UC [13], shown in Figure 3.4. This allows the battery to be used for the constant power applications, such as highway driving. At the same time, the UC provides additional power to supplement peak power demands when accelerating or regenerative braking. The addition of the DC/DC enables the control of the charge and discharge rates of the two sources resulting in extended battery life and improving the overall efficiency of the system.

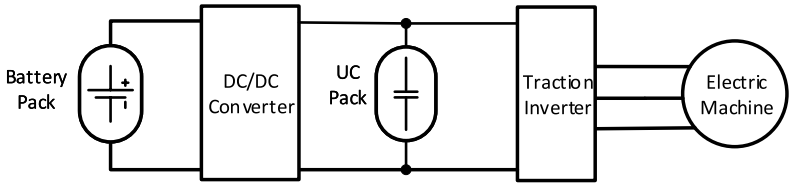

Figure 3.4: Parallel Active HESS

3.3 Battery Modelling

There are many methods for modelling batteries, but researchers generally use models that can be classified into three main groups: empirical models, electrochemical models, and equivalent circuit models [10]. Empirical models are often considered black-boxes and simulate the battery cells. These models consist of a series of math

functions with unknown parameters, and the model calculates these unknown parameters by trying to minimize the output error. Electrochemical modelling aims to show the base chemical reactions happening inside the battery cells. They simulate the internal electrochemical dynamics of the cell using a set of partial differential equations. Equivalent circuit models make use of basic circuit elements such as resistors and capacitors to simulate the dynamics of the cells. When parameterizing these models, the type and quality of data are essential. The values of these parameters can be calculated using input-output data combined with numerical optimization. The lack of sufficient high-quality data will cause inaccuracies in certain aspects of the battery's behaviour. Based on the required level of modelling complexity, the model may be comprised of first-order, second-order, or more resistor-capacitor branches.

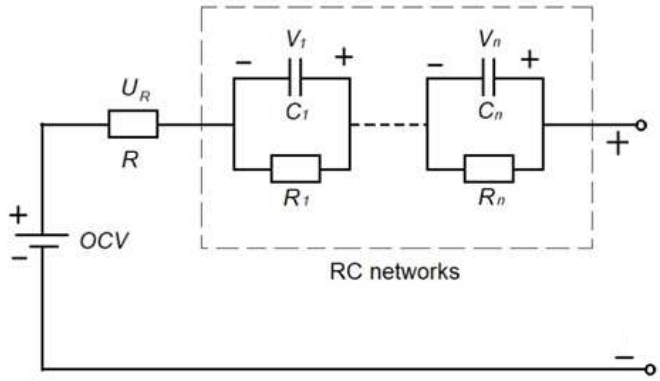

Figure 3.5: n-order R-RC-RC Equivalent Circuit Model

An equivalent circuit model simulates the battery dynamics resistors and capacitors to make RC branches, as seen below. The branches are comprised of three primary parameters, the modelling resistance $R_{\#}$, the modelling capacitance $C_{\#}$, and the internal resistance or Ohmic resistance of a battery cell R. The Ohmic resistance

is made up of R_{0+} for charging, and R_{0-} for a discharging. Figure 3.5 shows a circuit diagram for an n-order R-RC-RC model. Higher-order equivalent circuit models produce more accurate results but have the tradeoff of increased computational complexity. The following sets of equations give the state-space representation of the second-order R-RC-RC model.

$$\begin{bmatrix} V_{1,k+1} \\ V_{2,k+1} \\ z_{k+1} \end{bmatrix} = \begin{bmatrix} 1 - \frac{\Delta t}{R_1 C_1} & 0 & 0 \\ 0 & 1 - \frac{\Delta t}{R_2 C_2} & 0 \\ 0 & 0 & 1 \end{bmatrix} \begin{bmatrix} V_{1,k} \\ V_{2,k} \\ z_k \end{bmatrix} + \begin{bmatrix} \frac{\Delta t}{C_1} \\ \frac{\Delta t}{C_2} \\ \frac{-\eta \Delta t}{C} \end{bmatrix} i_k \tag{3.3.1}$$

$$V_{t,k} = OCV(z_k) - V_{1,k} - V_{2,k} - R_0 i_k \tag{3.3.2}$$

Chapter 4

Reconfigurable Multi-Source Inverter

A Reconfigurable Multi-Source Inverter (ReMSI) is a novel MSI topology that was first introduced in the paper "On the Concept of a Novel Reconfigurable Multi-Source Inverter" by Ephrem Chemali and Ali Emadi [15]. The paper introduces the concept and potential applications for a ReMSI, including using it in combination with a HESS. A ReMSI is similar in topology to that of an MSI but contains two additional switches, S_1 and S_2, which allow for an additional operating mode over the MSI. Its primary purpose is to connect two separate DC sources to a single AC output, because of the use of two DC sources, this power converter is best implemented in power-split architectures, such as the one shown below in Figure 4.2 below.

The simulations performed for [15] were done in Simulink and makes use of ideal switching, as [15] is proof of concepts for the new topology ideal switching is enough. The Figure 4.2 below shows the ReMSI circuit connections using these ideal switches. This thesis will expand upon their work, replacing the ideal switches with IGBTs in

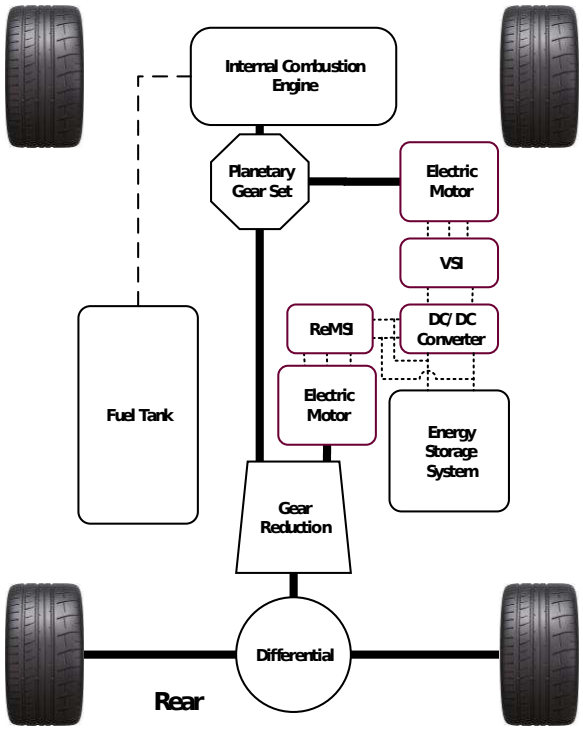

Figure 4.1: Reconfigurable Multi-Source Inverter in a Power-Split Hybrid Vehicle

a T-Type Neutral Point Clamped (TNPC) configuration, which will be discussed in more detail in Chapter 6.

Additionally, the S_1 and S_2 switches must be rated to withstand the full load requirements of DC input and should ideally be solid-state to avoid the switches welding under load. This thesis will also make use of the same Space Vector Pulse Width Modulation (SVPWM) control scheme used in [15]. These simulations will be used towards creating a prototype benchtop version of the ReMSI topology, which is discussed in Chapter 6.

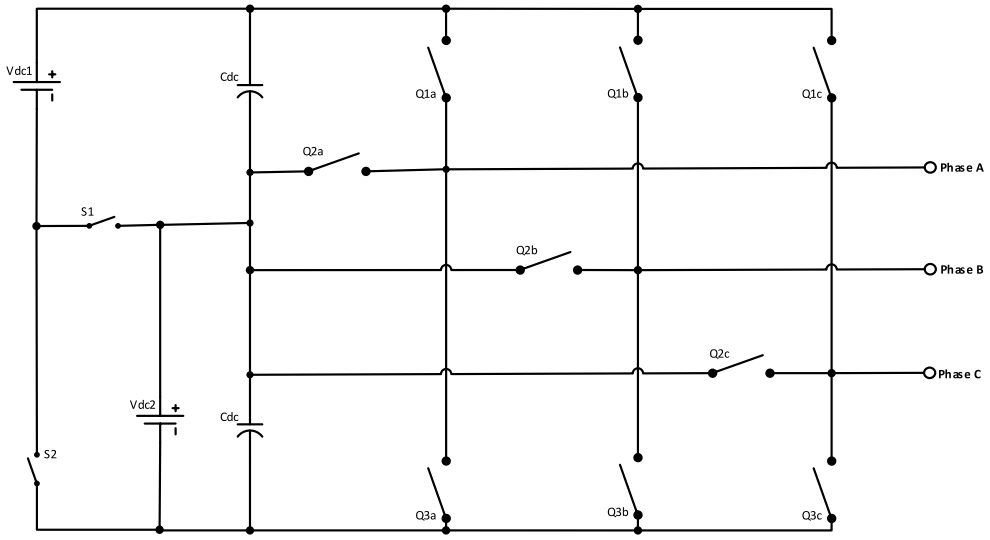

Figure 4.2: Ideal Switch Topology for an ReMSI

4.1 Operating Voltages

The ReMSI has four distinct operating modes, taking full advantage of both sources connected to the input of the inverter.

- Mode 1: This mode would be used for low-speed applications as the battery pack V_{DC2} is only supplying the inverter.
- Mode 2: In this mode, the first source V_{DC1} is being used to charge V_{DC2}, since the sources are connected in series in this situation and V_{DC2} smaller than V_{DC1} the remaining current is used to power the traction inverter.
- Mode 3: The traction inverter is only supplied from V_{DC1}; depending on the size V_{DC1}, this mode would be used for steady-state highway driving.
- Mode 4: This mode could be classified as a charge depleting drive mode, in which the traction motor is being supplied by both sources in series to produce

peak power for the tractive motor. This configuration is achieved when S_2 is open, and S_1 is closed.

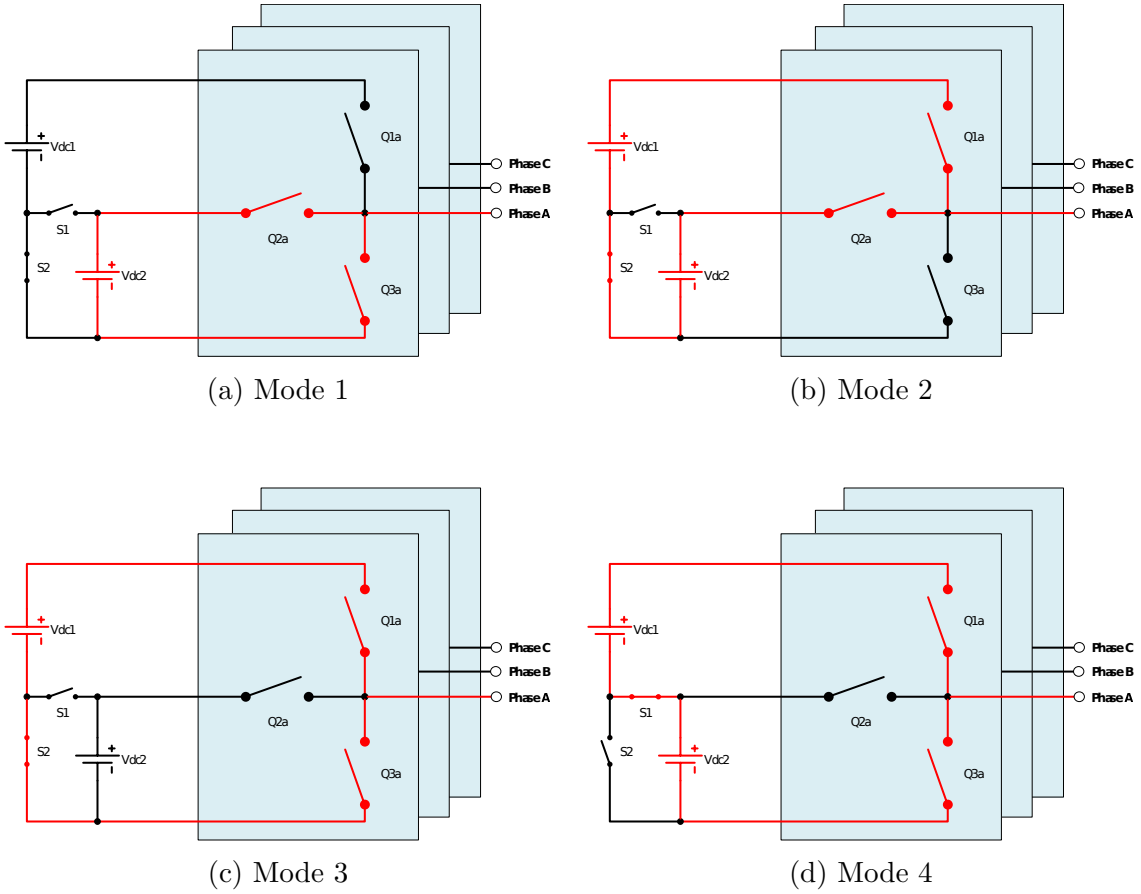

(a) Mode 1 (b) Mode 2

(c) Mode 3 (d) Mode 4

Figure 4.3: ReMSI Operating Modes Switching Paths

The operating phase voltages, V_{AN}, V_{BN}, V_{AN}, and the line-to-line voltages, V_{AB}, V_{BC}, and V_{AC} are calculated below.

$$\begin{bmatrix} V_{AN} \\ V_{BN} \\ V_{CN} \end{bmatrix} = \frac{1}{3} \begin{bmatrix} 2 & -1 & -1 \\ -1 & 2 & -1 \\ -1 & -1 & 2 \end{bmatrix} \times \begin{bmatrix} V_{AO} \\ V_{BO} \\ V_{CO} \end{bmatrix} \tag{4.1.1}$$

$$V_{AB} = V_{AN} - V_{BN} \tag{4.1.2}$$

$$V_{BC} = V_{BN} - V_{CN} \tag{4.1.3}$$

$$V_{CA} = V_{CN} - V_{AN} \tag{4.1.4}$$

4.2 Inverter Control

To understand how to control the inverter, one must first understand how the switches operate in order to achieve their desired output. A component is considered to be off, if it is in a zero state, and denoted a 0. If the switch is turned on, it shall be denoted as a 1. Great care should be taken to avoid any short circuits which could quickly become dangerous when operating the device at high voltages. Kirchhoff's Voltage Law (KVL) proves that two unequal voltage sources should never be connected in series to any element in between which can account for the difference in the two voltages [16]. By knowing the status of the upper switches, the user can also know the position of the lower switches as they are always opposite their upper counterpart; this is called complementary switching. When designing a control scheme with Pulse Width Modulation (PWM), there are two major design requirements. First, the user must minimize the number of switching per sampling period to avoid any unnecessary losses. Second, when transitioning from one switching state to the next, only two switches from the same inverter leg should be used [17].

In the ReMSI, the switches Q2 and Q3 are complementary in Mode 1; Q1 and Q2 are complementary in Mode 2; Q1and Q3 are complementary in Mode 3 and Mode 4; for each of their respective phase legs. Additionally, S_1 and S_2 are also complimentary in all operating modes. The inverter can shift through its' four operating modes to

allow for more efficient energy consumption in an automotive application. Depending on the driving conditions, whether using an ICE, EM's, or a blended combination of both, the ReMSI control scheme can select the most suitable option for the given scenario. With this topology, nine different line-to-line voltage outputs can be achieved and are outlined in the Table 4.1.

Table 4.1: Switching States of the ReMSI with Ideal Switches

Mode	**Switching States**											**Line-to-Line Voltages**		
	$\mathbf{S}_1$	$\mathbf{S}_2$	$\mathbf{Q}_{1a}$	$\mathbf{Q}_{1b}$	$\mathbf{Q}_{1c}$	$\mathbf{Q}_{2a}$	$\mathbf{Q}_{2b}$	$\mathbf{Q}_{2c}$	$\mathbf{Q}_{3a}$	$\mathbf{Q}_{3b}$	$\mathbf{Q}_{3c}$	$\mathbf{V}_{AB}$	$\mathbf{V}_{BC}$	$\mathbf{V}_{AC}$
1	0	1				0	1	1	1	0	0	V_{DC2}	0	-V_{DC2}
	0	1				0	0	1	1	1	0	0	V_{DC2}	-V_{DC2}
	0	1				1	0	1	0	1	0	-V_{DC2}	V_{DC2}	0
	0	1		0		1	0	0	0	1	1	-V_{DC2}	0	V_{DC2}
	0	1				1	1	0	0	0	1	0	-V_{DC2}	V_{DC2}
	0	1				0	1	0	1	0	1	V_{DC2}	-V_{DC2}	0
2	0	1	1	0	0	0	1	1				V_{DC1}-V_{DC2}	0	-(V_{DC1}-V_{DC2})
	0	1	1	1	0	0	0	1				0	V_{DC1}-V_{DC2}	-(V_{DC1}-V_{DC2})
	0	1	0	1	0	1	0	1				-(V_{DC1}-V_{DC2})	V_{DC1}-V_{DC2}	0
	0	1	0	1	1	1	0	0		0		-(V_{DC1}-V_{DC2})	0	V_{DC1}-V_{DC2}
	0	1	0	0	1	1	1	0				0	-(V_{DC1}-V_{DC2})	V_{DC1}-V_{DC2}
	0	1	1	0	1	0	1	0				V_{DC1}-V_{DC2}	-(V_{DC1}-V_{DC2})	0
3	0	1	1	0	0				0	1	1	V_{DC1}	0	-V_{DC1}
	0	1	1	1	0				0	0	1	0	V_{DC1}	-V_{DC1}
	0	1	0	1	0				1	0	1	-V_{DC1}	V_{DC1}	0
	0	1	0	1	1		0		1	0	0	-V_{DC1}	0	V_{DC1}
	0	1	0	0	1				1	1	0	0	-V_{DC1}	V_{DC1}
	0	1	1	0	1				0	1	0	V_{DC1}	-V_{DC1}	0
4	0	1	1	0	0				0	1	1	V_{DC1}+V_{DC2}	0	-(V_{DC1}+V_{DC2})
	1	0	1	1	0				0	0	1	0	V_{DC1}+V_{DC2}	-(V_{DC1}+V_{DC2})
	1	0	0	1	0				1	0	1	-(V_{DC1}+V_{DC2})	V_{DC1}+V_{DC2}	0
	1	0	0	1	1		0		1	0	0	-(V_{DC1}+V_{DC2})	0	V_{DC1}+V_{DC2}
	1	0	0	0	1				1	1	0	0	-(V_{DC1}+V_{DC2})	V_{DC1}+V_{DC2}
	1	0	1	0	1				0	1	0	V_{DC1}+V_{DC2}	-(V_{DC1}+V_{DC2})	0

The remaining states, not shown below, produce zero output line-to-line voltages and would be considered a fault state if all switches are on, [111], or a zero state where all switches are off [000].

4.2.1 Sinusoidal Pulse Width Modulation Scheme

Various modulation techniques can be used to control the gating signals for switching the power semiconductors in the desired pattern to achieve the DC to AC power

conversion. Sinusoidal Pulse Width Modulation (SPWM) technology is one of the most used modulation methods used by the industry for inverter control [18]. This technique allows the designer to control the output fundamental frequency and fundamental voltage. The gating signal is achieved by imposing a higher frequency triangular carrier wave, V_{cr} onto the sinusoidal waveform called the modulating wave V_m. In a three-phase inverter, there are three modulating waves, one per phase, V_{mA}, V_{mB}, and V_{mC} with each wave being out of phase by 120°.

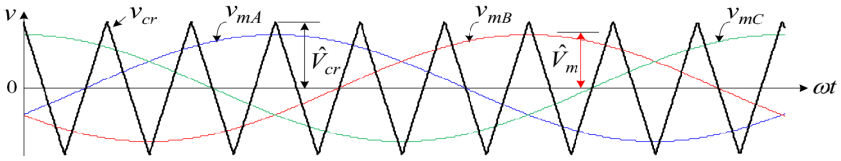

Figure 4.4: Sinusoidal Pulse Width Modulation Scheme

The output line-to-line voltages' magnitude and frequency can be independently controlled by the amplitude modulation index, m_a, and frequency of the modulation sine wave, f_m, respectively. These fundamental-frequency components of the inverter output voltage are calculated in the below equations. The frequency modulation index, m_f, is comprised of the carrier frequency and the modulation sine wave frequency.

$$m_a = \frac{\hat{V}_m}{\hat{V}_{cr}} \tag{4.2.1}$$

$$m_f = \frac{f_{cr}}{f_m} \tag{4.2.2}$$

After comparing the V_{cr} and the V_m the switching states for phase leg of the inverter can be determined based on the following rules:

- $V_m > V_{cr}$: The upper switch is turned on and the lower switch is turned off
- $V_m < V_{cr}$: The lower switch is turned on and the upper switch is turned off

Therefore, the peak-to-peak voltage of V_{cr} is restricted to the DC-link voltage V_{DC} forcing the maximum amplitude of the fundamental output phase voltage to be $\frac{V_{DC}}{2}$ and $0.612V_{DC}$ line-to-line voltage [19]. Additionally, the SPWM scheme causes higher harmonic losses than other modulation schemes, making it less ideal for the ReMSI.

4.2.2 Space Vector Pulse Width Modulation Scheme

SSVPWM (SPWM) is another modulation scheme used by vehicle manufacturers for inverter gating control. SVPWM has become increasingly popular due to more straightforward digital implementation with the advancement of digital signal processors. Additionally, SVPWM compares only one modulating wave with a carrier, even when used in three-phase applications. There is also the added benefit of allowing for a higher DC bus utilization than the SPWM method, with a maximum phase output of $\frac{V_{DC}}{\sqrt{3}}$ and a line-to-line voltage of 0.707 V_{DC}, which is a 15.47% improvement over the SPWM method. Additional bus utilization can be achieved by injecting third order harmonics, but this method is not explored within this research.

SVPWM switching states use the polar representation of the possible switch states within the inverter and are referred to as space vectors. To implement space vector modulation, a reference signal V_{ref} rotates about the $\alpha\beta$ reference plane, also known as the state space, where v_α and v_β are the vector components of vector reference

signal V_{ref} [20].

$$\vec{V}(t) = v_\alpha(t) + jv_\beta(t) \tag{4.2.3}$$

$$\begin{bmatrix} v_\alpha(t) \\ v_\beta(t) \end{bmatrix} = \frac{2}{3} \begin{bmatrix} \cos 0 & \cos \frac{2\pi}{3} & \cos \frac{4\pi}{3} \\ \sin 0 & \sin \frac{2\pi}{3} & \sin \frac{4\pi}{3} \end{bmatrix} \begin{bmatrix} v_{AO}(t) \\ v_{BO}(t) \\ v_{CO}(t) \end{bmatrix} \tag{4.2.4}$$

The state space is broken into sectors, which each represent the different sets of switches that are turned on or off for the given time period. For a given length and position in the state space, V_{ref} can be approximated by three nearby stationary vectors and based on the chosen stationery vectors, switching states are selected, and the gating signals are generated [21]. V_{ref} passes through sectors one by one, and when V_{ref} rotates one complete revolution in space, the inverter output voltage varies one cycle over time. V_{ref} is sampled with a frequency f_s, $T_s = \frac{1}{f_s}$ and the inverter output frequency corresponds to the rotating speed of V_{ref}. The inverter output voltage can be controlled by adjusting the magnitude of V_{ref}. In the conventional VSI, there are eight possible combinations with six active vectors and two zero space vectors. Due to the nature of complementary switching, SVPWM active only refers to the state of the upper switches. These eight switch states are calculated below.

$$\vec{V}(t) = \frac{2}{3}[v_{AO}(t)e^{j0} + v_{BO}(t)e^{j\frac{2\pi}{3}} + v_{CO}(t)e^{j\frac{4\pi}{3}}] \tag{4.2.5}$$

$$e^{jx} = \cos x + j \sin x \tag{4.2.6}$$

$$\begin{aligned}
V_S(000) &= V_0 = 0 \\
V_S(100) &= V_1 = V_{DC} e^{j0} \\
V_S(110) &= V_2 = V_{DC} e^{j\frac{\pi}{3}} \\
V_S(010) &= V_3 = V_{DC} e^{j\frac{2\pi}{3}} \\
V_S(011) &= V_4 = V_{DC} e^{j\pi} \\
V_S(001) &= V_5 = V_{DC} e^{j\frac{4\pi}{3}} \\
V_S(101) &= V_6 = V_{DC} e^{j\frac{5\pi}{3}} \\
V_S(111) &= V_7 = 0
\end{aligned} \tag{4.2.7}$$

In the ReMSI, there are 24 active vectors to allow for its four distinct operating modes. There are three possible voltage states -1, 0, and 1, which represent the potential phase voltage levels of each phase leg output. The spatial vector representation of the alpha-beta diagram is shown in Figure 4.5 and is composed of four concentric hexagons separated into six sectors each. The size of the hexagon varies with applied voltage, while the inner coloured circle of each hexagon represents the maximum line-to-line voltage. After the mode and sector identification stage, the switching duration of each vector is calculated; this is referred to as a dwell time calculation and is explained further in Chapter 5. Finally, a symmetric switching sequence is used to reduce the harmonic distortion and the number of switching periods, allowing for reduced power losses.

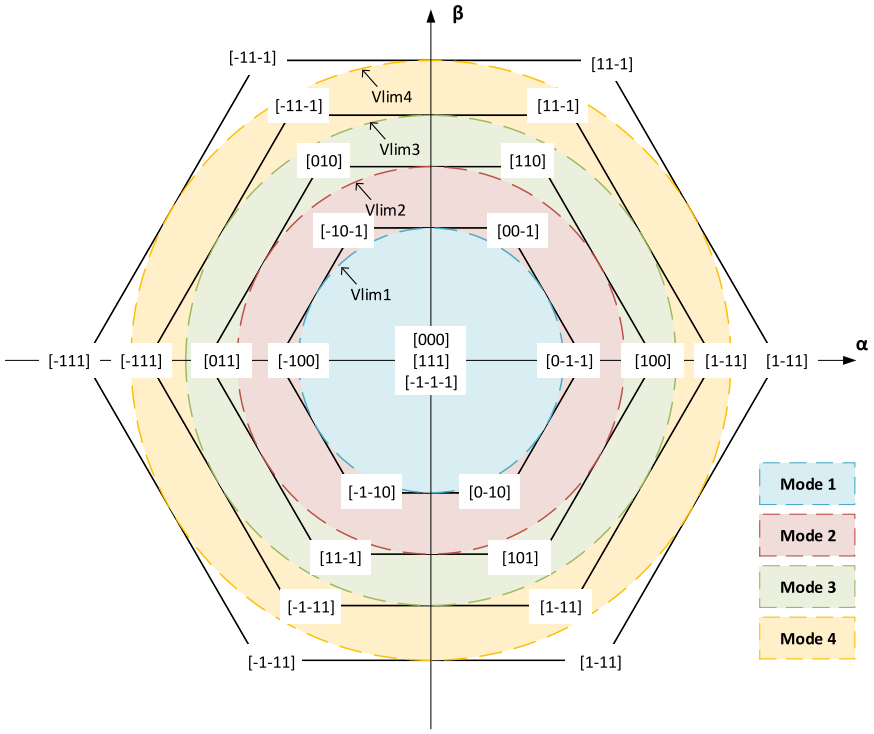

Figure 4.5: Alpha-Beta Reference Plane

Chapter 5

Modelling & Simulation of an ReMSI in an Electrified Vehicle

Modelling and simulation is a necessary tool to help understand a system and its' behaviour without having to build a real-world prototype. Mathworks MATLAB and Simulink is an industry-grade modelling and simulation tool, commonly used throughout the automotive industry. It is within the Simulink environment that the modelling and simulation work of this thesis is done. When an inverter is modelled as an independent system, a switching model is used. This type of modelling allows the internals for the inverter to be simulated and the switching frequency can be controlled and adjusted as needed. Although switching models are not useful as part of a larger vehicle model, the sampling time for the two systems would be independent of each other, thus requiring a large amount of computational power. In this thesis, the ReMSI is first discussed as a switching model and then is mapped into an efficiency look-up table to be used in a larger vehicle level model.

5.1 Inverter Modelling and Control

In the paper [15], ideal switches were used for the simulations; while this is enough to show a proof of concept, it is not accurate for real-world modelling. In order to achieve a more accurate simulation, the ideal switches were replaced with IGBT's. For this simulation, the Simulink SimPowerSystem toolbox was used to model the required IGBTs and diodes. Figure 5.1 shows a block diagram of the closed-loop control strategy used in this simulation to generate the SVPWM gating signals.

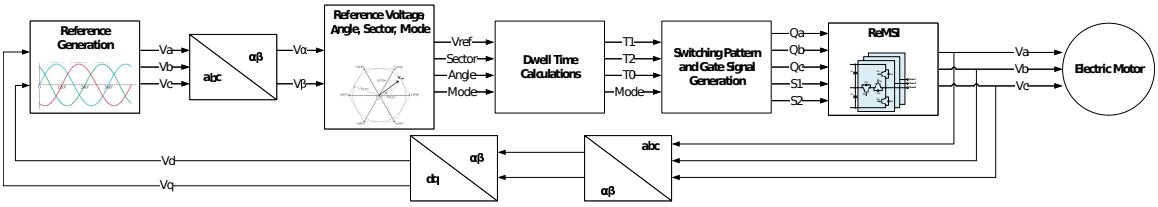

Figure 5.1: Block Diagram of SVPWM Control Strategy for the ReMSI

The voltage for $V_{DC1} = 450V$, and $V_{DC2} = 150V$, and the switching frequency is 10 kHz. When the magnitude and rotational angle of V_{ref} is sampled, the sector of the $\alpha\beta$ reference plane is determined as well as the operating mode of the inverter. The controller selects the two vectors which encompass the sector, to synthesize the AC waveforms. The dwell time is then given by T_1, T_2, and T_0, to minimize the number of switchings per sampling period T_S.

$$T_1 = \frac{\sqrt{3}T_s V_{ref}}{V_{DC}} \sin(\frac{\pi}{3} - \theta) \tag{5.1.1}$$

$$T_2 = \frac{\sqrt{3}T_s V_{ref}}{V_{DC}} \sin\theta \tag{5.1.2}$$

$$T_0 = T_s - T_1 - T_2 \tag{5.1.3}$$

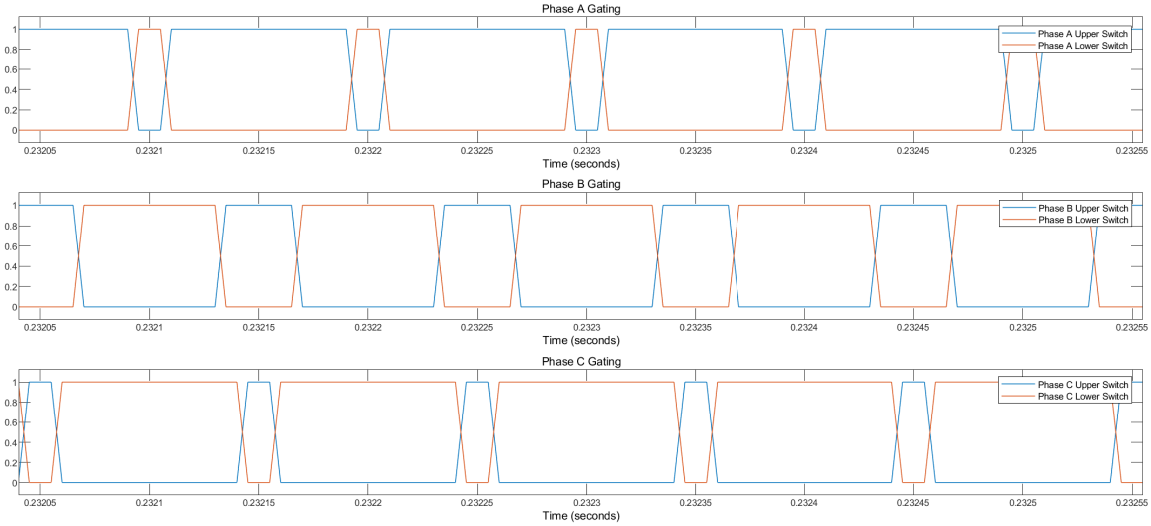

Figure 5.2: Gating Signals for each Phase Output

Gate driver signals are then sent to switch on/off the required IGBTs, shown in Figure 5.2, and the desired output voltage and current are achieved. The line-to-line voltage is shown with the output phase current in Figure 5.3, and the 3phase currents are highlighted in Figure 5.4.

The magnitude of the reference voltage vector was increased by a constant step second to highlight the complete operating range of the ReMSI. The magnitude of the V_{ref} is increased from 0 V, and the control algorithm determines that the operation of the ReMS should be limited to Mode 1 with a bus voltage of V_{DC2}. Switch S_2 is turned on, and switching banks Q_2 and Q_3 are activated as the reference voltage vector exceeds $\frac{V_{DC2}}{\sqrt{3}}$ the controller switches into Mode 2 where a bus voltage of $V_{DC1} - V_{DC2}$ is applied across the DC bus. This mode is activated by using switching banks Q_1 and Q_2, while Q_3 is turned off. When V_{ref} reaches $\frac{V_{DC1}-V_{DC2}}{\sqrt{3}}$ it switches into operational

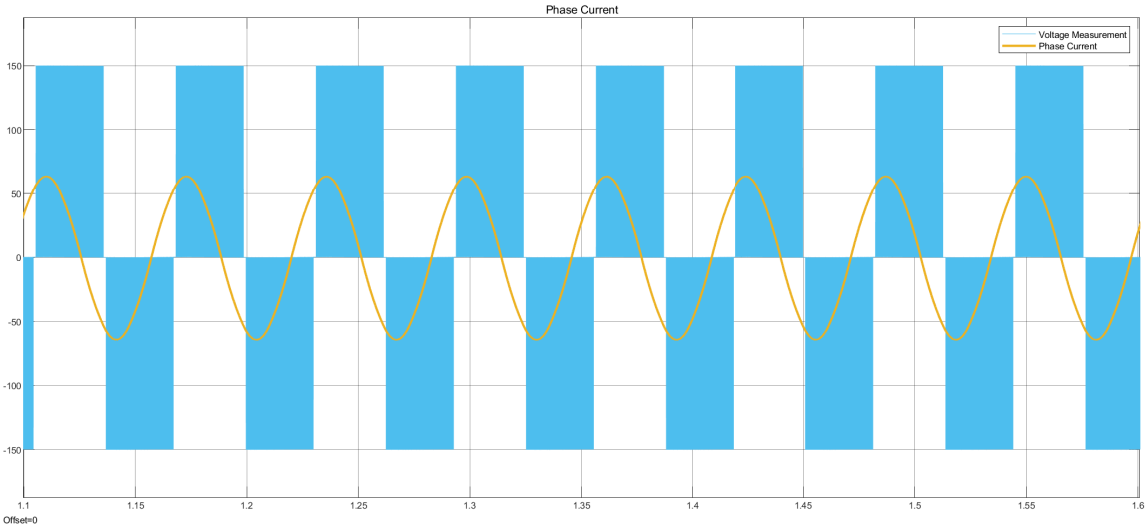

Figure 5.3: Line-to-Line Voltage and Output Phase Current

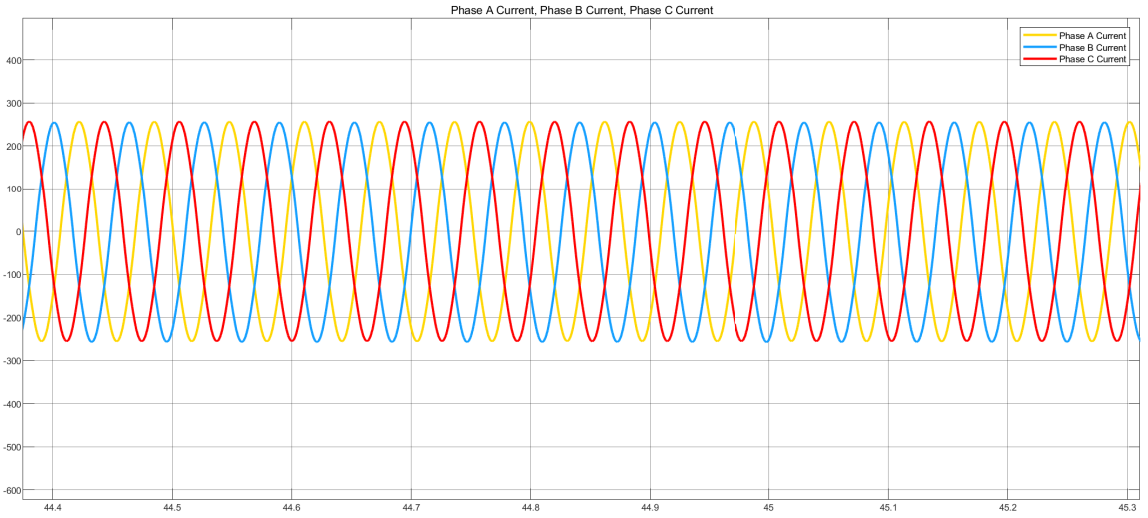

Figure 5.4: Output Phase Current

Mode 3, and switching bank Q_2 is shut off and banks Q_1 and Q_3 are switched. The load voltage across the input terminals is now V_{DC1}. The final operational mode, Mode 4, is achieved as the reference vector achieves a voltage of $\frac{V_{DC1}}{\sqrt{3}}$ and S_2 is turned off and S_1 is now closed, and the source voltage is now $V_{DC1} + V_{DC2}$. These

changes in voltage can be seen in Figure 5.5. Additionally, the commutation paths of the operating areas during sector one are detailed in the Appendix.

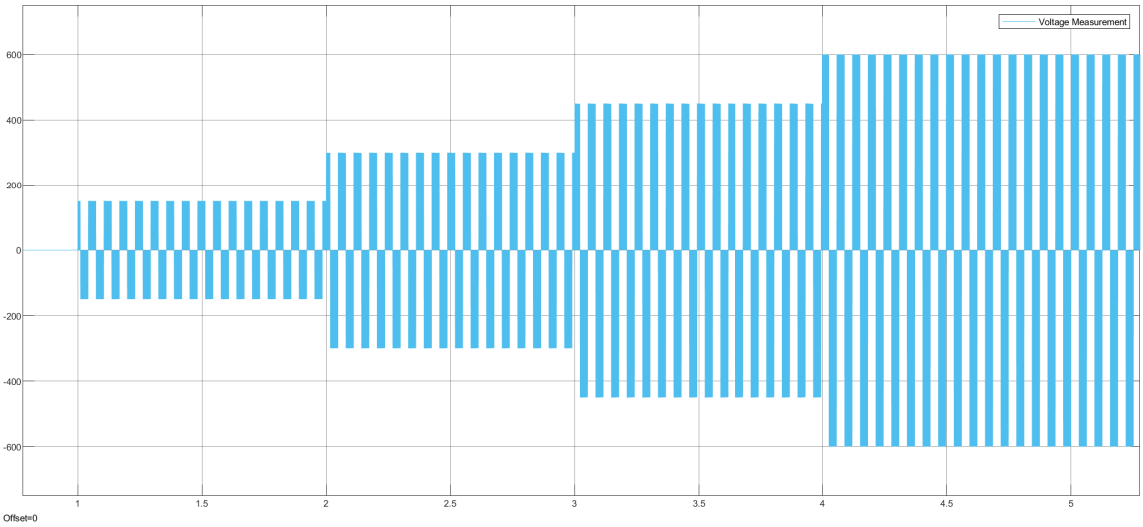

Figure 5.5: Output Voltages

5.1.1 IGBT and Diode Loss Modelling

The Infineon IGBT modules F3L50R06W1E3-B11 were selected for use with each of the phase legs. The parameters used for the loss calculations are based on the specifications found within the manufacturer's data sheets. Each IGBT has a co-packaged anti-parallel diode to help with reverse conducting requirements. The IGBTs losses calculated were the turn-on, turn-off and conduction losses. When the IGBT switches on the load current flows through the diode of the complimentary switch. At turn-on the IGBT sees the load current plus the reverse recovery current of the diode. Due to this the reverse recovery of the diode turn-on losses are normally higher than turn-off losses. The turn-on loss energy, E_{on} was calculated using a 2-D lookup table of the pre-switching voltage across the device, post-switching current flowing into the device.

The turn-off E_{off} losses were calculated in a similar manner with the pre-switching current and post-switching voltage. The conduction loss, V_{on} values were found using the current and operating temperature to determine the saturation voltage across the IGBT using a 2-D look-up table [22]. The diode's loss energy was calculated in a similar manner to achieve values for the reverse recovery losses as well as the conduction losses. The reverse recovery losses were found using the pre-switching current and the post switching voltage. Finally, the conduction energy for the diode was computed with the diode forward current and junction temperature to determine what the on-state voltage was across the diode using a 2-D look-up table [22]. The losses for each diode and IGBT pair was calculated individually and then combined to give a final result in the simulation.

5.2 Inverter Modelling with a HESS

The paper [23] presents a novel active HESS topology which consists of a battery and a UC connected to a multi-source inverter. The work from this paper can be expanded up to include the additional switches and operating mode of the ReMSI to achieve an output voltage of $V_{DC1} + V_{DC2}$. This setup aims to achieve similar performance to an active HESS architecture but without the additional DC/DC converter. By using the UC's on the main DC bus, they act as low-pass filters, which smooth the output current. This new inverter control scheme was studied and the affects on the battery showed that the average current ripple could be reduced by up to 60%, compared to traditional battery only ESS.

5.3 Vehicle Modelling

The first distinction that should be made when modelling vehicles is the type of modelling to use, choosing between steady-state and dynamic vehicle models. Steady-state models consider all transient states negligible and generally require less computational time at the expense of real-life modelling accuracy [24]. Dynamic vehicle models, on the other hand, factor in transient states and attempt to model with greater accuracy using more general and sophisticated methods [24]. Furthermore, it is also beneficial to define the differences between structural and functional models. Many of the current software packages used for vehicle modelling and simulation are structural systems, meaning that the system is composed of interconnected devices, each modelling a real-life component [24]. These devices are typically organized into component libraries, and users drag and drop graphical representation of physical components to create a vehicle propulsion system model. Functional models, on the other hand, are entirely mathematical; the system is represented through the interconnection of functions, each representing a unique physical component. While system analysis can be improved with a functional model system, the graphical simplicity and ease of design are removed throughout the vehicle control system design process.

The final model method distinction that must be made is between forward and backward based models. Forward and backward models refer to the direction in which model calculations are performed [24]. In the forward or engine-to-wheel method, calculations begin with the vehicle torque sources, were transmitted and reflected torque values are applied to the remainder of the model towards the vehicle chassis or other power consumers [24]. In the mechanical domain, vehicle speed and rotational speed of the respective components are sent back to the torque sources. Similarly,

in the electrical domain, current and voltages are used. In the case of a backwards, or wheel-to-engine model approach, calculations begin with the required traction effort at the wheels, and then send this information to the torque sources and other propulsion system components [24]. Backwards model approaches require pre-defined speed drive cycles in order to calculate the force acting on the wheels and therefore calculate the required propulsion system power command. This approach can be used for dynamic programming applications.

Most vehicle models consist of three major components: the torque controller model, a vehicle plant model, and the driver mode. The torque controller model is a time-based design of the simulation that forces the controller inputs from the driver plant model and the vehicle plant model. The controller takes in the acceleration and deceleration pedal position commands, propulsion system component information, and resulting vehicle speed. The vehicle plant model is where the vehicle and power-train specific details come are added. This where the ESS, ICE, EM's, inverters, and other components efficiency and outputs are calculated.

The driver model is used to simulate a human driver operating the modelled vehicle over a real-world drive cycle. It also allows the model to be evaluated for its acceleration and deceleration capabilities, fuel efficiency, and battery usage and recharge. By running the driver model in simulations, the user can adjust the implementation of its controllers to iteratively improve and optimize the design and performance of the system. The driver model works by taking the desired input and current vehicle velocity and outputting speed, positive and negative torque values. The desired velocity is the speed that the driver would like to achieve, given the current surrounding environment. The current velocity is the speed the vehicle is currently travelling at

and is fed to the driver system through a feedback loop in the model. The positive and negative torques values are representative acceleration and braking within the vehicle.

5.4 ReMSI in an Electrified Powertrain

The following simulation was run to get baseline results for the experimental test setup planned in Chapter 6. Two DC sources were used, with $V_{DC1} = 450V$ acting as a generator and $V_{DC2} = 150V$ acting as a battery pack. The battery was modelled using an equivalent circuit R-RC model and was initialized to 70% State-of Charge (SOC). The model was parameterized using experimental cell data from a 5.4 Ah Lithium polymer cell [14], and this data was used to generate a function of the state of charge using the open circuit voltage. Figure 5.6 shows the affects on the inverter on the batteries voltage as it sweeps through its' various operating modes.

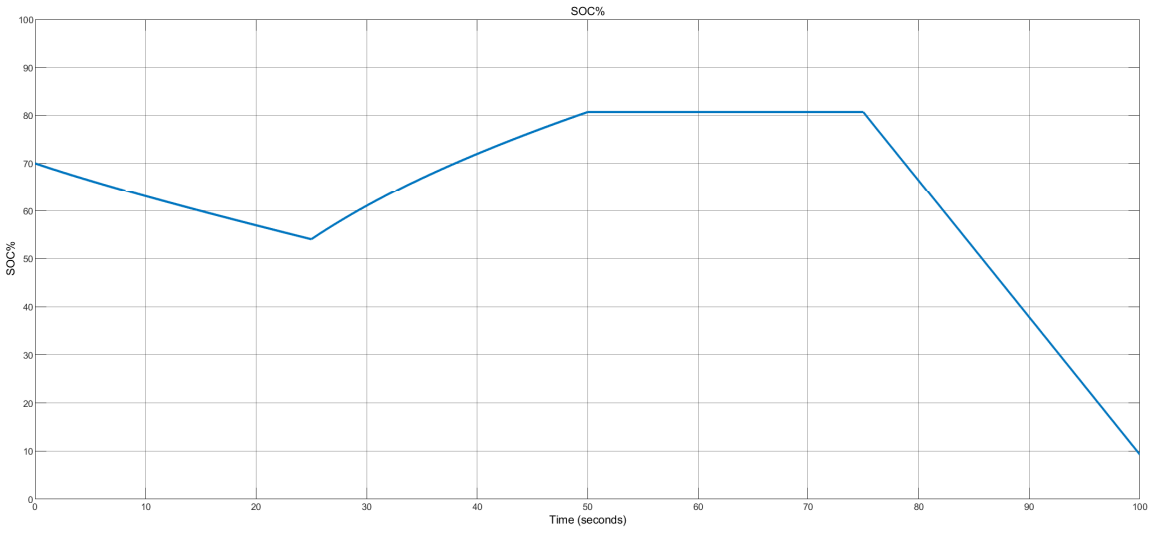

Figure 5.6: SOC of V_{DC2} Throughout the Different Operating Modes

Mode 1 uses just V_{DC2} and As a result the battery SOC is decreasing. This mode

is most effective a lower EM speeds where a smaller bus voltage can reduce switching losses. As the inverter enters Mode 2 the SOC of V_{DC2} begins to increase again as the bus voltage reaches $V_{DC1} - V_{DC2}$. The higher voltage generator to recharges the battery while simultaneously supplying the load. In Mode 3 the inverter is only supplied by V_{DC1} therefore the SOC of the battery remains unchanged throughout this operation mode. Finally, in Mode 4, the generator and the battery are connected in series to achieve $V_{DC1} + V_{DC2}$. This is of significance as it would allow an OEM the freedom to significantly undersize the battery without sacrificing performance. Due to the series connection of the sources battery's voltage no longer needs to be sized to the traction motor. This is shown at the end of the graph where the SOC begins to decrease faster than in Mode 1 because the reference voltage in Mode 4 is larger than in Mode 1. Therefore much more energy is discharged in this final mode of operation. These results validate the theoretical principle operation of the ReMSI discussed in Chapter 4.

Chapter 6

Power Circuitry and Plans for Experimentation of the ReMSI

6.1 Existing Experimental Setup

A scaled-down prototype of an MSI was already built and available for use at the McMaster Automotive Resource Centre. This setup was built to validate the effectiveness of the inverter and is composed of three Infineon IGBT modules of type F3L50R06W1E3-B11. These were selected for their compact nature, as well as higher power ratings which would allow for use with other experimental setups. Experiments were performed with a 5.9 kWh battery pack of 50 V and a HV DC-link of 150 V provided by a power supply. An induction motor was then connected back-to-back with an induction generator, which can be used as a load for testing and validation purposes. The control of the gate signals and signals for current, voltage, and speed, is done using a real-time system called a MicroAutoBox II from dSPACE [25]. A new circuit board was designed for use with this setup, which allowed for the addition of S_1

and S_2, this new board would interface with the existing setup. The Printed Circuit Board (PCB) was designed using Altium, an industry-grade PCB routing tool. The schematics for this PCB can be found in the appendix. Additionally, this setup is to be modified to include an updated version of the control scheme to account for the additional operating mode of the ReMSI.

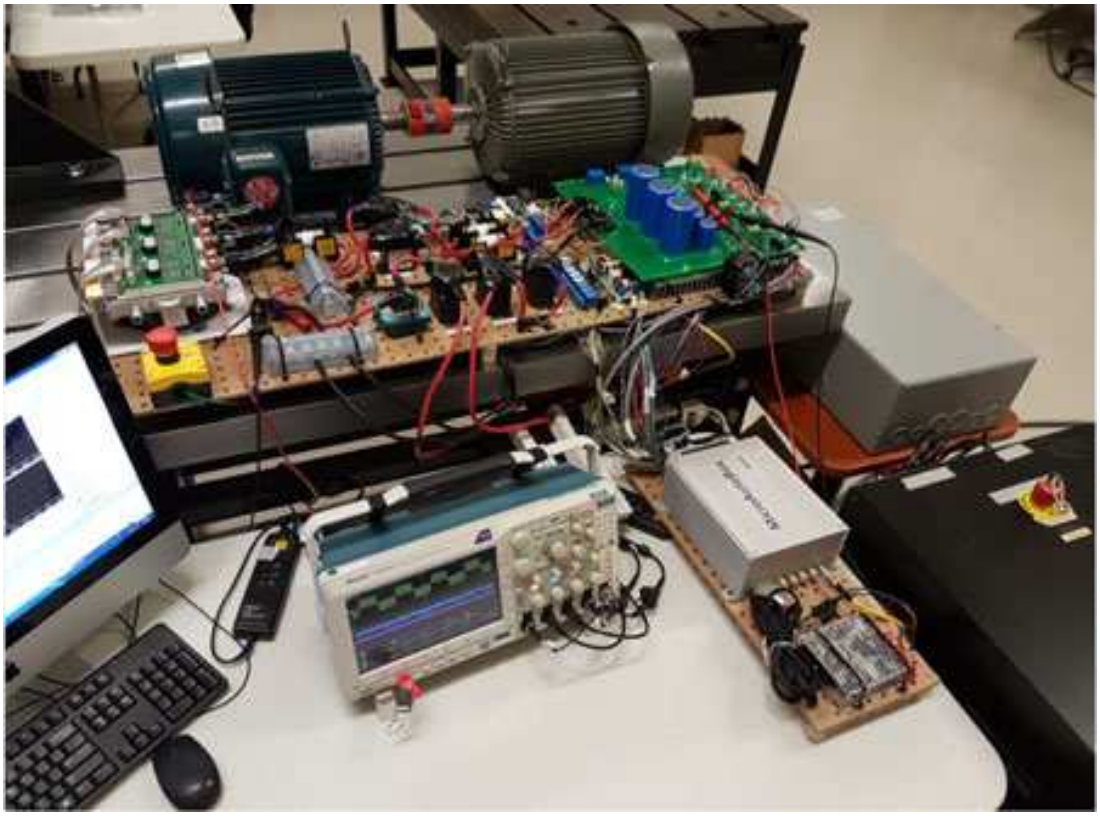

Figure 6.1: Experimental Test Setup

Various safety precautions were integrated into the experimental setup by the previous user, including fuses, an emergency stop button, pre-charge circuits, and inrush current detection. The Figure 6.1 shows the complete experimental setup.

6.2 IGBT Setup

The power conduction stage of both the MSI and ReMSI has been designed to make use of IGBT's. Among the many switching topologies that have been developed for IGBT's, the Neutral Point Clamped (NPC) and the T-type NPC (TNPC) are the most competitive solutions. The paper [8] compares the efficiencies for a wide range of switching frequencies that have been conducted to compare the NPC and the TNPC topologies for a VSI inverter. The results showed that the TNPC is more efficient for medium band frequencies between 10 kHz to 30 kHz, while the NPC becomes slightly more efficient for higher frequencies above 30 kHz [8]. These switching topologies provide output voltages with lower harmonic distortion than the traditional VSI but require additional control complexity due to a high part count.

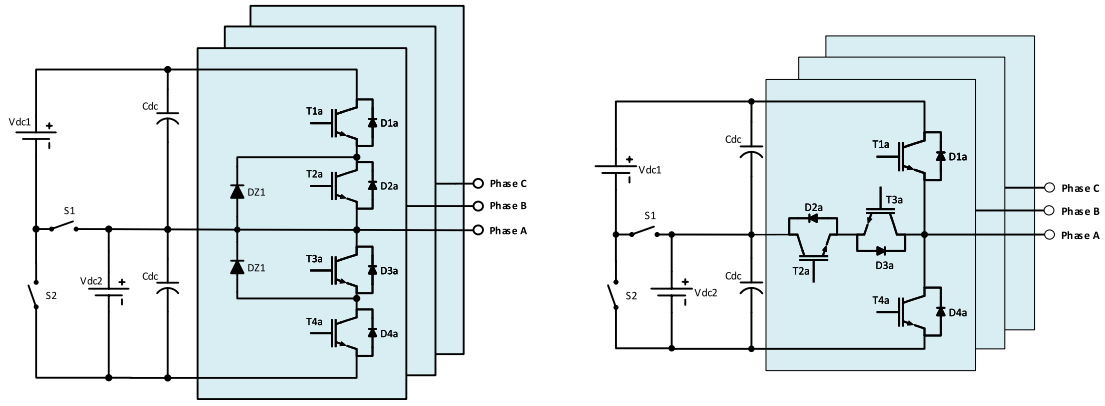

(a) Phase Leg A with a NPC Setup

(b) Phase Leg A with a TNPC Setup

Figure 6.2: NPC vs. TNPC IGBT Setup

A TNPC setup is often preferred over a traditional NPC configuration due to the use of fewer components [17]. This helps reduce the overall cost of the setup. It also helps improve the reliability and longevity of the phase leg as the reduced number of components provides fewer points of failure for the device.

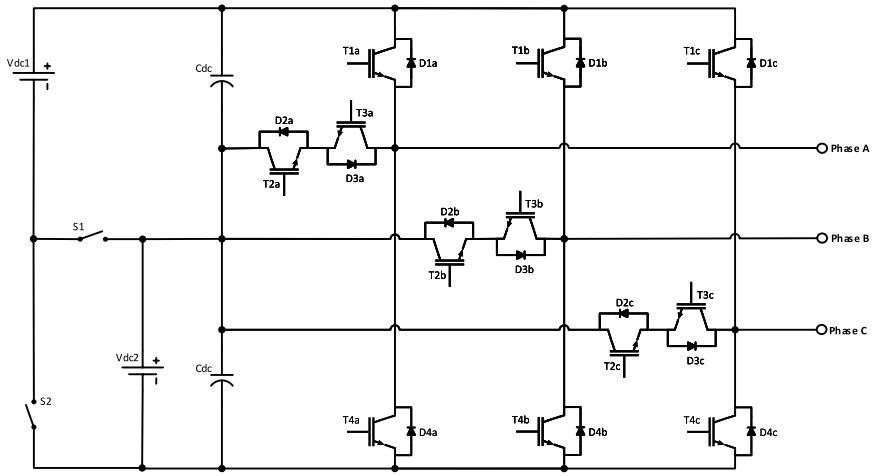

Figure 6.3: TNPC Switch Topology for an ReMSI

With the TNPC setup, the voltages V_{AO}, V_{BO}, and V_{CO} are expressed as the following set of equations.

$$V_{AO} = F_{2a}V_{DC1} + G_{2a}V_{DC2} - Z_a i_a \tag{6.2.1}$$

$$V_{BO} = F_{2b}V_{DC1} + G_{2b}V_{DC2} - Z_b i_b \tag{6.2.2}$$

$$V_{CO} = F_{2c}V_{DC1} + G_{2c}V_{DC2} - Z_c i_c \tag{6.2.3}$$

Where Z_k is the phase impedance of the load, and $F_{2k} = S_{T_{1k}}$ and $G_{2k} = S_{T_{2k}} \wedge S_{T_{3k}}$ are the switching functions of their respective IGBTs. Additionally the switches T_3 and T_4 are complementary to T_1 and T_2 respectively in Modes 1 and 2. While in Modes 3 and 4, the switches T_4 are complementary to T_1. Due to the nature of Mode 2, care should be taken in choosing the DC source voltages ensuring that $V_{DC1} > 2V_{DC2}$ as the voltage $V_{DC1} - V_{DC2}$ should be positive and greater than $V_{DC}2$.

Switches S_1 and S_2 were also planned to be discrete IGBT's from Infineon as well.

These semi-conductors and their accompanying anti-parallel diodes would need to be selected with the dual voltage sources in mind. S_1 would only need to be rated for V_{DC1} but S_2 would need to be rated for the voltage and current requirements seen in mode 4, $V_{DC1} + V_{DC2}$. Contactors are would not make a suitable choice for this application due to the potential for rapid transitions between the different operating modes. Contactors are prone to welding when switched under full load conditions and therefore could cause damage to the internal circuitry of the inverter.

6.3 Challenges

Due to the 2020 COVID-19 global pandemic, all in-person work at McMaster University was stopped on March 13^{th} 2020 [26]. To help stop the spread of COVID-19, the province of Ontario then declared a state of emergency on March 17^{th}, 2020 [27]. Due to the university shut down and provincial order to shelter-in-place the experimental research planned for this thesis could not be completed as intended. As of August 2020, McMaster University is still conducting online classes and has restricted in-person work until 2021.

Chapter 7

Conclusion

This thesis focused on the concept, design, simulation, and implementation of a ReMSI for electrified vehicle applications.

Trends within both the Canadian and global automotive markets were reviewed with emphasis on the growing environmental concerns associated with combustion vehicles. Various vehicle configurations were presented and discussed with significance placed on electrified vehicles such as hybrids. With a shift in public attitude, vehicles are no longer being viewed as point-to-point fossil-fuel-burning transportation devices but rather an efficient, connected, and intelligent technology.

The fundamental components of an electrified power were introduced and reviewed, with a specific focus on EM's, traction inverters, power electronics and energy storage systems. The energy conversion and transfer between the electric machine and the ESS were discussed along with the use cases and applications. The different hybrid vehicle architectures were introduced with their respective practical design considerations. For any component to be seriously considered by the automotive industry, it must be competitive on cost, reliability, and efficiency.

By far, the most expensive aspect of an EV is the energy storage system, which is comprised primarily of HV batteries. Typically, the cost of the battery pack is driven by the output voltage and rated output power; therefore, there is a need within the automotive industry designs that enable the use of a battery pack with lower output voltages in order to minimize cost. The different methods to reduce costs are discussed in this chapter, along with battery modelling and simulation methods.

The concept of the ReMSI was introduced, using ideal switches, which would eventually be swapped out for IGBTs. With the addition of two switches, S_1 and S_2, the inverter can make use of two DC sources and can operate in four distinct modes during the DC/AC conversion. The ReMSI can be driven by either one or both sources, allowing for four voltage levels, namely V_{DC1}, V_{DC2}, $V_{DC1} - V_{DC2}$ and $V_{DC1} + V_{DC2}$. When operating as a rectifier for AC/DC conversion, two operating modes are achievable where the power generated by the EM is supplied to one of the two DC sources. Different inverter modulation techniques were investigated to be used in the ReMSI simulation environment.

The SVPWM modulation technique was explored and used in the simulation to achieve the desired IGBT gating patterns. The ReMSI was first modelled as an individual component and then as a part of a more extensive vehicle simulation. Simulation results are consistent with the proposed theory, which validated the effectiveness of the proposed topology and concept. An experimental setup was then proposed to validate the simulation results, but due to the COVID-19 pandemic could not be realized.

7.1 Future Work

Concerning future work on the ReMSI, many aspects could be expanded upon to improve further the work achieved. Some suggestions have been included below of potential next steps.

In chapter 4, the voltage balancing of the two input capacitors on the DC side of the inverter could be further investigated, including the required sizing calculations. Additionally other IGBT topologies could be researched, including further analysis of the NPC topology.

In chapter 5, a more comprehensive model could be created to better capture the losses throughout the model. For instance, more accurate results could be achieved by using experimental measurements rather than values from the datasheet for the IGBT switching parameters. Additionally, the forward voltage drop of the switch and diode combination could be measured for several currents to improve the conduction loss model. Finally, it could also be improved by the addition of thermal losses throughout the system.

In chapter 6, the experiments that were planned could be performed to validate the inverter topology further. The PCB that was designed would need to be manufactured and put together with the required components before being integrated into the experimental test setup. Additionally, the bench could be modified to include the HESS designed and built by the students of the EcoCAR 3 McMaster team to highlight the benefits of both systems in combination with each other.

While many safety precautions were integrated into the experimental setup by the previous user, including fuses, an emergency stop button, pre-charge circuits, and inrush current detection. These were bulky additional components that were

connected on the test bench externally. Further research could be done the decrease the size and of these components as well as update the pre-charge circuitry to account for mode 4. Additional analysis should also be completed to insure the pre-charge circuity will respond to the switching time between the different operating modes of the ReMSI.

Appendix A

Commutation Paths

The commutation paths of the operating areas during the interval $[\frac{\pi}{6}; \frac{\pi}{2}]$ are detailed in Figure A.2, Figure A.3, Figure A.4, Figure A.5 for the TNPC ReMSI for Modes 1 through 4 respectively. It is assumed that the phase currents $i_a(t)$ and $i_c(t)$ are positive and $i_b(t)$ is negative.

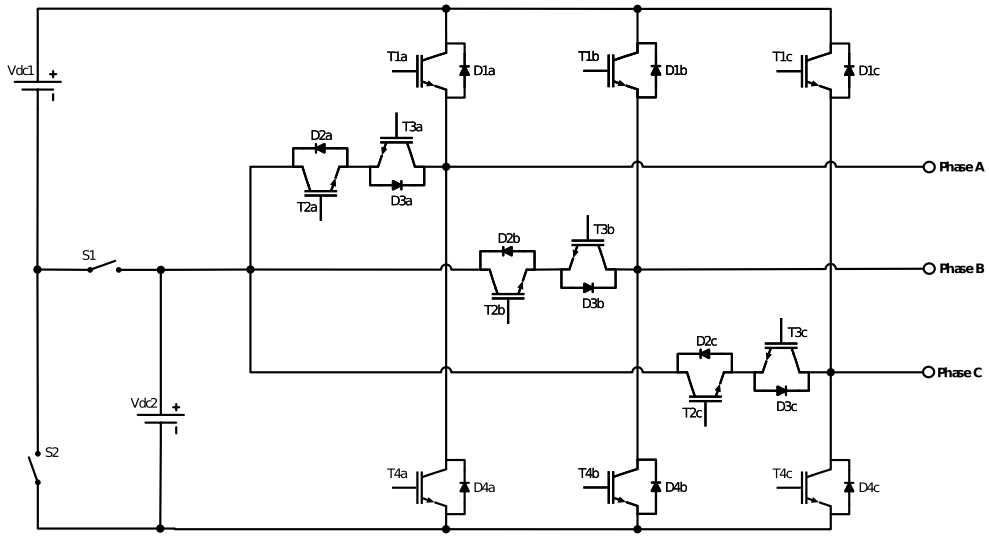

Figure A.1: Original TNPC ReMSI Circuit

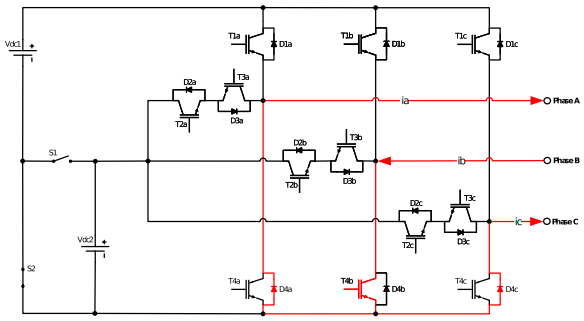

(a) Operating area I

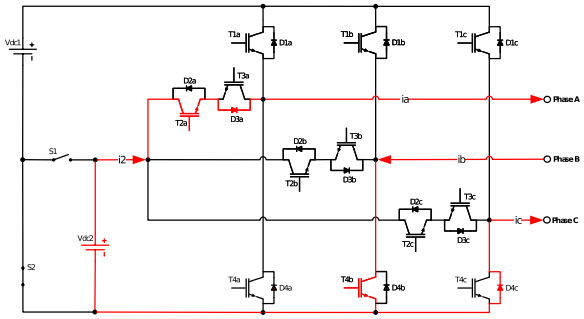

(b) Operating area II

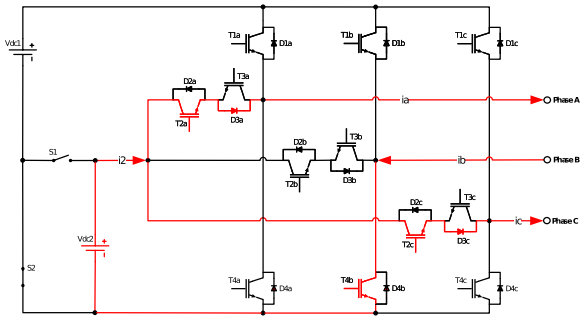

(c) Operating area III

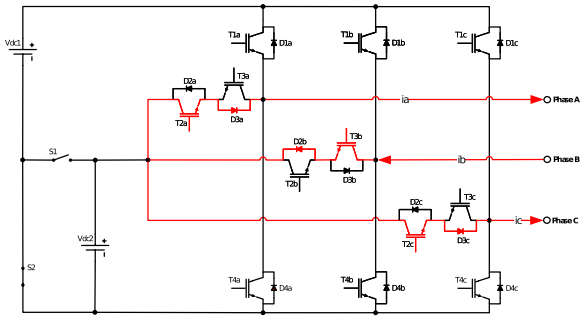

(d) Operating area IV

Figure A.2: Commutation Paths in Operating Mode 1

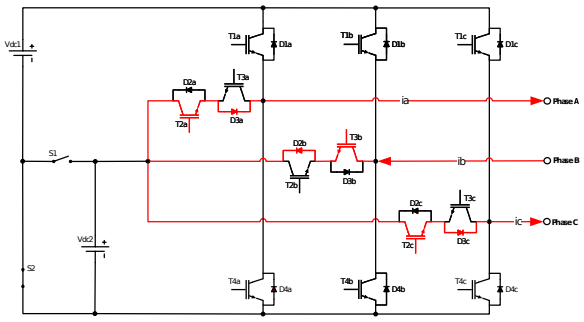

(a) Operating area I

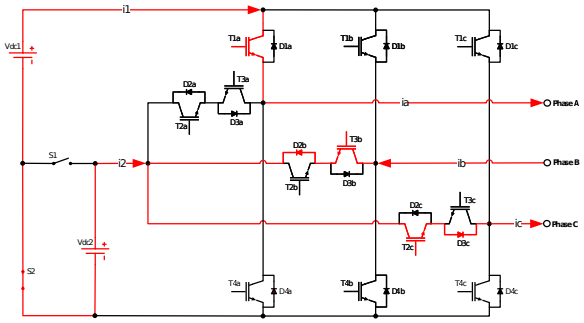

(b) Operating area II

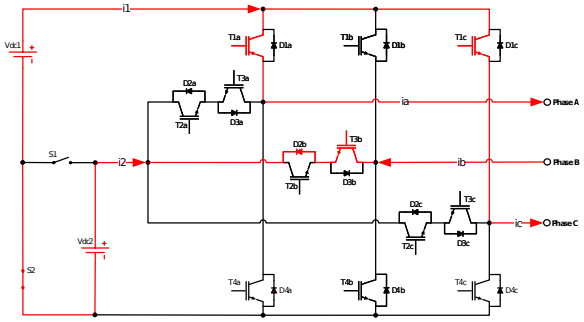

(c) Operating area III

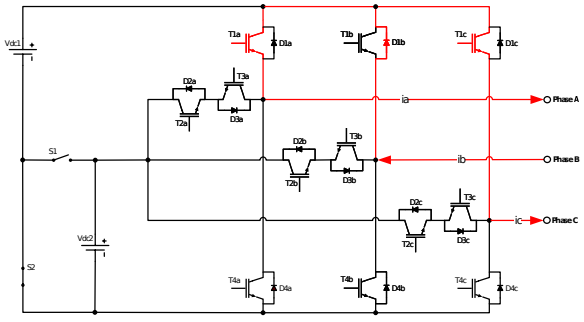

(d) Operating area IV

Figure A.3: Commutation Paths in Operating Mode 2

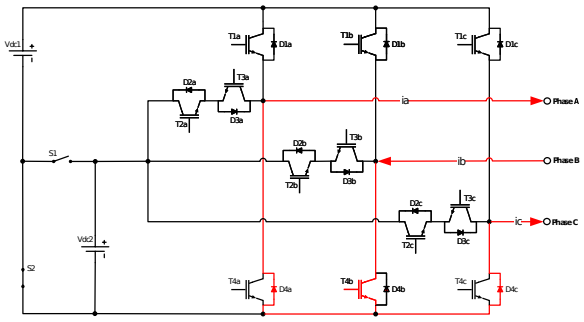

(a) Operating area I

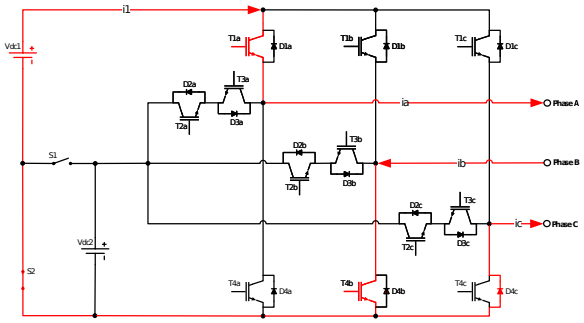

(b) Operating area II

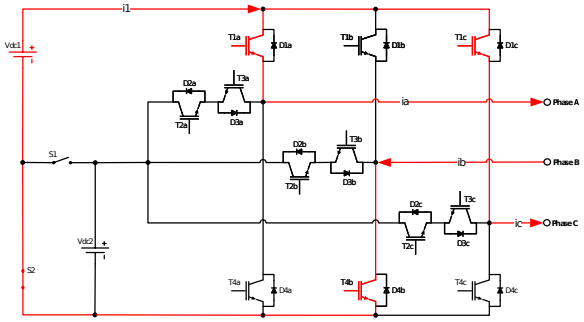

(c) Operating area III

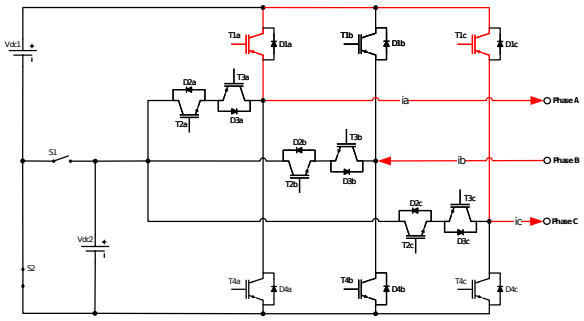

(d) Operating area IV

Figure A.4: Commutation Paths in Operating Mode 3

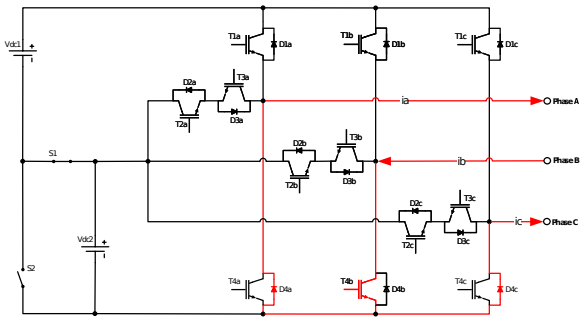

(a) Operating area I

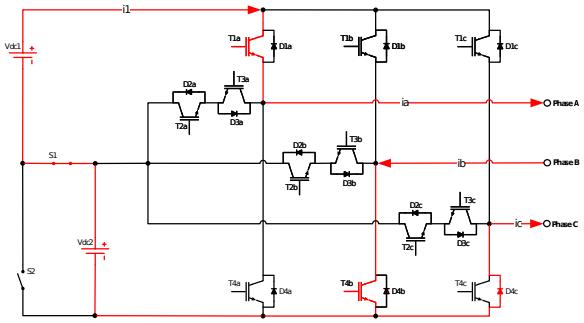

(b) Operating area II

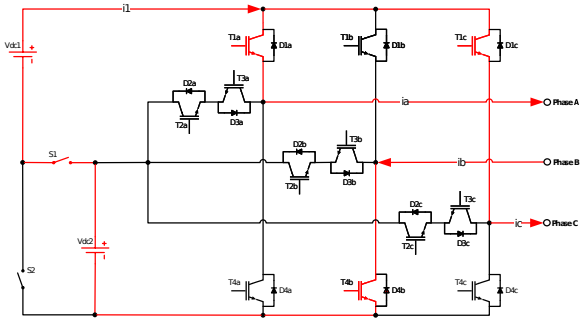

(c) Operating area III

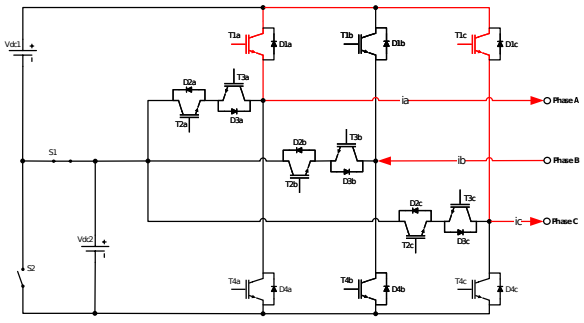

(d) Operating area IV

Figure A.5: Commutation Paths in Operating Mode 4

Appendix B

Printed Circuit Board Schematics

The following schematics are from the first revision of the printed circuit board designed for the ReMSI experimental setup. This circuit board does not include the discrete IGBTs for S_1 and S_2.

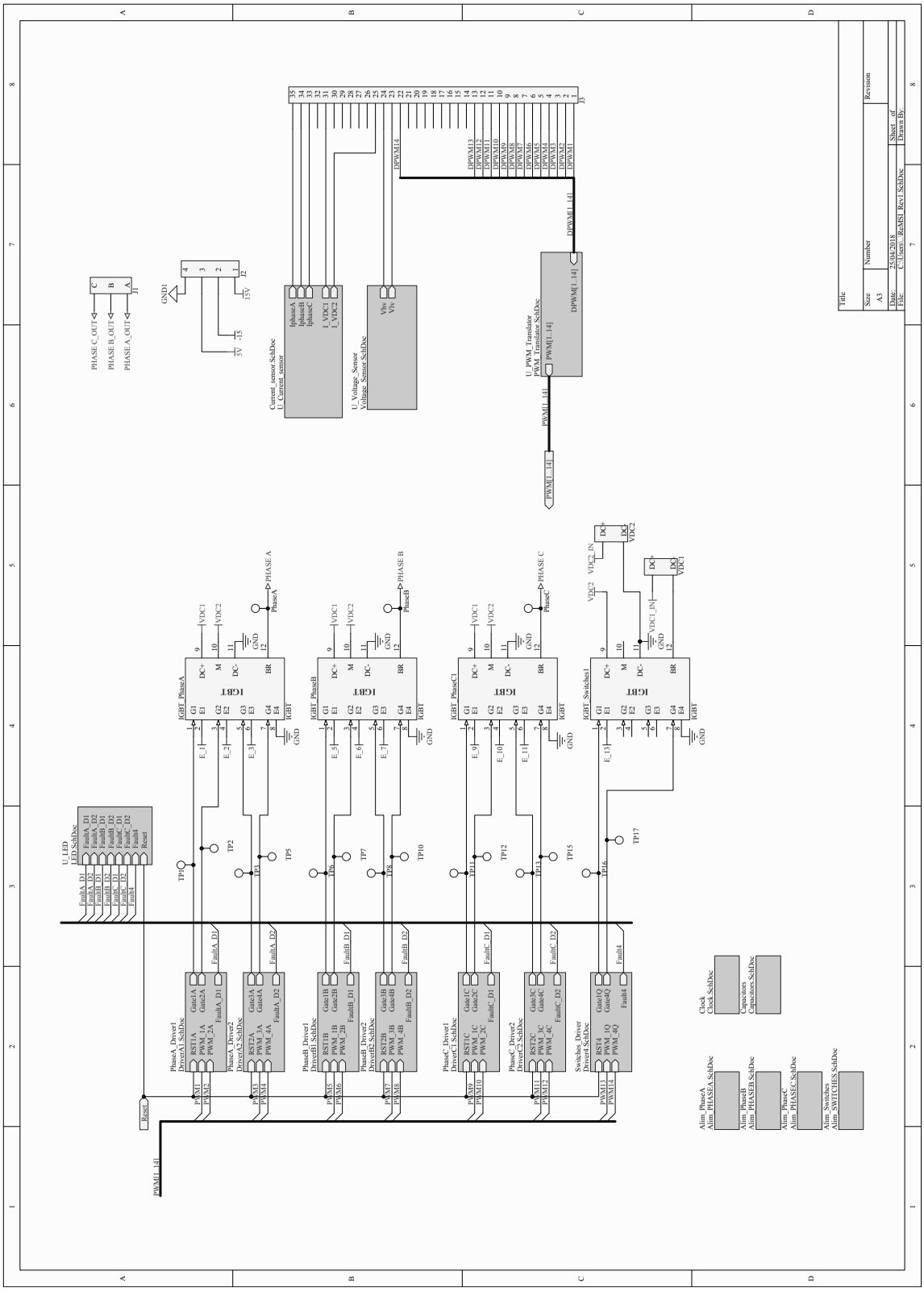

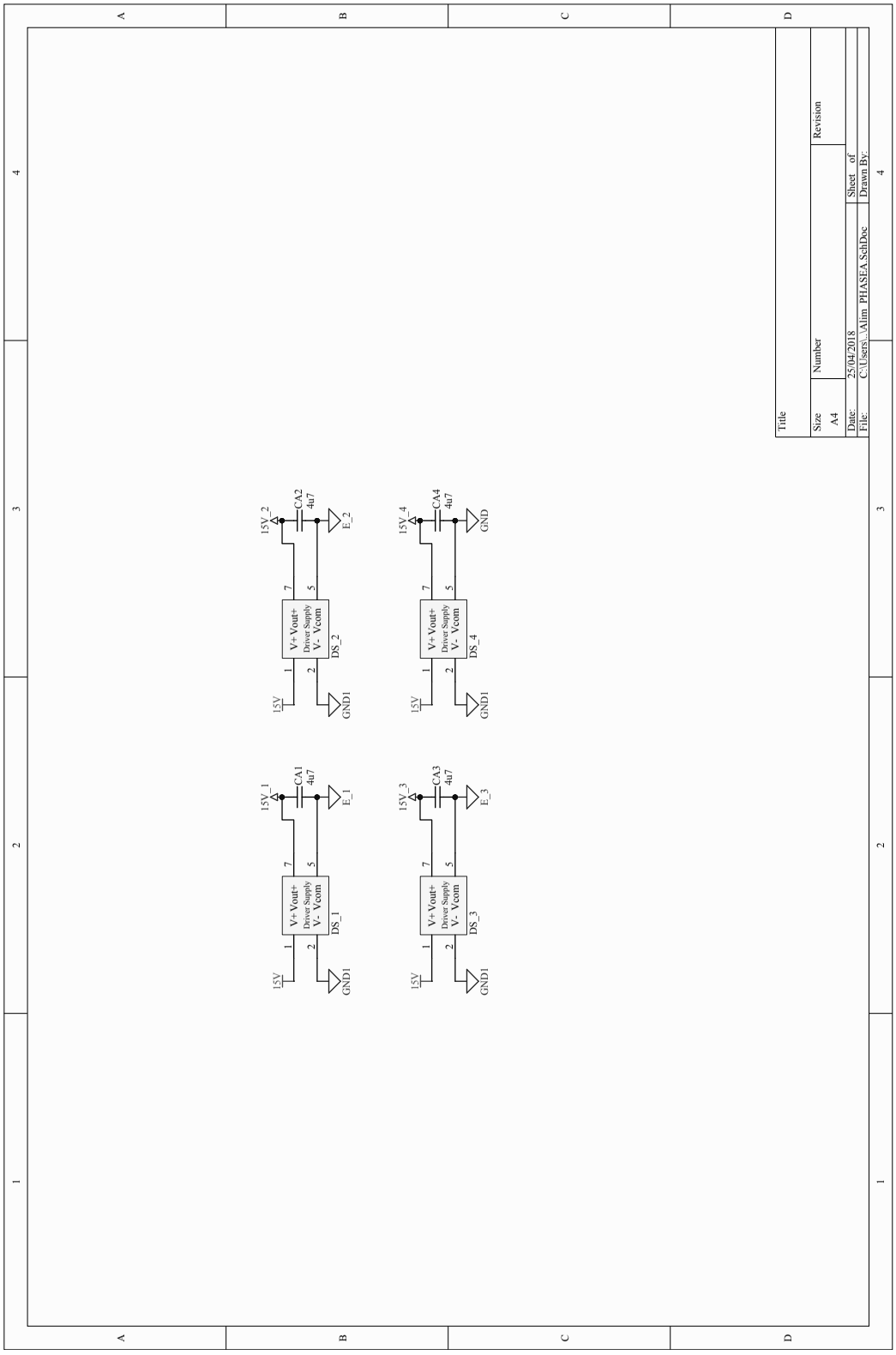
Title
Size
A4
Number
Revision
Date: 25/04/2018
File: C:\Users\...\Alim_PHASEA.SchDoc
Sheet of
Drawn By:
15V_1
CA1
4u7
E_1
15V
V+ Vout+
Driver Supply
V- Vcom
DS_1
GND1
15V_2
CA2
4u7
E_2
DS_2
15V_3
CA3
4u7
E_3
DS_3
15V_4
CA4
4u7
GND
DS_4

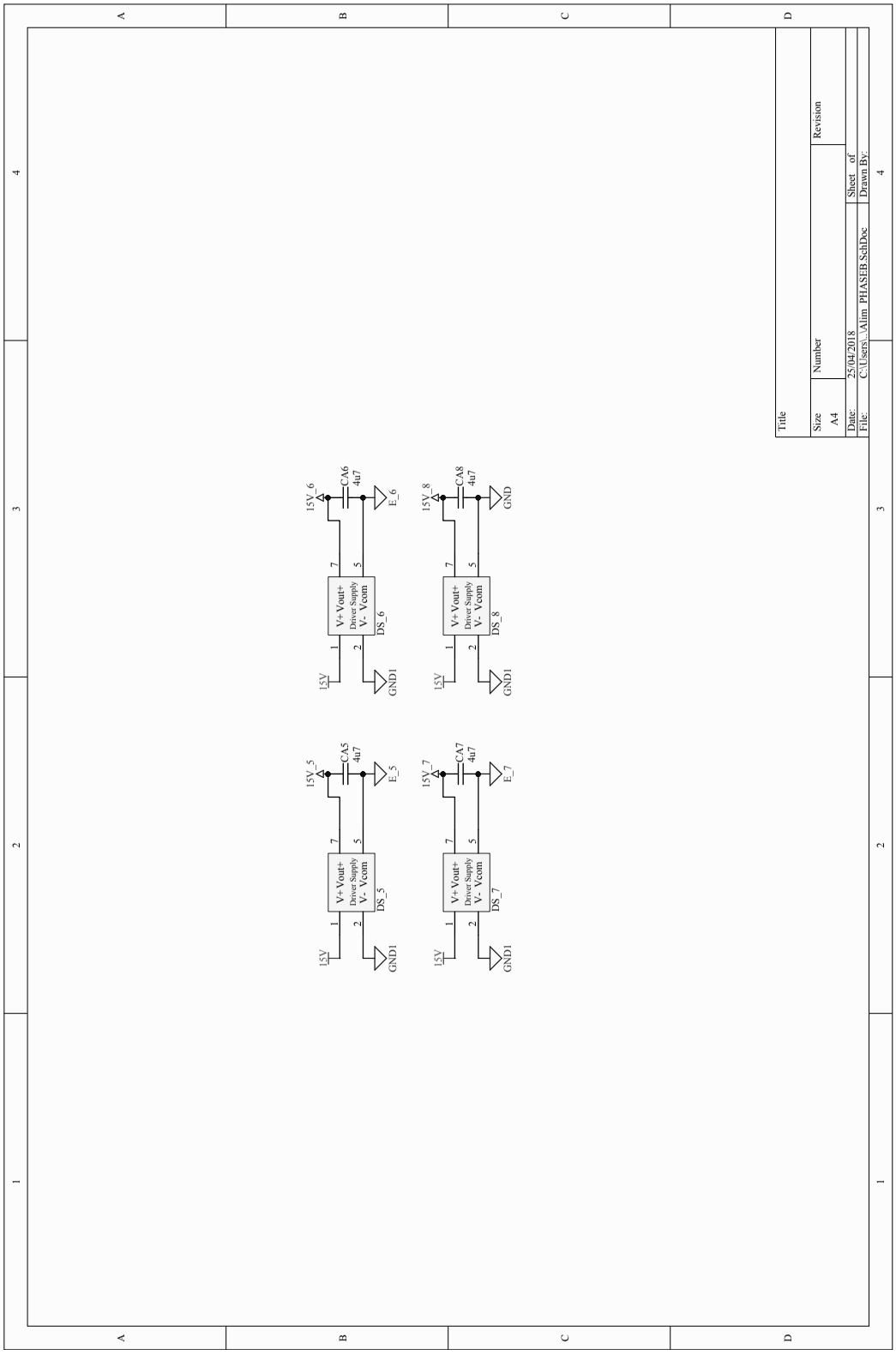
Title
Size A4
Number
Revision
Date: 25/04/2018
File: C:\Users\...\Alim_PHASEB.SchDoc
Sheet of
Drawn By:
15V_6
CA6 4u7
E_6
V+ Vout+ Driver Supply V- Vcom
DS_6
15V
GND1
15V_8
CA8 4u7
GND
DS_8
15V_5
CA5 4u7
E_5
DS_5
15V_7
CA7 4u7
E_7
DS_7

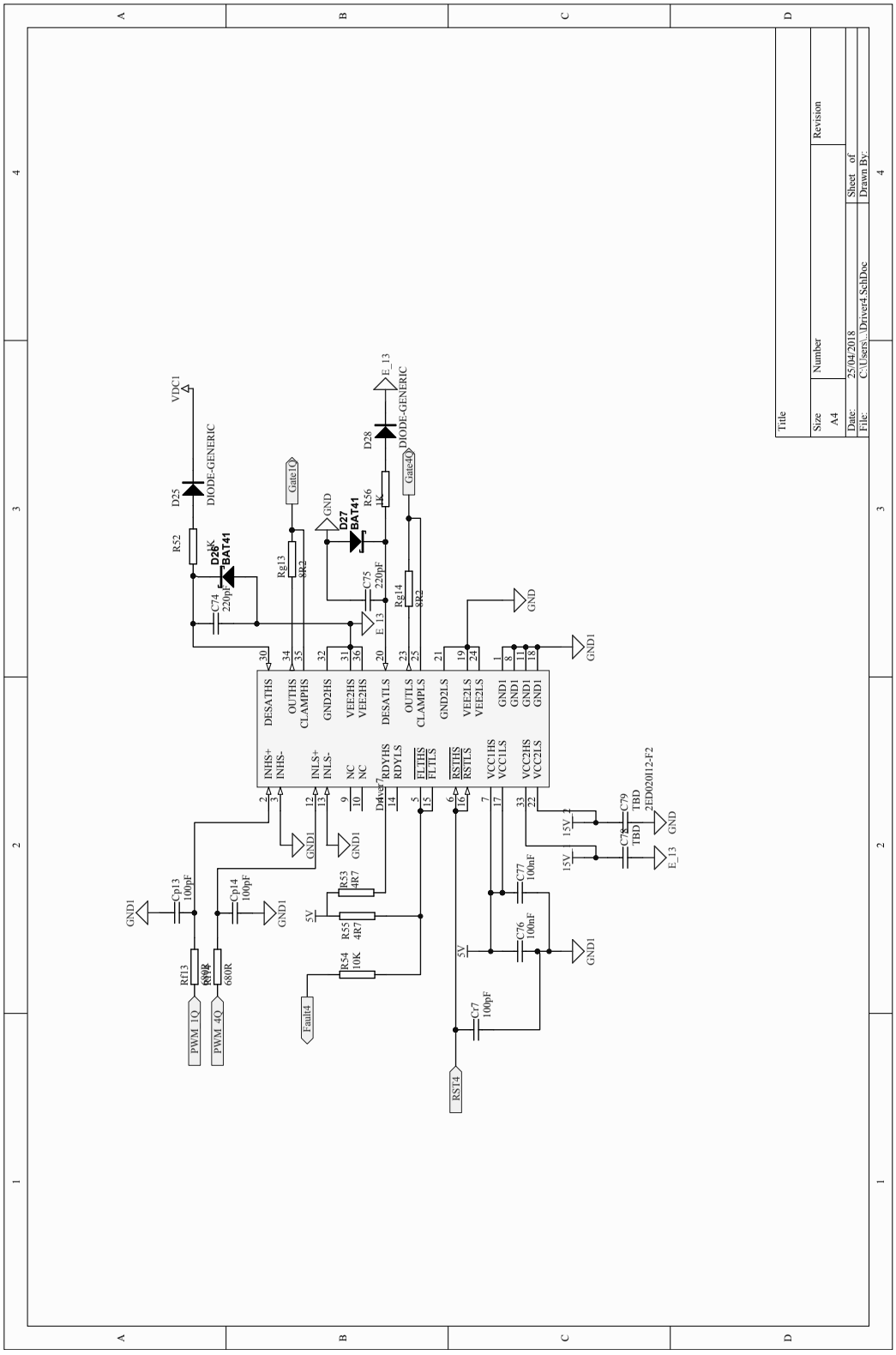
VDC1
D25
DIODE-GENERIC
R52
D26
BAT41
C74
220pF
Rg13
8R2
Gate1Q
GND
D27
BAT41
R56
1K
C75
220pF
D28
DIODE-GENERIC
E_13
Gate4Q
Rg14
8R2
DESATHS
OUTHS
CLAMPHS
GND2HS
VEE2HS
VEE2HS
DESATLS
OUTLS
CLAMPLS
GND2LS
VEE2LS
VEE2LS
GND1
GND1
GND1
INHS+
INHS-
INLS+
INLS-
NC
NC
RDYHS
RDYLS
FLTHS
FLTLS
RSTHS
RSTLS
VCC1HS
VCC1LS
VCC2HS
VCC2LS
Cp13
100pF
Cp14
100pF
Rf13
680R
680R
PWM_1Q
PWM_4Q
R53
4R7
R55
4R7
R54
10K
Fault4
C77
100nF
C76
100nF
C7
100pF
RST4
15V
C78
TBD
C79
TBD
2ED020I12-F2
Title
Size
A4
Number
Revision
Date:
25/04/2018
Sheet of
File:
C:\Users\...\Driver4.SchDoc
Drawn By:

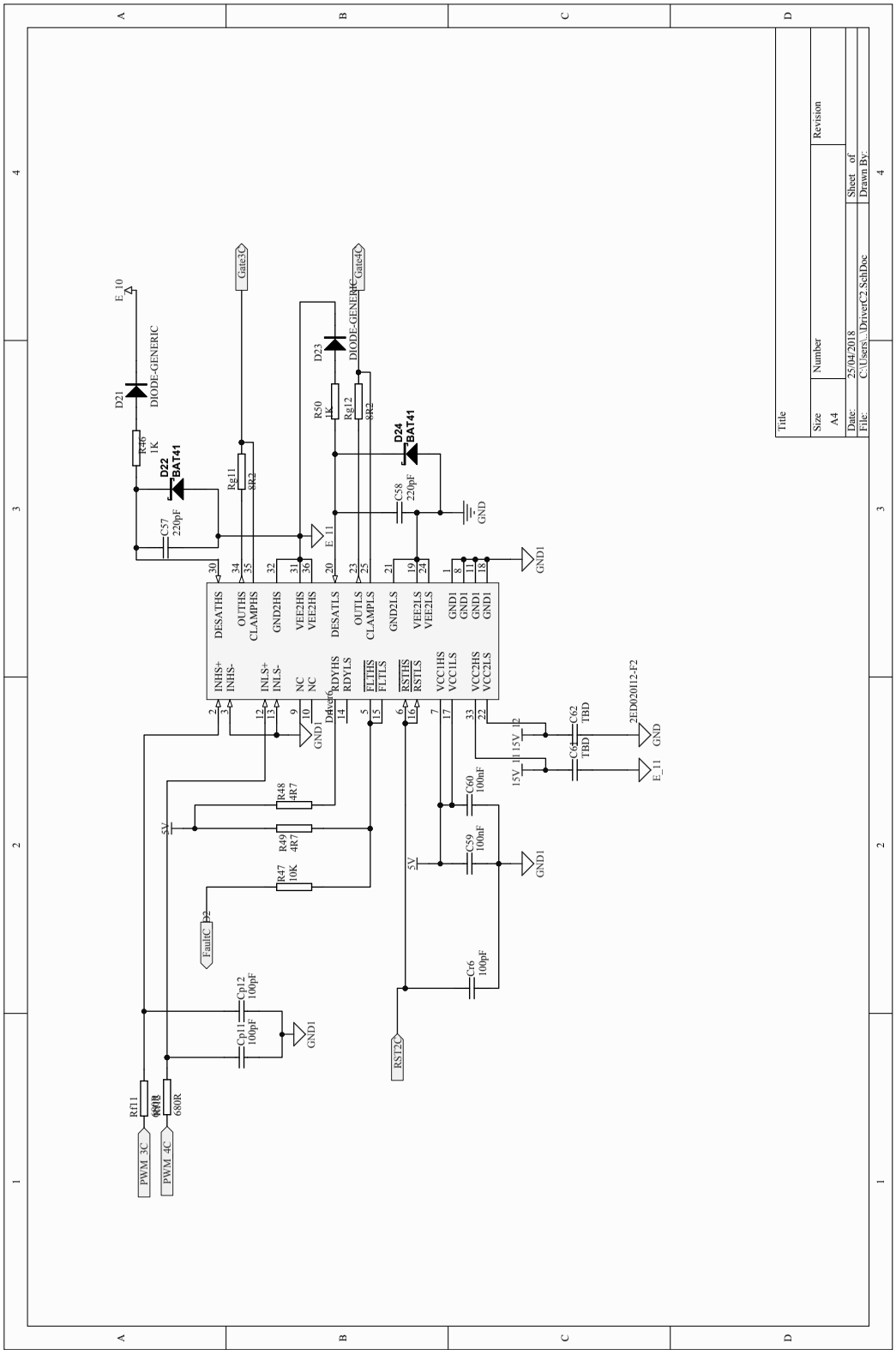
Title
Size A4
Number
Revision
Date: 25/04/2018
Sheet of
File: C:\Users\...\DriverC2.SchDoc
Drawn By:
DESATHS
OUTHS
CLAMPHS
GND2HS
VEE2HS
VEE2HS
DESATLS
OUTLS
CLAMPLS
GND2LS
VEE2LS
VEE2LS
GND1
GND1
GND1
INHS+
INHS-
INLS+
INLS-
NC
NC
RDYHS
RDYLS
FLTHS
FLTLS
RSTHS
RSTLS
VCC1HS
VCC1LS
VCC2HS
VCC2LS
D21
DIODE-GENERIC
D22
BAT141
D23
DIODE-GENERIC
D24
BAT141
R46 1K
R50 1K
Rg11 8R2
Rg12 8R2
C57 220pF
C58 220pF
C59 100nF
C60 100nF
C62 TBD
C63 TBD
Cr6 100pF
Cp11 100pF
Cp12 100pF
R47 10K
R48 4R7
R49 4R7
R11 680R
Gate3C
Gate4C
E_10
E_11
5V
15V_I2
GND
GND1
PWM_3C
PWM_4C
FaultC
RST2C
2EDO20112-F2

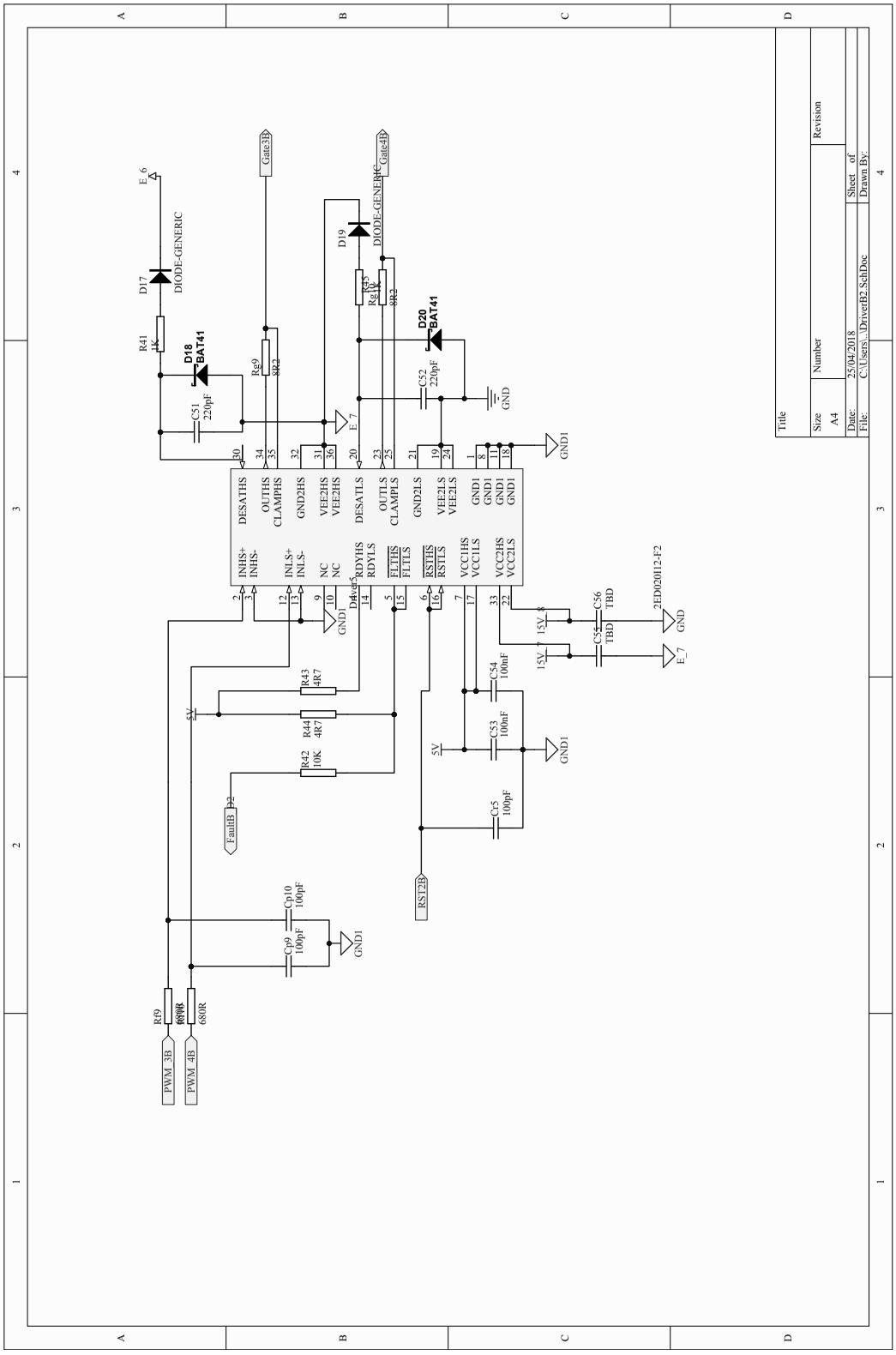
Title
Size A4
Number
Revision
Date: 25/04/2018
Sheet of
File: C:\Users\...\Driver82.SchDoc
Drawn By:
DESATHS
OUTHS
CLAMPHS
GND2HS
VEE2HS
VEE2HS
DESATLS
OUTLS
CLAMPLS
GND2LS
VEE2LS
VEE2LS
GND1
GND1
GND1
INHS+
INHS-
INLS+
INLS-
NC
NC
RDYHS
RDYLS
FLTHS
FLTLS
RSTHS
RSTLS
VCC1HS
VCC1LS
VCC2HS
VCC2LS
D17 DIODE-GENERIC
D18 BAT41
D19 DIODE-GENERIC
D20 BAT41
R41 1K
Rg9 8R2
Rg10 8R2
R45 10K
C51 220pF
C52 220pF
Gate3B
Gate4B
E_6
E_7
GND
GND1
R43 4R7
R44 4R7
R42 10K
C53 100nF
C54 100nF
C55 TBD
C56 TBD
Cr5 100pF
Cp9 100pF
Cp10 100pF
R19
680R
PWM_3B
PWM_4B
FaultB
RST2B
5V
15V
2ED020I12-F2

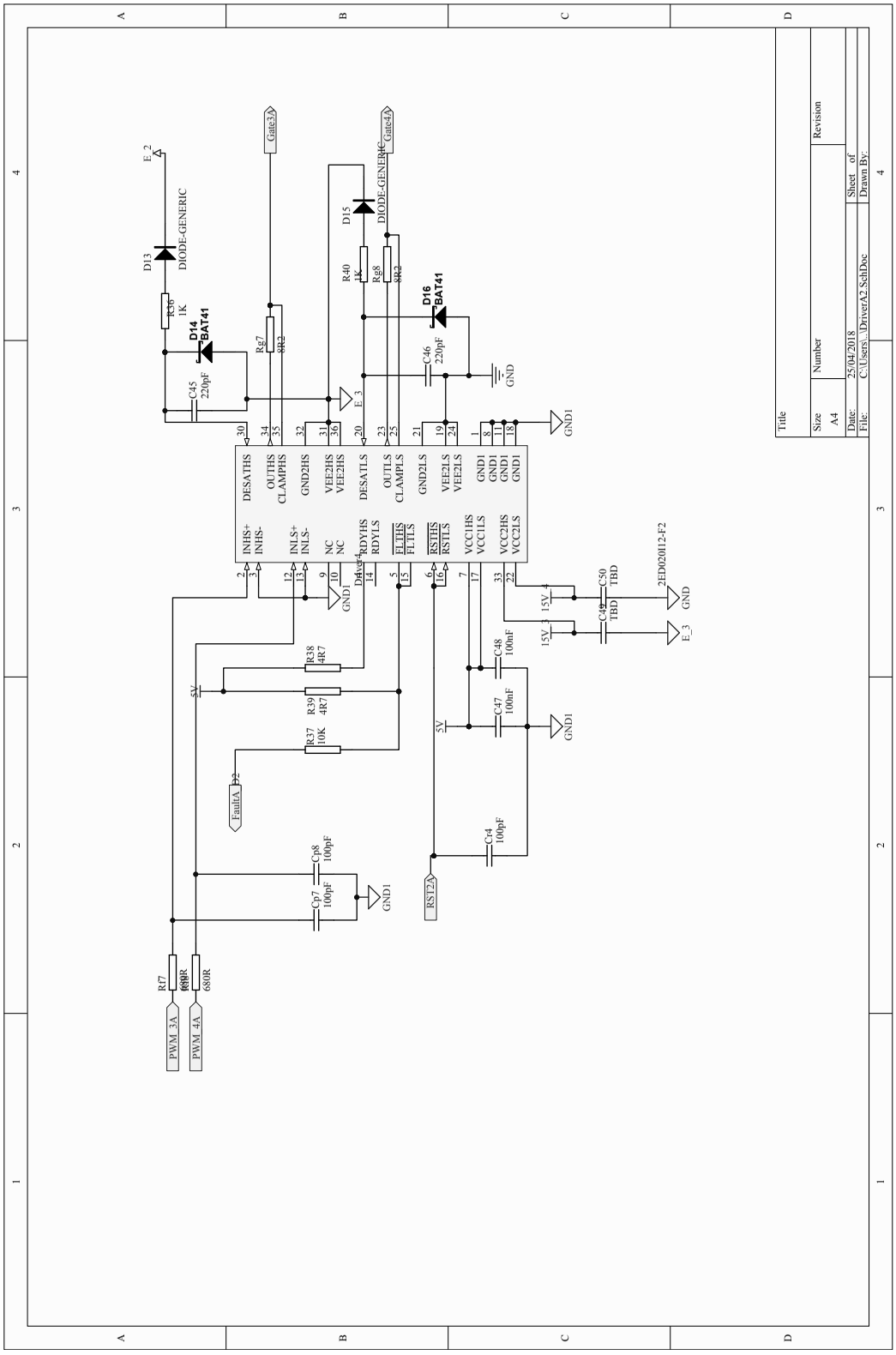
Title
Size A4
Number
Revision
Date: 25/04/2018
Sheet of
File: C:\Users\...\DriverA2.SchDoc
Drawn By:
DESATHS
OUTHS
CLAMPHS
GND2HS
VEE2HS
VEE2HS
DESATLS
OUTLS
CLAMPLS
GND2LS
VEE2LS
VEE2LS
INHS+
INHS-
INLS+
INLS-
NC
NC
RDYHS
RDYLS
FLTHS
FLTLS
RSTHS
RSTLS
VCC1HS
VCC1LS
VCC2HS
VCC2LS
GND1
GND1
GND1
D13
DIODE-GENERIC
D14
BAT41
D15
DIODE-GENERIC
D16
BAT41
R36
1K
R40
1K
Rg7
8R2
Rg8
8R2
C45
220pF
C46
220pF
Gate3A
Gate4A
E_2
E_3
GND
GND1
R38
4R7
R39
4R7
R37
10K
5V
FaultA
C48
100nF
C47
100nF
C4
100pF
Cp8
100pF
Cp7
100pF
RST2A
15V_4
15V_3
C50
TBD
C49
TBD
2ED020I12-F2
GND
R47
680R
680R
PWM 3A
PWM 4A

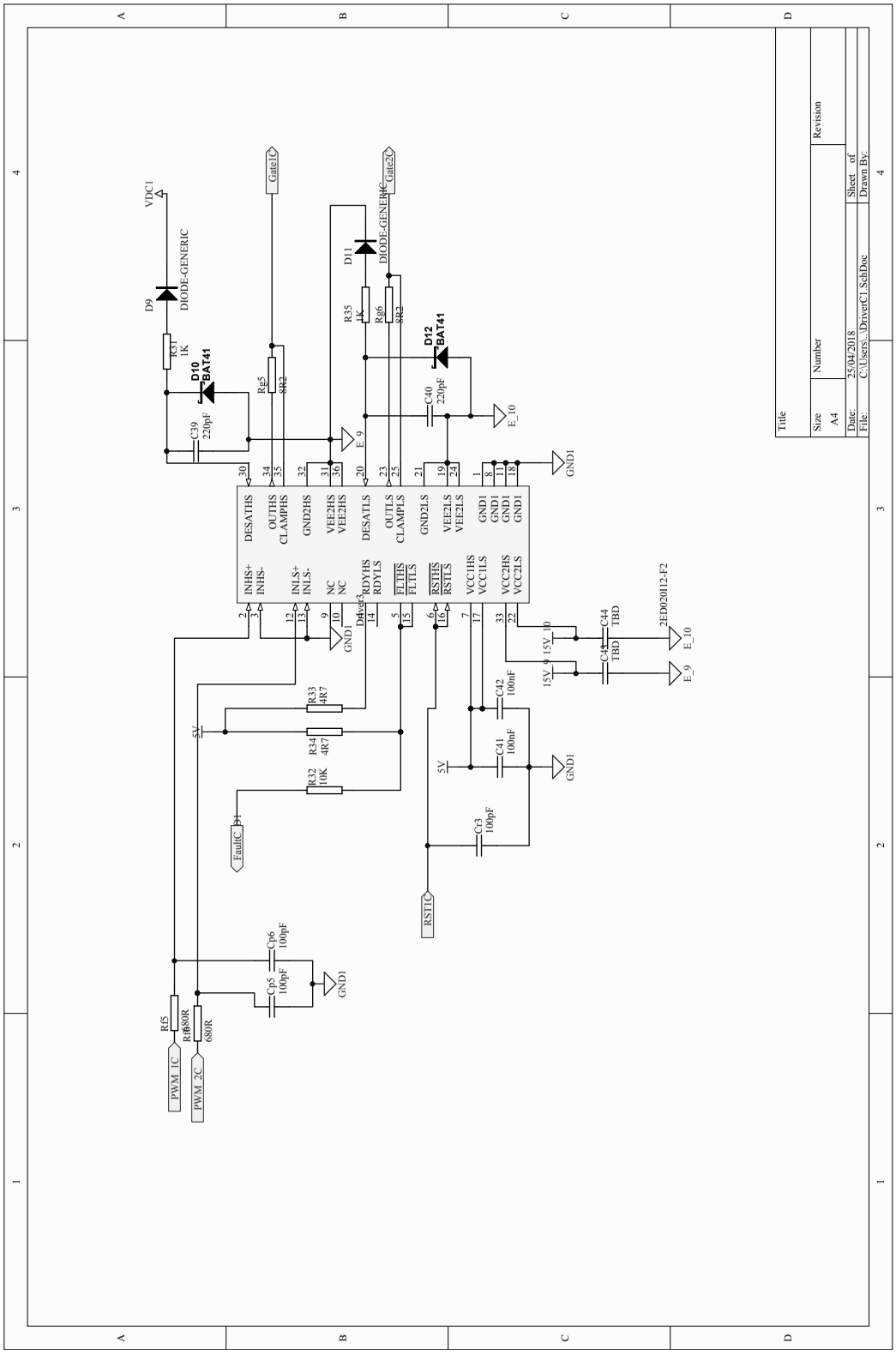
VDC1
D9
DIODE-GENERIC
R31
1K
D10
BAT41
C39
220pF
Rg5
4R2
Gate1C
D11
DIODE-GENERIC
Gate2C
R35
1K
Rg6
4R2
D12
BAT41
C40
220pF
E_10
E_9
GND1
DESATHS
OUTHS
CLAMPHS
GND2HS
VEE2HS
VEE2HS
DESATLS
OUTLS
CLAMPLS
GND2LS
VEE2LS
VEE2LS
INHS+
INHS-
INLS+
INLS-
NC
NC
RDYHS
RDYLS
FLTHS
FLTLS
RSTHS
RSTLS
VCC1HS
VCC1LS
GND1
GND1
GND1
VCC2HS
VCC2LS
Dwg2
R33
4R7
R34
4R7
R32
10K
5V
FaultC
C42
100nF
C41
100nF
C3
100pF
15V_10
C43
TBD
C44
TBD
2ED020I12-F2
E_9
E_10
RSTIC
Cp6
100pF
Cp5
100pF
R45
680R
R46
680R
PWM_1C
PWM_2C
Title
Size
A4
Number
Revision
Date:
25/04/2018
Sheet of
File:
C:\Users\...\DriverC1.SchDoc
Drawn By:

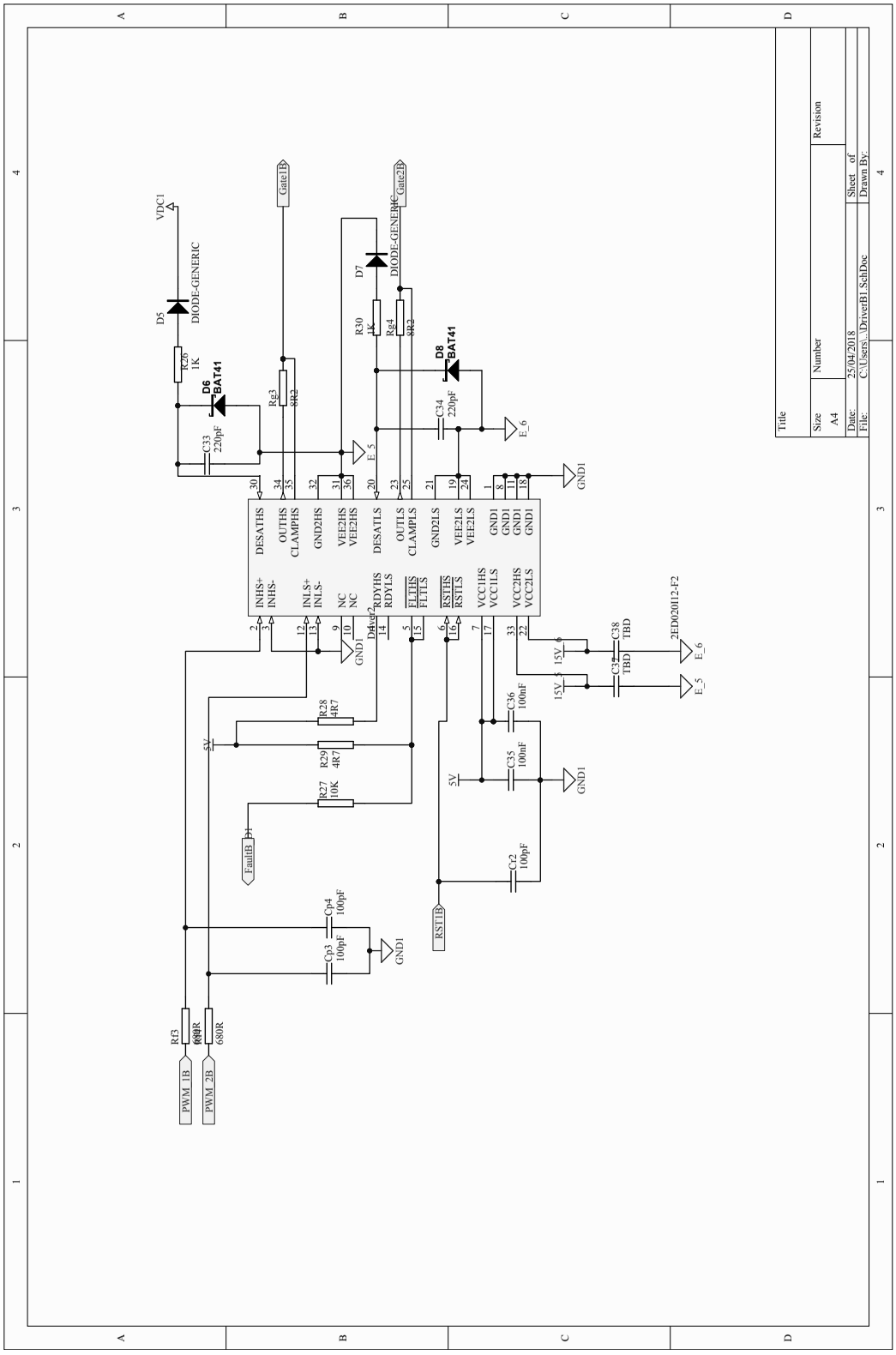
VDC1
D5
DIODE-GENERIC
D6
BAT41
D7
DIODE-GENERIC
D8
BAT41
Gate1B
Gate2B
R26
1K
R30
1K
Rg3
8R2
Rg4
8R2
C33
220pF
C34
220pF
E_5
E_6
GND1
DESATHS
OUTHS
CLAMPHS
GND2HS
VEE2HS
VEE2HS
DESATLS
OUTLS
CLAMPLS
GND2LS
VEE2LS
VEE2LS
GND1
GND1
GND1
INHS+
INHS-
INLS+
INLS-
NC
NC
RDYHS
RDYLS
FLTHS
FLTLS
RSTHS
RSTLS
VCC1HS
VCC1LS
VCC2HS
VCC2LS
Driver2
2EDO2012-F2
15V_6
15V_5
C38
TBD
C37
TBD
C36
100nF
C35
100nF
Cr2
100pF
5V
R28
4R7
R29
4R7
R27
10K
FaultB
Cp4
100pF
Cp3
100pF
RSTIB
R3
680R
680R
680R
PWM_1B
PWM_2B
Title
Size
A4
Number
Revision
Date:
25/04/2018
Sheet of
File:
C:\Users\...\DriverB1.SchDoc
Drawn By:

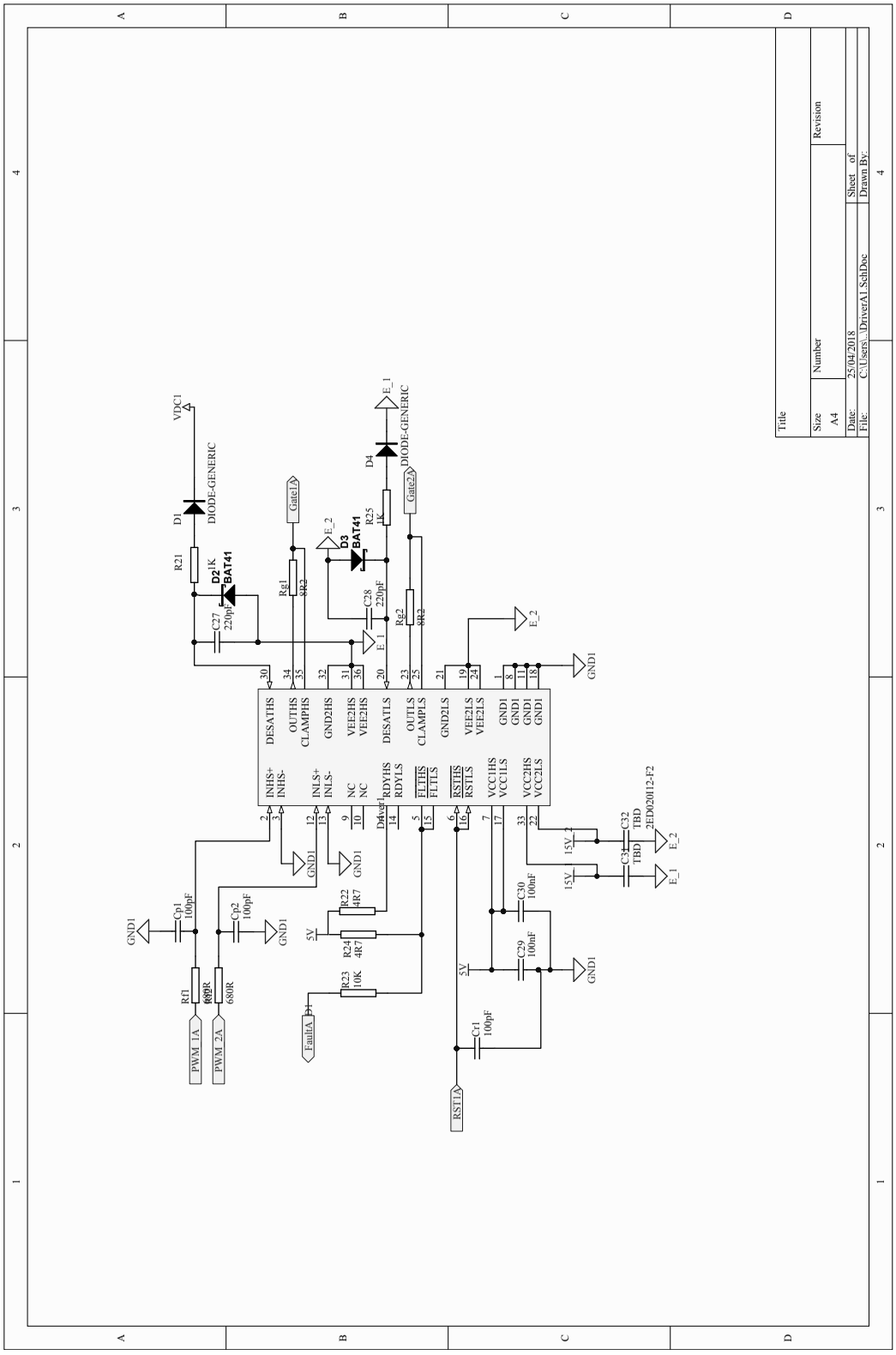
VDC1
D1
DIODE-GENERIC
R21
1K
D2
BAT41
C27
220pF
Rg1
8R2
Gate1A
E_2
D3
BAT41
R25
1K
C28
220pF
E_1
D4
DIODE-GENERIC
Gate2A
Rg2
8R2
E_2
GND1
DESATHS
OUTHS
CLAMPHS
GND2HS
VEE2HS
VEE2HS
DESATLS
OUTLS
CLAMPLS
GND2LS
VEE2LS
VEE2LS
GND1
GND1
GND1
INHS+
INHS-
INLS+
INLS-
NC
NC
RDYHS
RDYLS
FLTHS
FLTLS
RSTHS
RSTLS
VCC1HS
VCC1LS
VCC2HS
VCC2LS
Driver1
GND1
GND1
Cp1
100pF
Cp2
100pF
GND1
GND1
Rf1
680R
680R
PWM_1A
PWM_2A
5V
R22
4R7
R24
4R7
R23
10K
FaultA
C1
100pF
5V
C29
100nF
GND1
RST1A
15V_2
15V
C30
100nF
C32
TBD
C34
TBD
2ED020I12-F2
E_2
E_1
Title
Size
A4
Number
Revision
Date:
25/04/2018
Sheet of
File:
C:\Users\...\DriverA1.SchDoc
Drawn By:

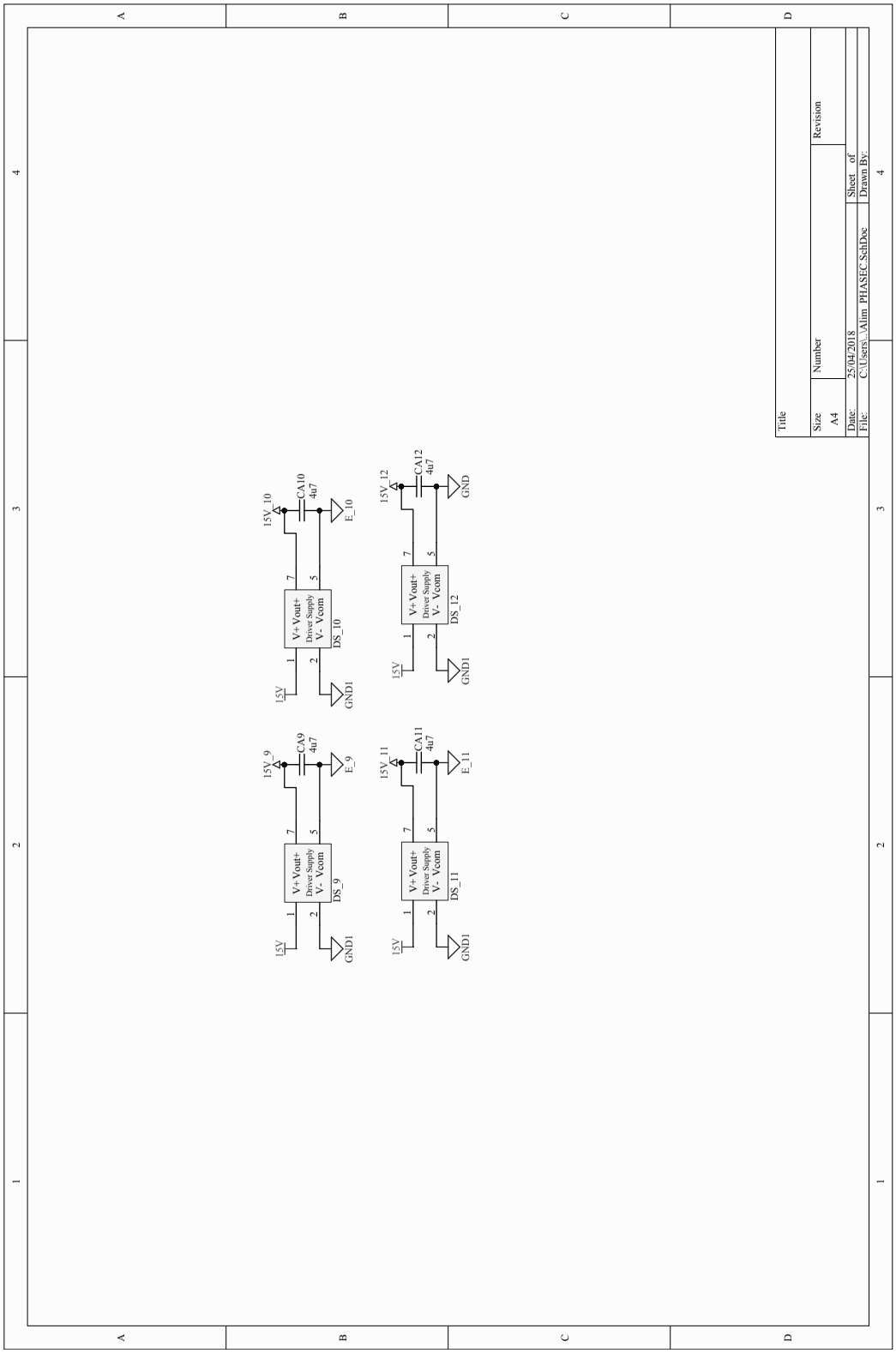
Title
Size
A4
Number
Revision
Date: 25/04/2018
File: C:\Users\...\Alim_PHASEC.SchDoc
Sheet of
Drawn By:
15V_10
CA10
4u7
E_10
V+ Vout+
Driver Supply
V- Vcom
DS_10
15V
GND1
15V_12
CA12
4u7
GND
DS_12
15V_9
CA9
4u7
E_9
DS_9
15V_11
CA11
4u7
E_11
DS_11

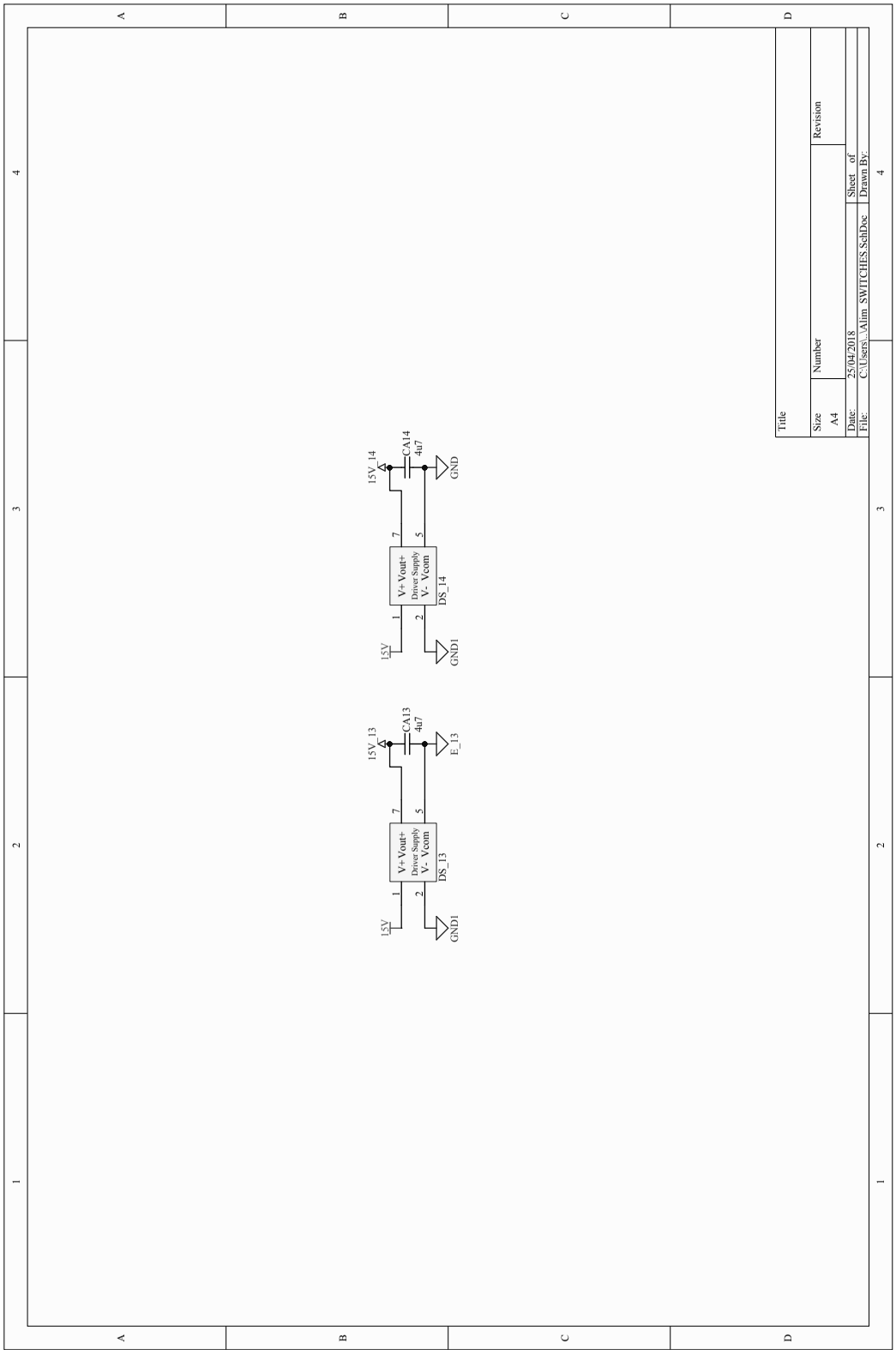
15V_14
CA14
4u7
GND
V+ Vout+
Driver Supply
V- Vcom
DS_14
15V
GND1
15V_13
CA13
4u7
E_13
V+ Vout+
Driver Supply
V- Vcom
DS_13
15V
GND1
Title
Size
A4
Number
Revision
Date: 25/04/2018
File: C:\Users\...\Alim_SWITCHES.SchDoc
Sheet of
Drawn By:

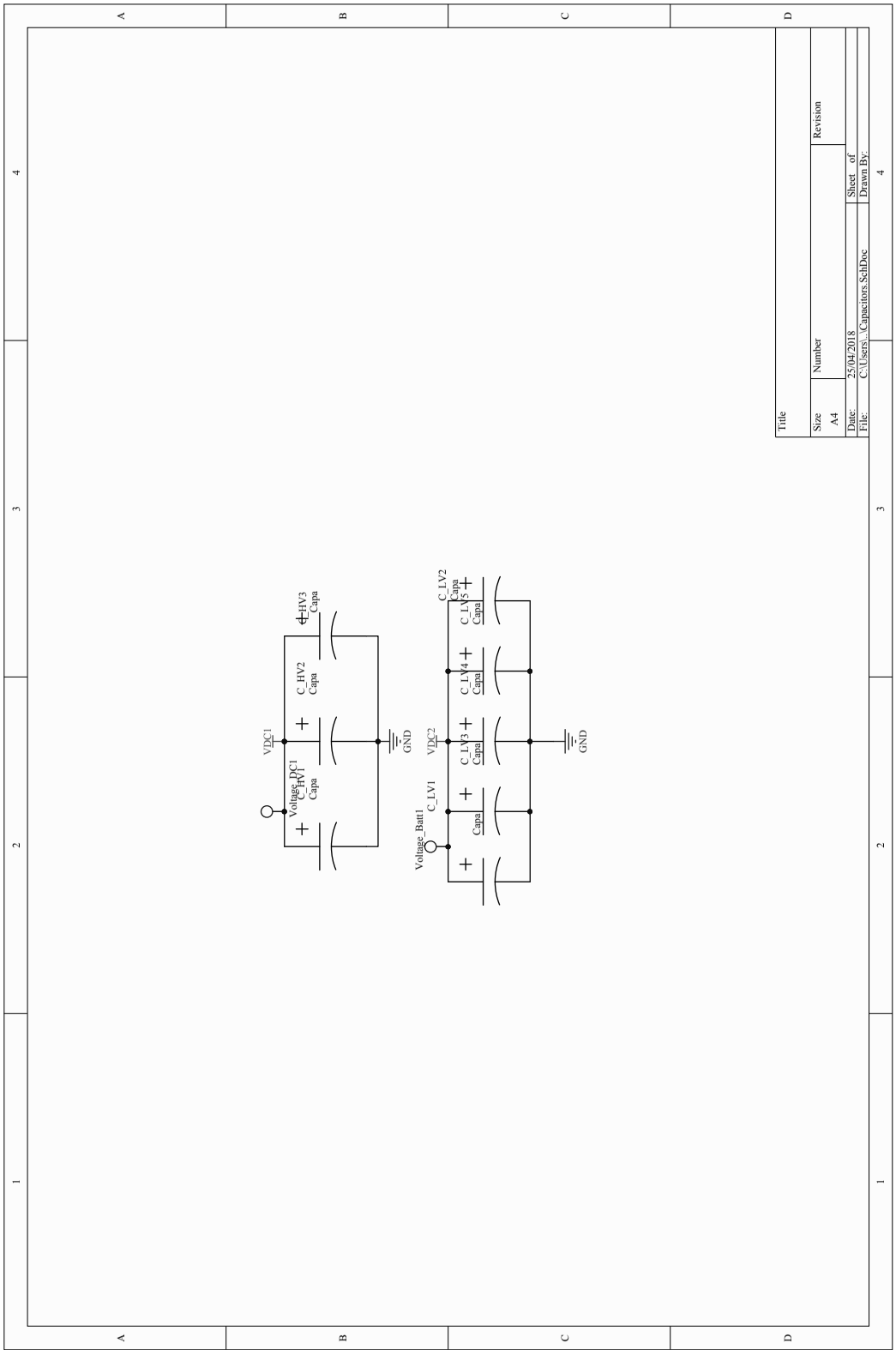
Title
Size
A4
Number
Revision
Date: 25/04/2018
Sheet of
File: C:\Users\...\Capacitors.SchDoc
Drawn By:
Voltage_DC1
VDC1
C_HV1
Capa
C_HV2
Capa
C_HV3
Capa
GND
Voltage_Batt1
VDC2
C_LV1
Capa
C_LV2
Capa
C_LV3
Capa
C_LV4
Capa
C_LV5
Capa
GND

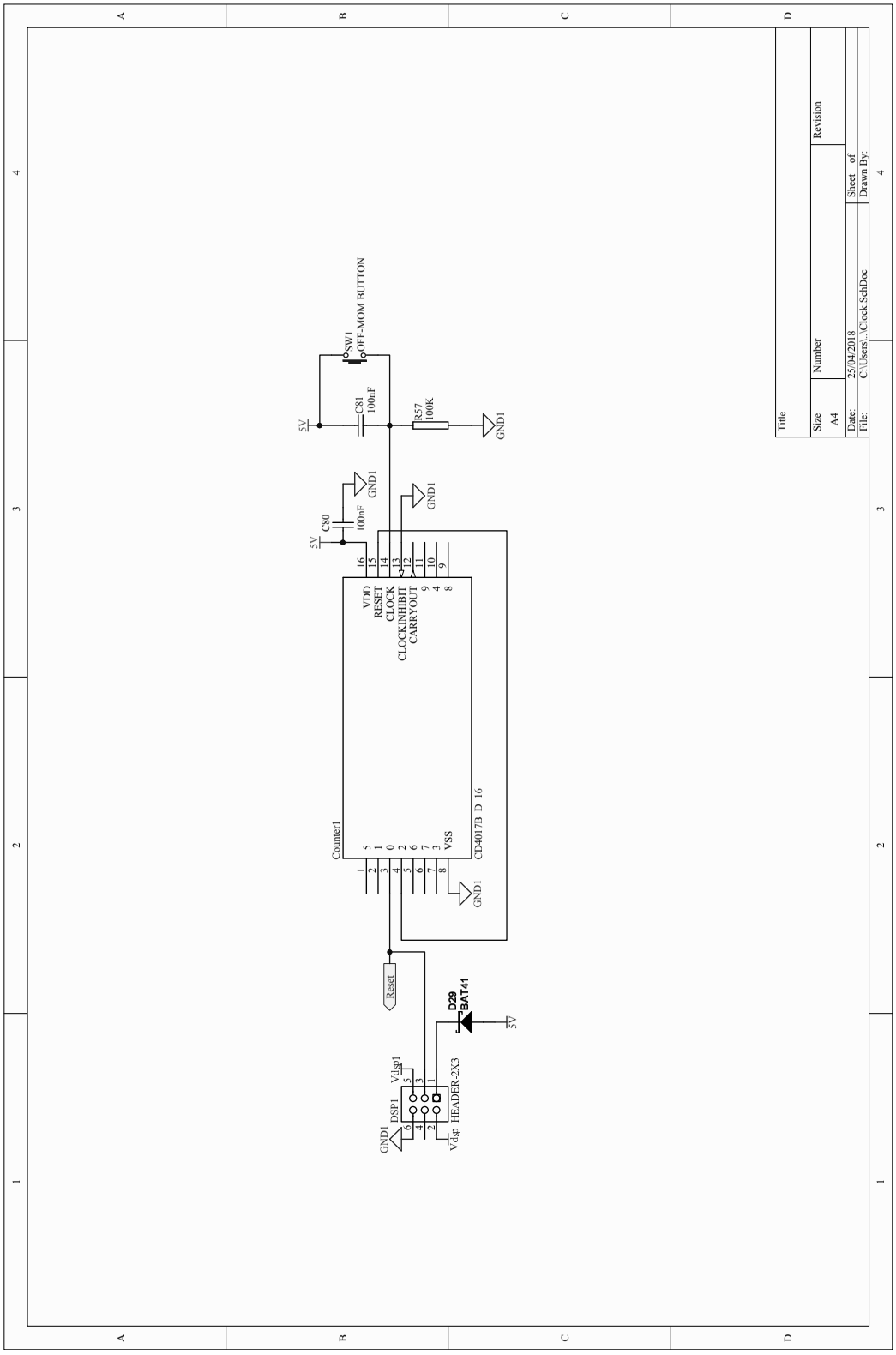
SW1
OFF-MOM BUTTON
5V
C81
100nF
R57
100K
GND1
C80
100nF
Counter1
VDD
RESET
CLOCK
CLOCKINHBIT
CARRYOUT
VSS
CD4017B_D_16
Reset
D29
BA141
DSP1
Vdsp1
HEADER-2X3
Vdsp
Title
Size
A4
Number
Revision
Date: 25/04/2018
File: C:\Users\...\Clock.SchDoc
Sheet of
Drawn By:

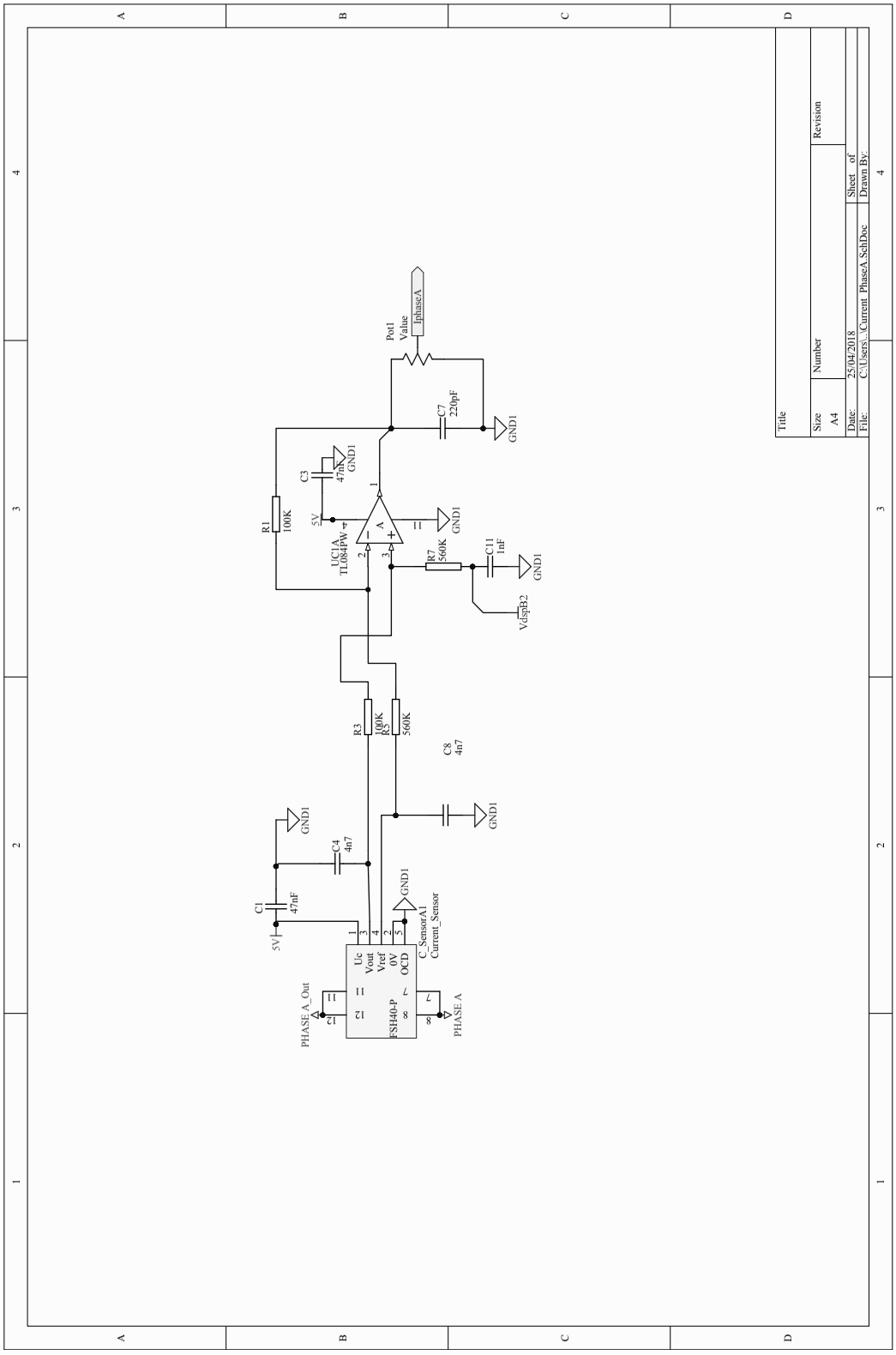
Pot1
Value
PhaseA
C7
220pF
GND1
C3
47nF
5V
R1
100K
U1:A
TL084PW
R7
560K
C11
1nF
Vusph2
R3
100K
R5
560K
C8
4n7
C4
4n7
C1
47nF
C_SensorA1
Current_Sensor
Uc
Vout
Vref
0V
OCD
FSH40-P
PHASE A_Out
PHASE A
Title
Size
A4
Number
Revision
Date: 25/04/2018
File: C:\Users\...\Current_PhaseA.SchDoc
Sheet of
Drawn By:

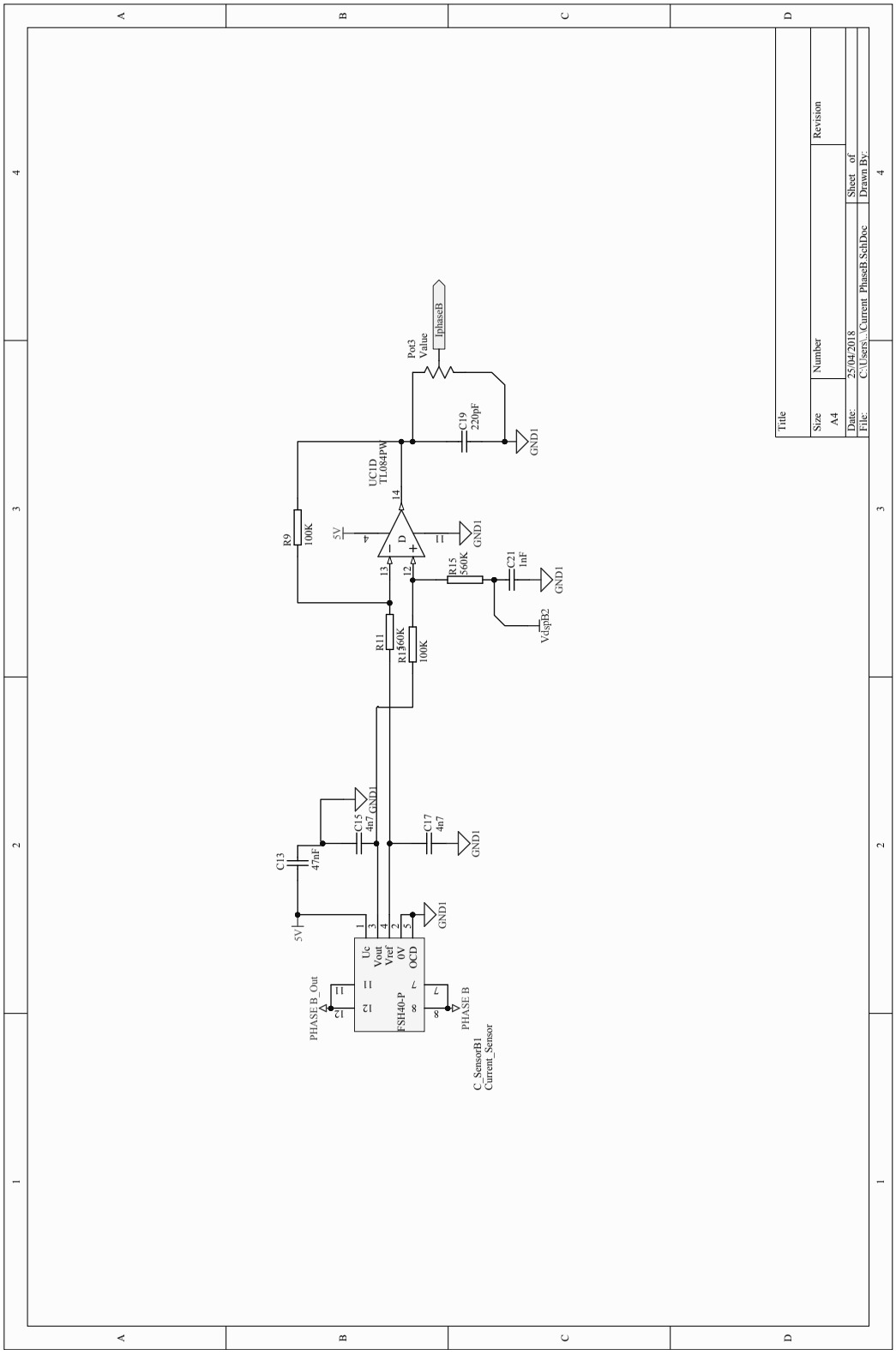
IphaseB
Pot3
Value
C19
220pF
GND1
UC1D
TL084PW
R9
100K
5V
R15
560K
C21
1nF
VdspB2
R11
560K
R13
100K
C15
4n7
C17
4n7
C13
47nF
PHASE B_Out
Uc
Vout
Vref
0V
OCD
FSH40-P
PHASE B
C_SensorB1
Current_Sensor
Title
Size
A4
Number
Revision
Date: 25/04/2018
File: C:\Users\...\Current_PhaseB.SchDoc
Sheet of
Drawn By:

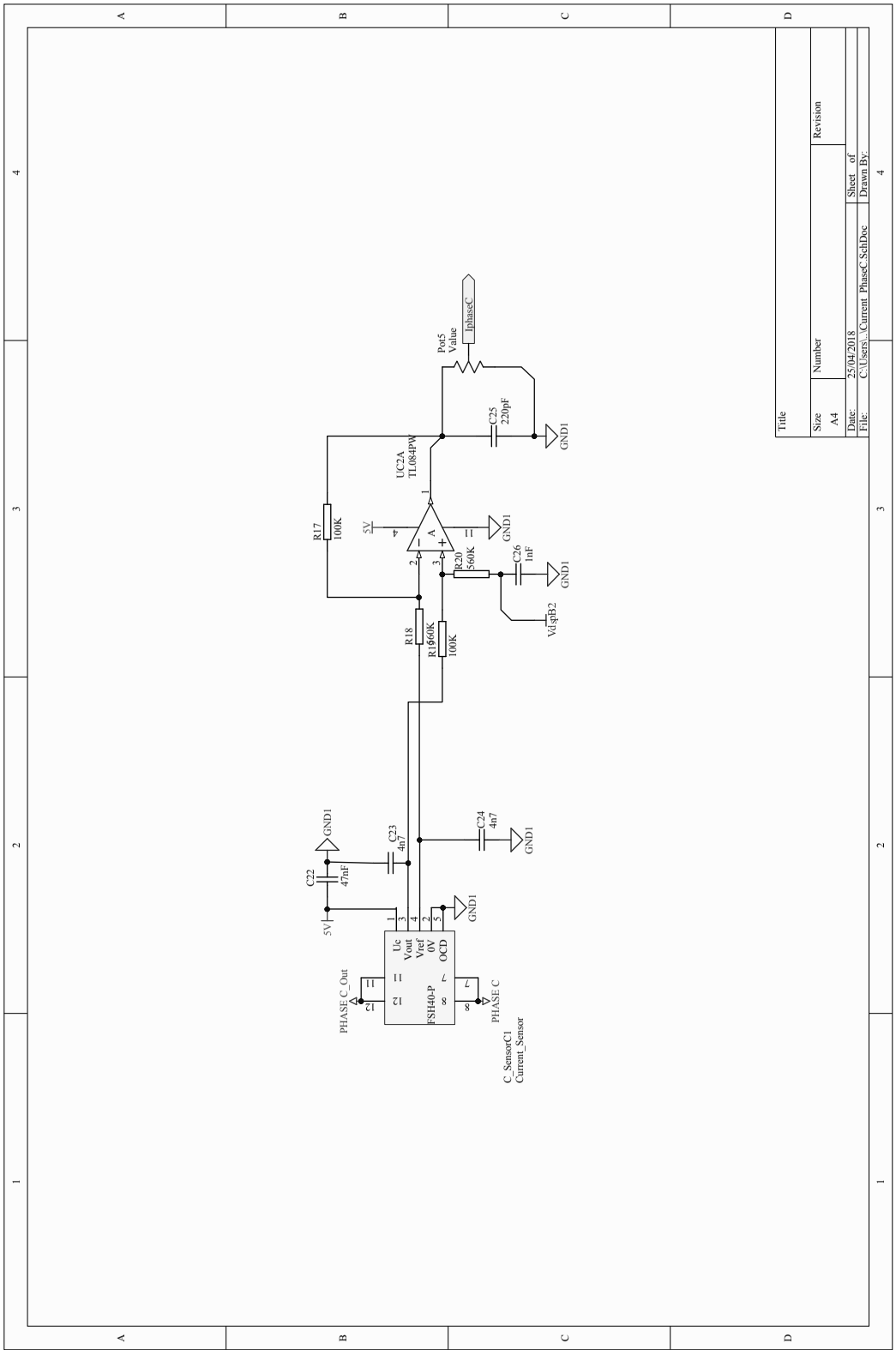
Pot5
Value
IphaseC
C25
220pF
GND1
UC2A
TL084PW
R17
100K
5V
R20
560K
C26
1nF
Vdsph2
R18
R19
560K
100K
C24
4n7
C23
4n7
C22
47nF
5V
Uc
Vout
Vref
0V
OCD
FSH40-P
PHASE C_Out
PHASE C
C_SensorC1
Current_Sensor
Title
Size
A4
Number
Revision
Date: 25/04/2018
Sheet of
File: C:\Users\...\Current_PhaseC.SchDoc
Drawn By:

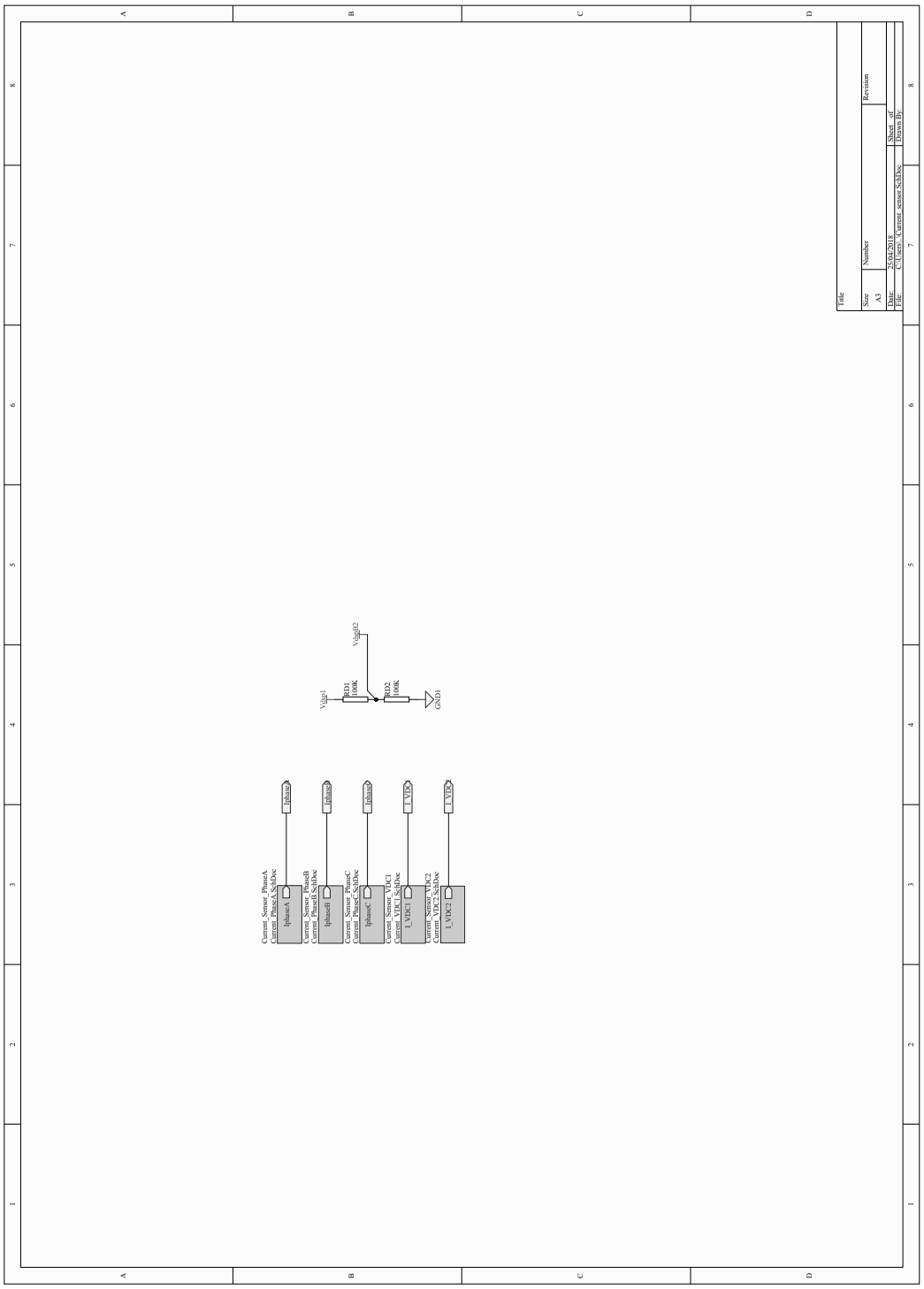
Title
Size
A3
Number
Revision
Date:
25/04/2018
Sheet of
File:
C:\Users\...\current_sensor.SchDoc
Drawn By:
Vsign1
R201
100K
R202
100K
Vsign2
GND1
Iphase1
Iphase2
Iphase3
I_VDC1
I_VDC2
Current_Sensor_PhaseA
Current_PhaseA_SchDoc
IphaseA
Current_Sensor_PhaseB
Current_PhaseB_SchDoc
IphaseB
Current_Sensor_PhaseC
Current_PhaseC_SchDoc
IphaseC
Current_Sensor_VDC1
Current_VDC1_SchDoc
I_VDC1
Current_Sensor_VDC2
Current_VDC2_SchDoc
I_VDC2

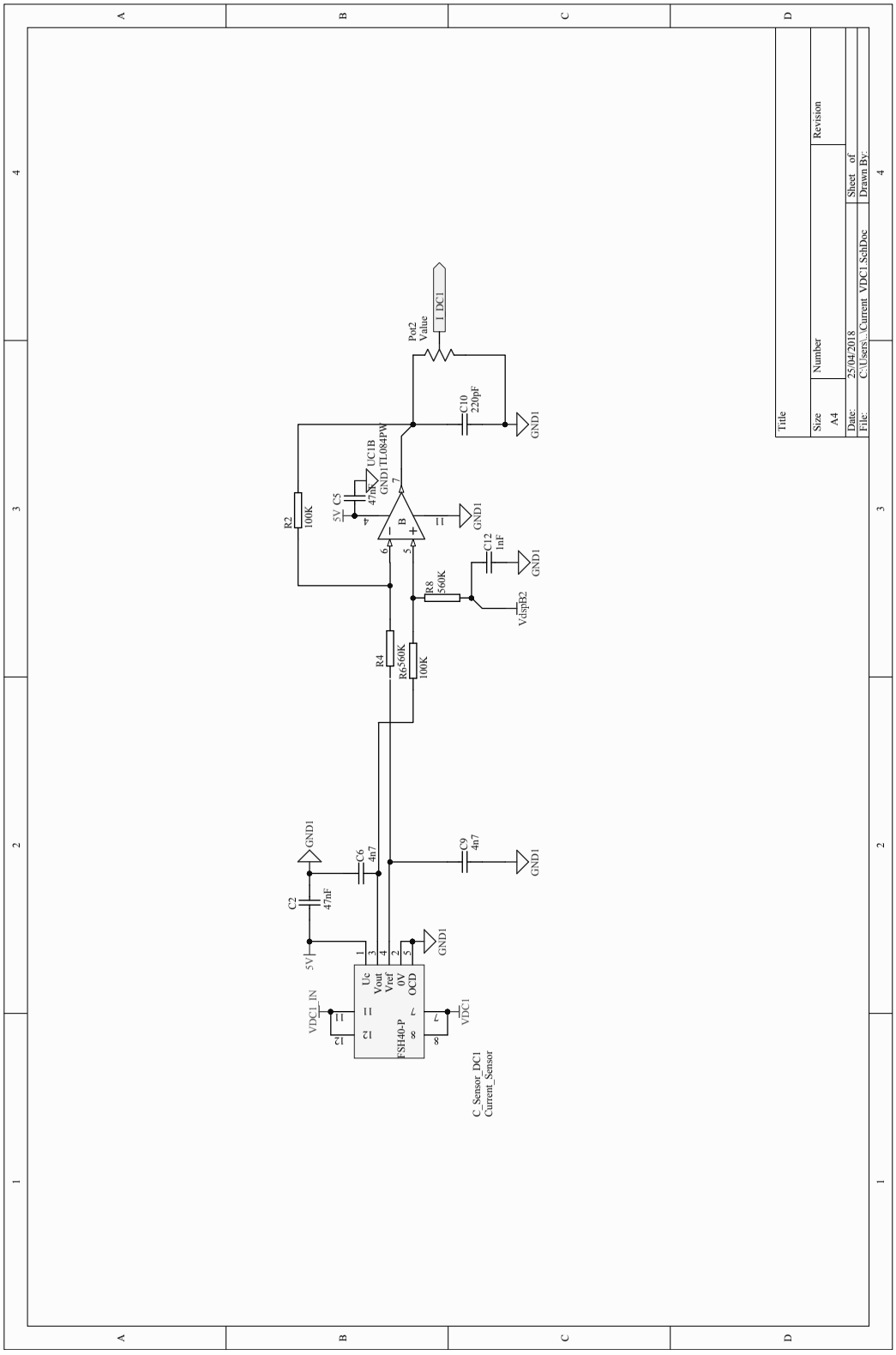
Pot2
Value
I_DC1
C10
220pF
GND1
UC1B
TL084PW
5V C5
47nF
R2
100K
R4
R6 560K
100K
R8
560K
C12
1nF
Vdiff82
C6
4n7
C9
4n7
C2
47nF
5V
Uc
Vout
Vref
0V
OCD
FSH40-P
VDC1_IN
VDC1
C_Sensor_DC1
Current_Sensor
Title
Size
A4
Number
Revision
Date: 25/04/2018
File: C:\Users\...\Current_VDC1.SchDoc
Sheet of
Drawn By:

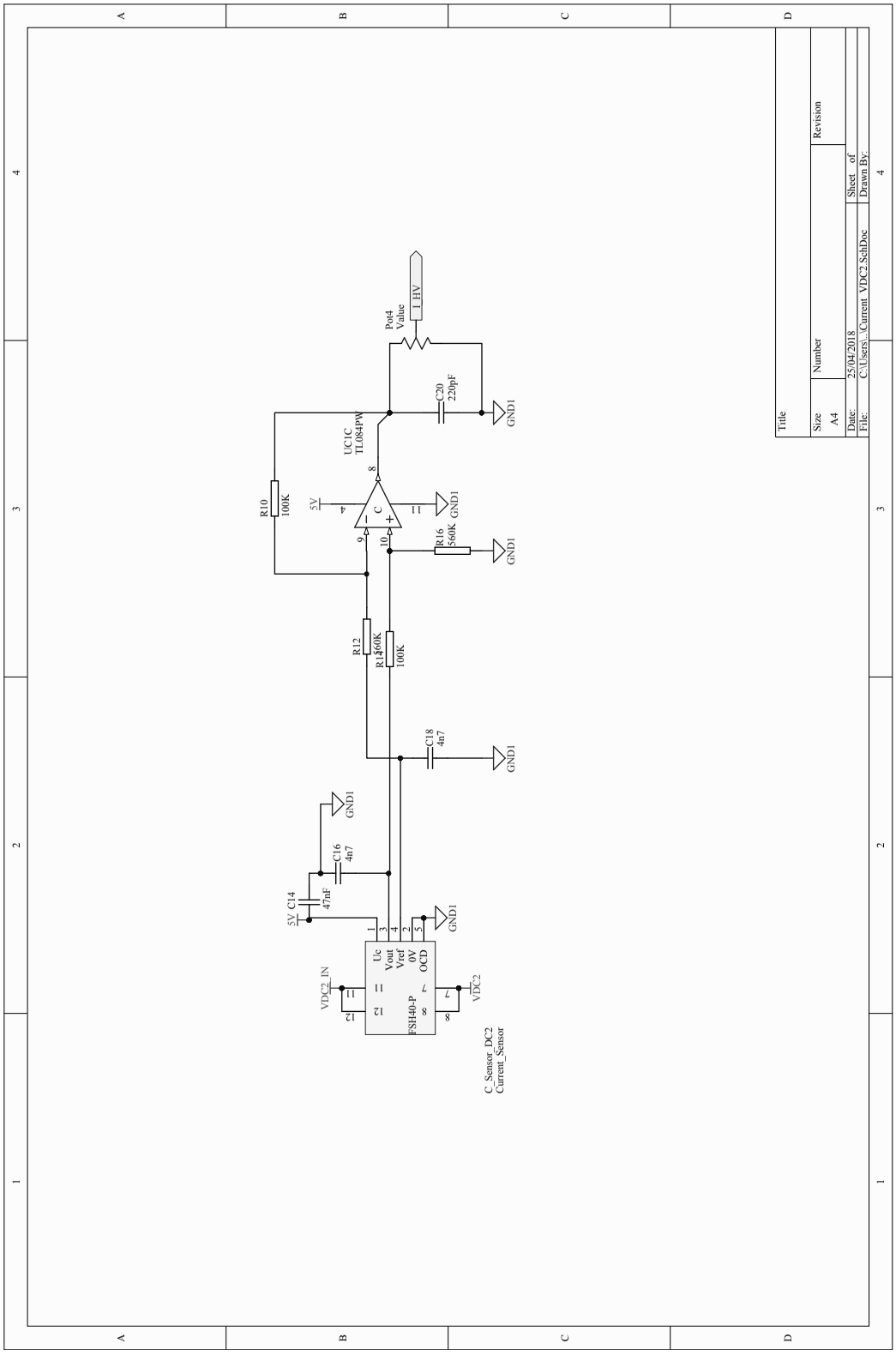
Title
Size
A4
Number
Revision
Date: 25/04/2018
File: C:\Users\...\Current_VDC2.SchDoc
Sheet of
Drawn By:
Pot4
Value
1_HV
C20
220pF
GND1
UC1C
TL084PW
R10
100K
5V
R16
560K
R12
560K
R14
100K
C18
4n7
C16
4n7
5V C14
47nF
Uc
Vout
Vref
0V
OCD
FSH40-P
VDC2_IN
VDC2
C_Sensor_DC2
Current_Sensor

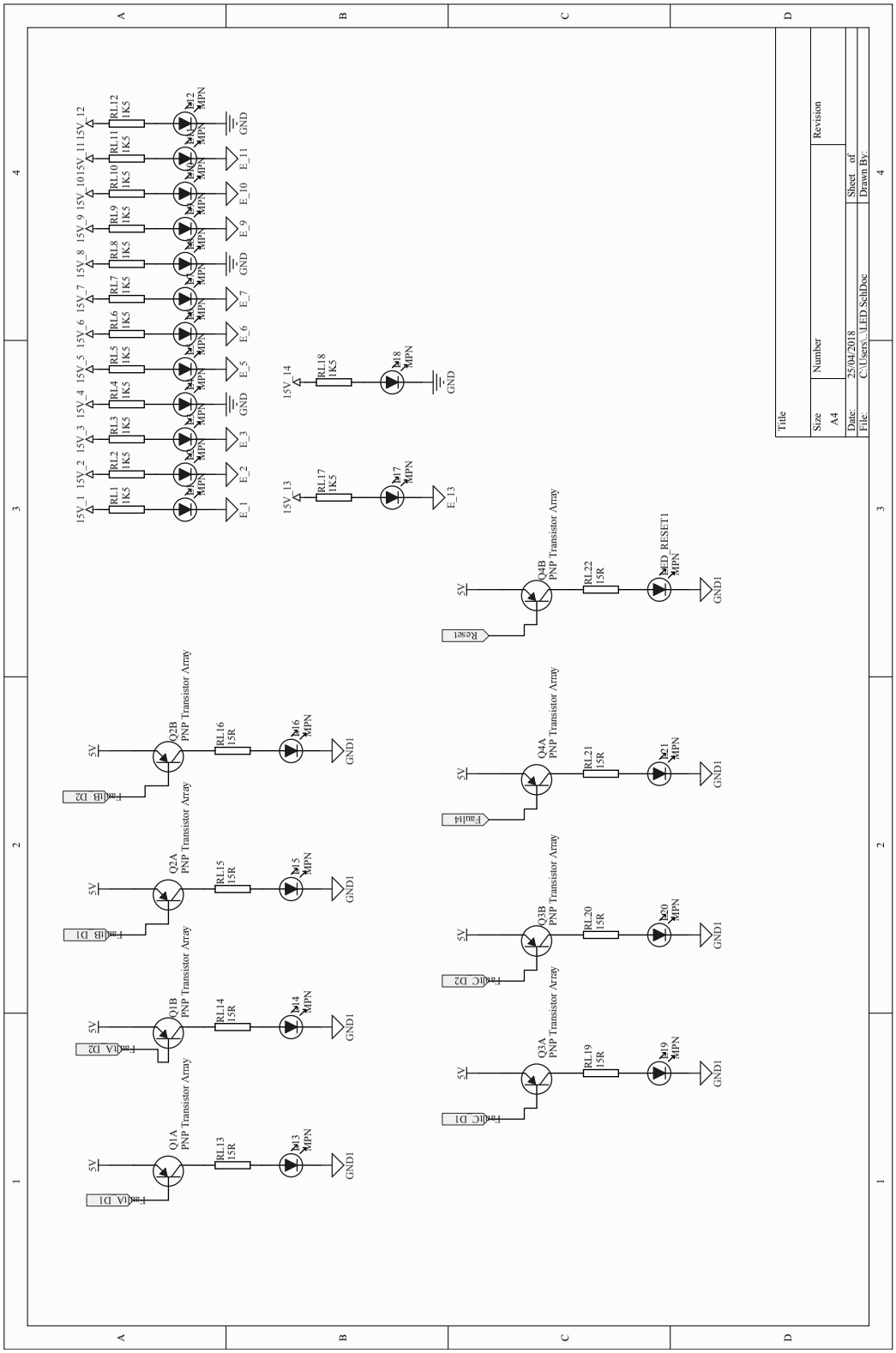
Title
Size A4
Number
Revision
Date: 25/04/2018
Sheet of
File: C:\Users\...\LED.SchDoc
Drawn By:
Q1A PNP Transistor Array
Q1B PNP Transistor Array
Q2A PNP Transistor Array
Q2B PNP Transistor Array
Q3A PNP Transistor Array
Q3B PNP Transistor Array
Q4A PNP Transistor Array
Q4B PNP Transistor Array
RL1 1K5
RL2 1K5
RL3 1K5
RL4 1K5
RL5 1K5
RL6 1K5
RL7 1K5
RL8 1K5
RL9 1K5
RL10 1K5
RL11 1K5
RL12 1K5
RL13 15R
RL14 15R
RL15 15R
RL16 15R
RL17 1K5
RL18 1K5
RL19 15R
RL20 15R
RL21 15R
RL22 15R
5V
GND
GND1
E_1
E_2
E_3
E_5
E_6
E_7
E_9
E_10
E_11
E_13
Reset
RESET1
Fault1A D1
Fault1A D2
Fault1B D1
Fault1B D2
Fault1C D1
Fault1C D2
Fault4

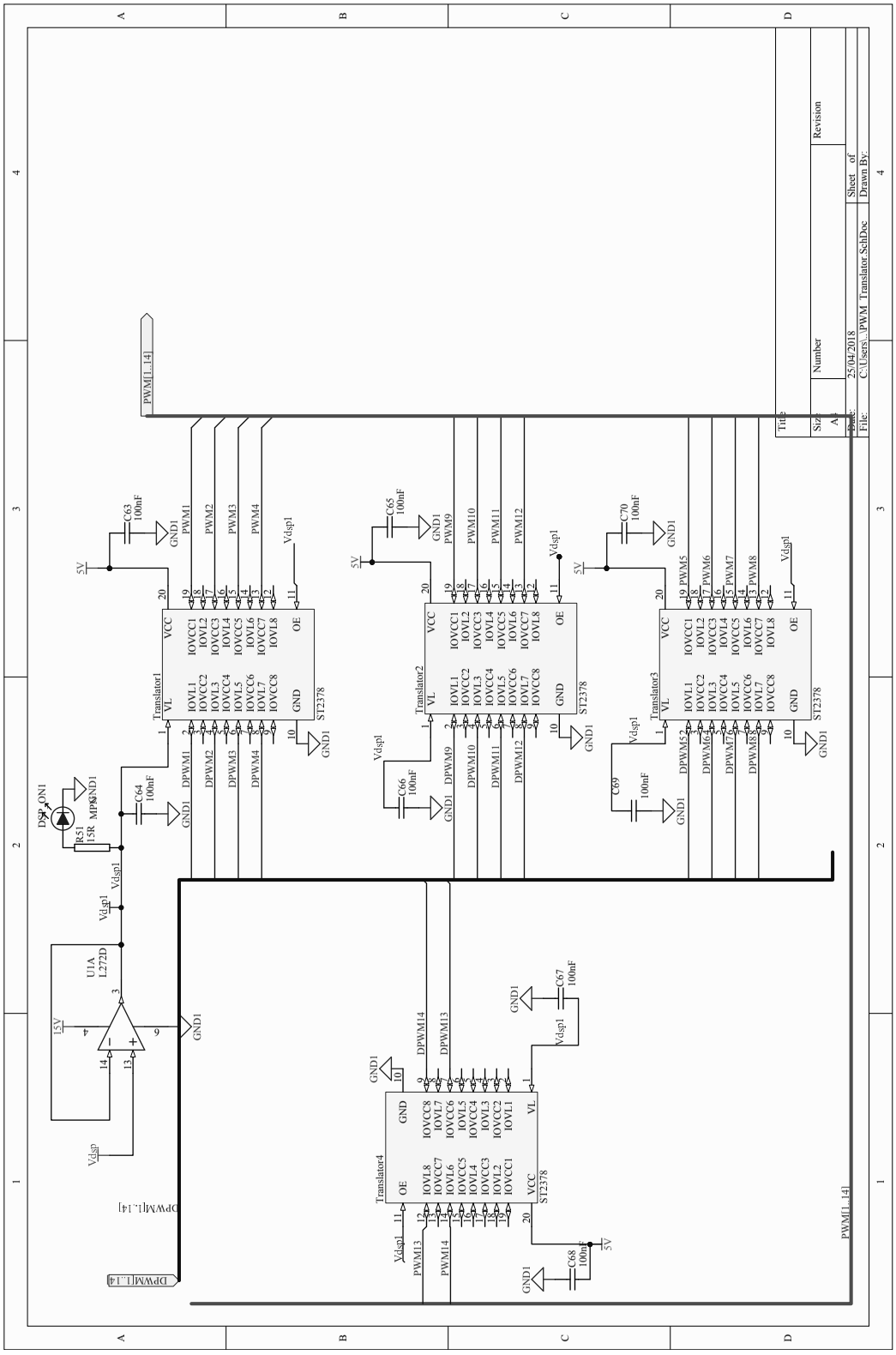
PWM[1..14]
Translator1
Translator2
Translator3
Translator4
ST2378
VCC
VL
GND
OE
IOVL1
IOVL2
IOVL3
IOVL4
IOVL5
IOVL6
IOVL7
IOVL8
IOVCC1
IOVCC2
IOVCC3
IOVCC4
IOVCC5
IOVCC6
IOVCC7
IOVCC8
DPWM1
DPWM2
DPWM3
DPWM4
DPWM5
DPWM6
DPWM7
DPWM8
DPWM9
DPWM10
DPWM11
DPWM12
DPWM13
DPWM14
PWM1
PWM2
PWM3
PWM4
PWM5
PWM6
PWM7
PWM8
PWM9
PWM10
PWM11
PWM12
PWM13
PWM14
C63 100nF
C64 100nF
C65 100nF
C66 100nF
C67 100nF
C68 100nF
C69 100nF
C70 100nF
R51 15R
U1A L272D
DSP ON1
MPWM
5V
Vdsp1
GND1
Title
Size: A4
Number
Revision
Date: 25/04/2018
File: C:\Users\...\PWM Translator.SchDoc
Sheet of
Drawn By:

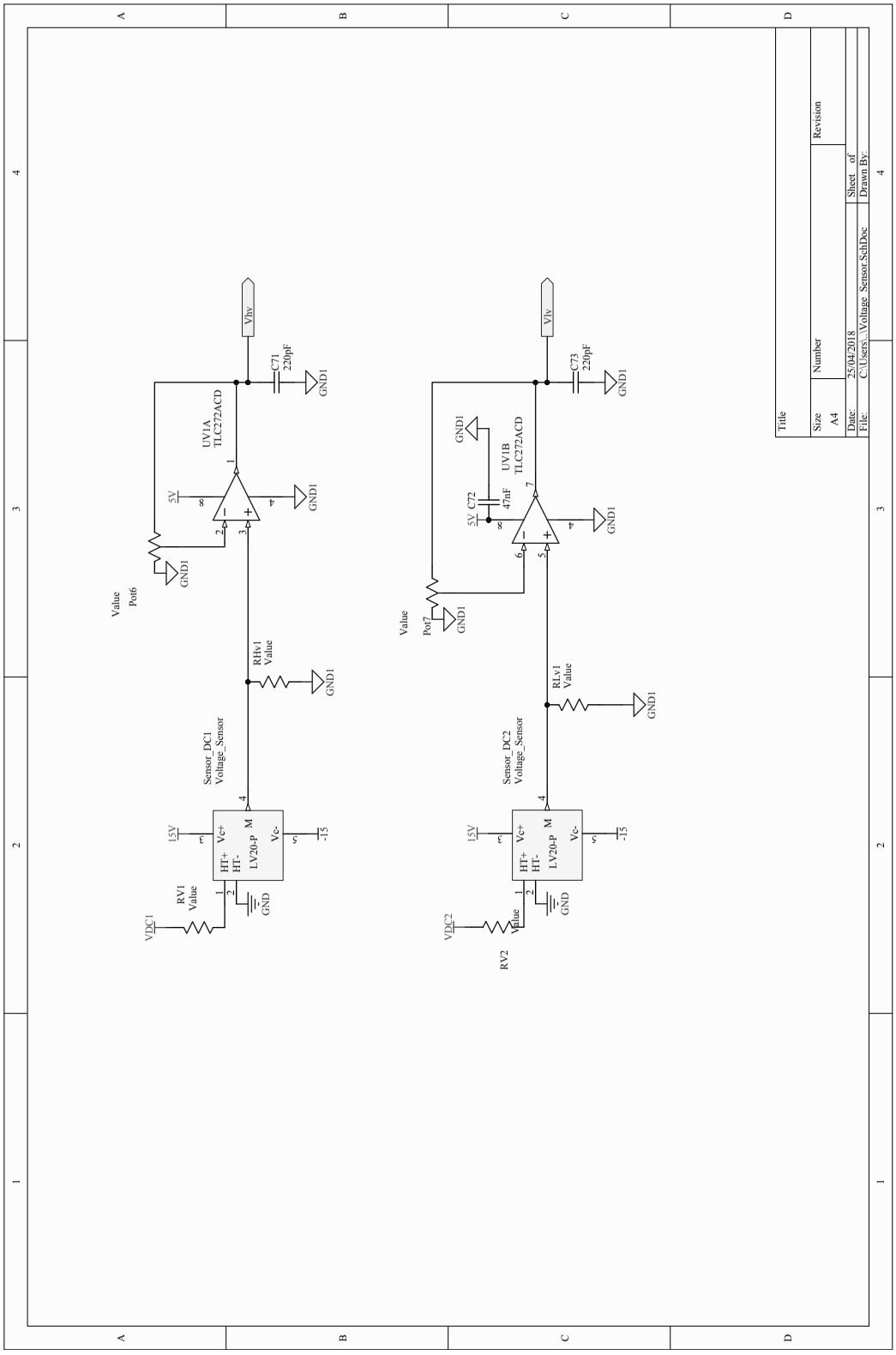
Vhv
C71
220pF
GND1
UV1A
TLC272ACD
5V
Value
Pot6
RHv1
Value
Sensor_DC1
Voltage_Sensor
15V
HT+
HT-
Vc+
Vc-
LV20-P
M
-15
RV1
Value
GND
VDC1
C73
C72
47nF
UV1B
Pot7
RLv1
Sensor_DC2
RV2
VDC2
Title
Size
A4
Number
Revision
Date:
25/04/2018
Sheet of
File:
C:\Users\...\Voltage_Sensor.SchDoc
Drawn By:

Bibliography

[1] N. R. C. Government of Canada, "2009 Canadian Vehicle Survey Summary Report," Sept. 2011. Last Modified: 2011-09-01.

[2] S. C. Government of Canada, "Automotive statistics," Dec. 2018.

[3] A. Emadi, *Advanced Electric Drive Vehicles*. CRC Press Taylor and Francis Group, Oct. 2014.

[4] IEA, "Global EV Outlook 2020 – Analysis."

[5] O. US EPA, "Explaining Electric & Plug-In Hybrid Electric Vehicles," Aug. 2015.

[6] Obama Whitehouse, "What the New Fuel Economy Standards Mean for You | whitehouse.gov."

[7] K. V. Singh, H. O. Bansal, and D. Singh, "A comprehensive review on hybrid electric vehicles: architectures and components," *Journal of Modern Transportation*, vol. 27, pp. 77–107, June 2019.

[8] J. Reimers, L. Dorn-Gomba, C. Mak, and A. Emadi, "Automotive Traction

Inverters: Current Status and Future Trends," *IEEE Transactions on Vehicular Technology*, vol. 68, pp. 3337–3350, Apr. 2019.

[9] L. Dorn-Gomba, P. Magne, C. Barthelmebs, and A. Emadi, "On the concept of the multi-source inverter," in *2016 IEEE Applied Power Electronics Conference and Exposition (APEC)*, pp. 453–459, Mar. 2016.

[10] R. Ahmed, "MODELING AND STATE OF CHARGE ESTIMATION OF ELECTRIC VEHICLE BATTERIES," p. 311.

[11] Toyota, "2020 Toyota Mirai Hydrogen Fuel Cell Electric Vehicle | The Future of Everyday."

[12] Maxwell Technologies, "Maxwell Ultracapacitors: Enabling Energy's Future."

[13] L. Dorn-Gomba, "MULTI-SOURCE INVERTER FOR ELECTRIFIED VEHICLES: CONCEPT, ANALYTICAL DESIGN, EFFICIENCY ANALYSIS, AND IMPLEMENTATION," p. 228.

[14] E. Chemali, L. McCurlie, B. Howey, T. Stiene, M. M. Rahman, M. Preindl, R. Ahmed, and A. Emadi, "Minimizing battery wear in a hybrid energy storage system using a linear quadratic regulator," in *IECON 2015 - 41st Annual Conference of the IEEE Industrial Electronics Society*, pp. 003265–003270, Nov. 2015.

[15] E. Chemali and A. Emadi, "On the concept of a novel Reconfigurable Multi-Source Inverter," in *2017 IEEE Transportation Electrification Conference and Expo (ITEC)*, (Chicago, IL, USA), pp. 707–713, IEEE, June 2017.

[16] J. F. Silva and S. F. Pinto, "36 - Advanced Control of Switching Power Converters," in *Power Electronics Handbook (Third Edition)* (M. H. Rashid, ed.), pp. 1037–1113, Boston: Butterworth-Heinemann, Jan. 2011.

[17] Mehdi Narimani, "ECE720_topic 7_ NPC Inverters."

[18] R. P. Aguilera, P. Acuna, G. Konstantinou, S. Vazquez, and J. I. Leon, "Chapter 2 - Basic Control Principles in Power Electronics: Analog and Digital Control Design," in *Control of Power Electronic Converters and Systems* (F. Blaabjerg, ed.), pp. 31–68, Academic Press, Jan. 2018.

[19] S.-H. Kim, "Chapter 7 - Pulse width modulation inverters," in *Electric Motor Control* (S.-H. Kim, ed.), pp. 265–340, Elsevier, Jan. 2017.

[20] A. Iqbal, S. Moinoddin, S. Ahmad, M. Ali, A. Sarwar, and K. N. Mude, "15 - Multiphase Converters," in *Power Electronics Handbook (Fourth Edition)* (M. H. Rashid, ed.), pp. 457–528, Butterworth-Heinemann, Jan. 2018.

[21] Mehdi Narimani, "ECE720_topic 5_voltage Source Inverters.pdf."

[22] Mathworks, "Loss Calculation in a Three-Phase 3-Level Inverter - MATLAB & Simulink."

[23] L. Dorn-Gomba, E. Chemali, and A. Emadi, "A novel hybrid energy storage system using the multi-source inverter," in *2018 IEEE Applied Power Electronics Conference and Exposition (APEC)*, pp. 684–691, Mar. 2018. ISSN: 2470-6647.

[24] C. C. Chan, A. Bouscayrol, and K. Chen, "Electric, Hybrid, and Fuel-Cell Vehicles: Architectures and Modeling," *IEEE Transactions on Vehicular Technology*,

vol. 59, pp. 589–598, Feb. 2010. Conference Name: IEEE Transactions on Vehicular Technology.

[25] L. Dorn-Gomba, P. Magne, B. Danen, and A. Emadi, "On the Concept of the Multi-Source Inverter for Hybrid Electric Vehicle Powertrains," *IEEE Transactions on Power Electronics*, vol. 33, pp. 7376–7386, Sept. 2018.

[26] McMaster University, "No more in-person classes and exams: President's letter," Mar. 2020.

[27] Ontario, "COVID-19: Government service changes and public closures," Apr. 2020.